From particles to plumes: Role of flocculation in turbidity flows

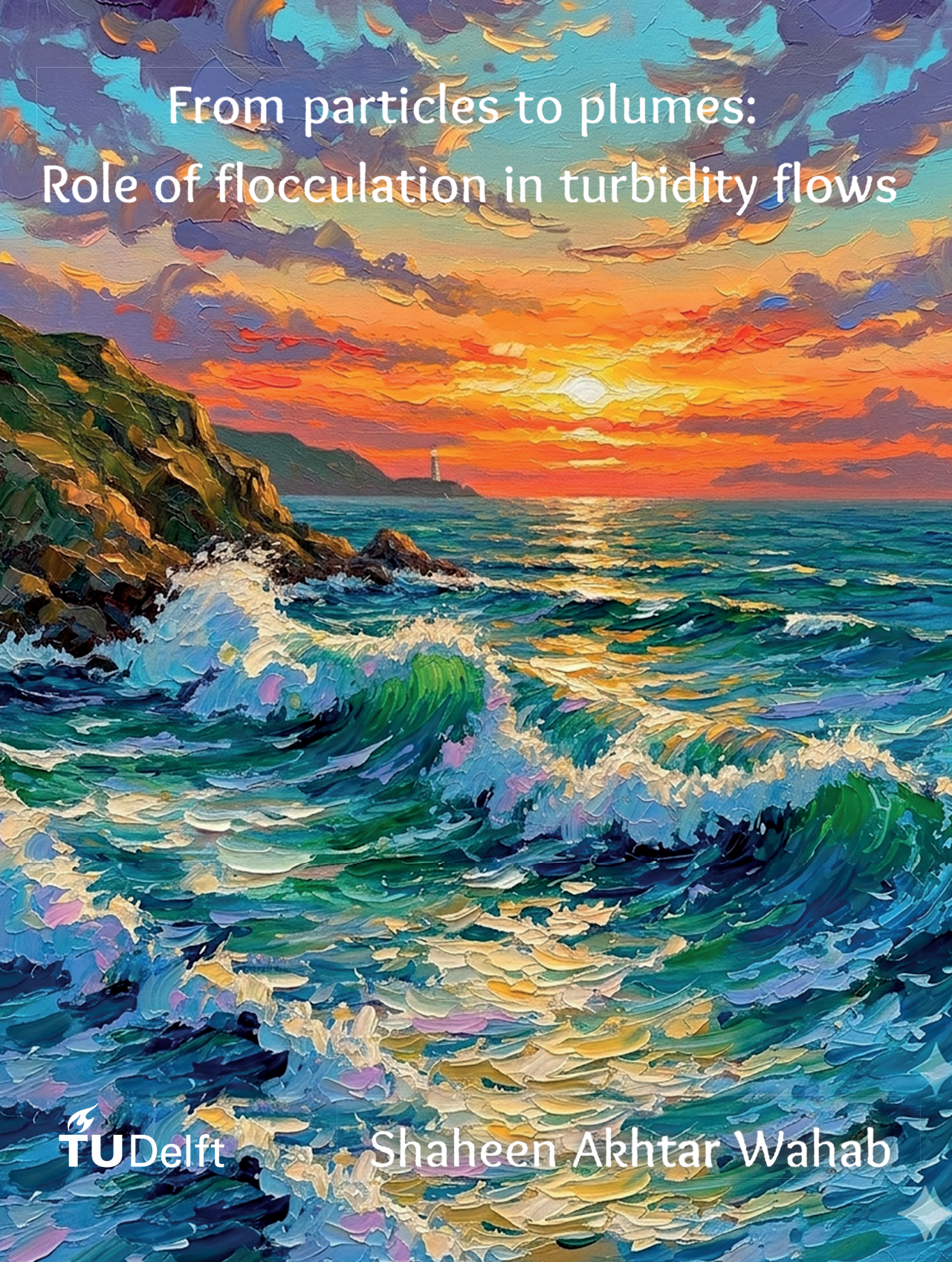

TU Delft

Shaheen Akhtar Wahab

FROM PARTICLES TO PLUMES: ROLE OF FLOCCULATION IN TURBIDITY FLOWS

FROM PARTICLES TO PLUMES: ROLE OF FLOCCULATION IN TURBIDITY FLOWS

Dissertation

for the purpose of obtaining the degree of doctor
at Delft University of Technology,
by the authority of the Rector Magnificus
Prof. dr. ir. H. Bijl,
chair of the Board for Doctorates,
to be defended publicly on
Thursday 2nd, July 2026 at 5:30 p.m.

by

Shaheen Akhtar WAHAB

This dissertation has been approved by the promotors.

Composition of the doctoral committee:

Rector Magnificus	Chairperson
Dr. ir. R.L.J. Helmons	Delft University of Technology, promotor
Dr. C. Chassagne	Delft University of Technology, promotor
Independent members:	
Prof. dr. ir. M. van Koningsveld	Delft University of Technology
Prof. dr. A.J. Manning	University of Plymouth, United Kingdom
Dr. ir. B.C. van Prooijen	Delft University of Technology
Dr. H. de Stigter	Nederlands Instituut voor Onderzoek der Zee
Prof. dr. L. Thomsen	University of Gothenburg, Sweden
Other members:	
Prof. G.D. Weymouth	Delft University of Technology, reserve member

This research has been funded by NWO.

Keywords: deep-sea mining, flocculation, turbidity flows, lock-exchange

Printed by: Proefschrift Specialist

Front & Back: Google Gemini 3.5 Flash

ISBN 978-94-93539-45-7

An electronic version of this dissertation is available at
http://repository.tudelft.nl/.

To my
grandfather Late. Dr. Abdul Wahab, grandmother Late. Rebecca Wahab (paternal),
and my grandfather, Late. Muhibur Rahman (maternal)

CONTENTS

SUMMARY

The work presented in this thesis investigates the role of flocculation in turbidity flows, with relevance to deep-sea mining but also dredging operations in more shallow waters, as the results are broadly applicable. Deep-sea mining is emerging as an alternative source for critical minerals needed for the transition to clean energy technologies. However, mining activities disturb the seabed, leading to the formation of sediment plumes. These sediment plumes propagate over long distances and impact sensitive marine ecosystems in the area. Similar environmental concerns also arise in the case of dredging projects, where resuspended sediments increase the turbidity in the surrounding waters. These challenges highlight the need for improved understanding of sediment plume dynamics and the processes that control their evolution. Flocculation (the aggregation of small particles into larger ones) could potentially limit turbidity flow propagation. This underpins the work presented in this thesis.

A series of laboratory experiments was designed to study the propagation of turbidity currents under controlled conditions. A lock-exchange flume setup was used to simulate sediment-laden turbidity currents, where detailed investigations of current propagation and floc formation were carried out. The work combines hydrodynamic measurements with advanced particle-sensing techniques to link micro-scale flocculation processes with turbidity current behavior. Experiments were first conducted with clay (illite) in the presence of flocculants (polyacrylamide), and then with a natural clay from the Clarion-Clipperton Fracture Zone (CCZ) that contains organic matter (acting as flocculants). Some experiments were also conducted with non-flocculating quartz as a reference. The results demonstrate that flocculation can occur rapidly, within tens of seconds, and significantly modifies particle size distributions and settling behavior.

The thesis further explores how seabed characteristics influence turbidity currents. Experiments were performed over beds of different compositions and ages to understand their roles in turbidity flows and floc evolution. The presence of polyacrylamide in the outflow compartment of the lock-exchange flume was found to increase the front velocity when no bed was present, which was attributed to the lubrication effect between the turbidity current and the plexiglass bottom of the flume. It was found that pre-existing beds and their consolidation state affect sediment entrainment and flow propagation. Bed roughness and material type can either enhance or suppress floc formation, thereby altering the mobility of the turbidity current. These findings are directly relevant to operational strategies in dredging and mining, where repeated disturbance of the seabed occurs.

In addition to physical mechanisms, this research also examines the ability of monitoring instruments to detect turbidity current properties, particularly particle size and concentration. Optical Backscatter Sensors (OBS), Acoustic Doppler Velocimeter (ADV), and Laser In-Situ Scattering and Transmissometry (LISST) were used in the lock-exchange setup. Malvern mastersizer and FlocCAM were used to further characterize samples

taken at different positions within the lock-exchange flume. The study demonstrates that sensor responses are highly sediment-dependent and that no single instrument can, in situ (lock-exchange) reliably distinguish between primary (unflocculated) particles and aggregates. A combination of lab measurements and in situ sensor techniques is therefore recommended for studying flocculation.

Overall, this thesis provides new experimental insights into the coupling between particle aggregation and turbidity current dynamics. It shows that flocculation, bed interactions, and sensor limitations must all be considered when predicting sediment plume behavior. The outcomes contribute to more reliable assessment and monitoring of environmental impacts associated with offshore engineering activities and offer guidance for future field measurements. The work ultimately strengthens the scientific basis for responsible and sustainable management of deep-sea mining and dredging operations.

SAMENVATTING

Dit proefschrift onderzoekt de rol van flocculatie in troebelheidsstromen (turbidity flows), met bijzondere relevantie voor diepzeemijnbouw, maar ook voor baggerwerkzaamheden in ondiepere wateren, aangezien de resultaten breed toepasbaar zijn. Diepzeemijnbouw wordt steeds vaker gezien als een alternatieve bron van kritieke mineralen die nodig zijn voor de energietransitie. Mijnbouwactiviteiten verstoren echter de zeebodem, waardoor sedimentpluimen ontstaan. Deze sedimentpluimen kunnen zich over grote afstanden verspreiden en kwetsbare mariene ecosystemen beïnvloeden. Vergelijkbare milieukwesties doen zich voor bij baggerprojecten, waarbij opgewervelde sedimenten de troebelheid van het omringende water verhogen. Deze uitdagingen benadrukken de noodzaak van een beter begrip van de dynamiek van sedimentpluimen en de processen die hun ontwikkeling bepalen. Flocculatie – het samenklonteren van kleine deeltjes tot grotere aggregaten – kan mogelijk de verspreiding van troebelheidsstromen beperken. Dit vormt de basis van het onderzoek dat in dit proefschrift wordt gepresenteerd.

Een reeks laboratoriumexperimenten werd ontworpen om de voortplanting van troebelheidsstromen onder gecontroleerde omstandigheden te bestuderen. Hiervoor werd gebruikgemaakt van een lock-exchange-opstelling waarin sedimentbeladen troebelheidsstromen werden gesimuleerd. Gedetailleerde metingen werden uitgevoerd naar zowel de voortplanting van de stroming als de vorming van flocs. Het onderzoek combineert hydrodynamische metingen met geavanceerde technieken voor de detectie van deeltjes om processen van flocculatie op microschaal te koppelen aan het gedrag van troebelheidsstromen. De experimenten werden eerst uitgevoerd met klei (illiet) in aanwezigheid van flocculanten (polyacrylamide), gevolgd door experimenten met natuurlijke klei uit de Clarion-Clipperton Zone (CCZ), die organisch materiaal bevat dat als natuurlijk flocculant werkt. Daarnaast werden experimenten uitgevoerd met niet-flocculerend kwarts als referentiemateriaal. De resultaten tonen aan dat flocculatie zeer snel kan optreden, binnen enkele tientallen seconden, en een aanzienlijke invloed heeft op de deeltjesgrootteverdeling en het bezinkgedrag.

Daarnaast onderzoekt dit proefschrift hoe eigenschappen van de zeebodem troebelheidsstromen beïnvloeden. Experimenten werden uitgevoerd boven bodems met verschillende samenstellingen en leeftijden om hun rol in troebelheidsstromen en de ontwikkeling van flocs te begrijpen. De aanwezigheid van polyacrylamide in het uitstroomcompartiment van de lock-exchange-opstelling bleek de frontsnelheid te verhogen wanneer geen bodem aanwezig was. Dit werd toegeschreven aan een smerend effect tussen de troebelheidsstroom en de plexiglazen bodem van de goot. Verder werd vastgesteld dat reeds aanwezige bodems en hun mate van consolidatie van invloed zijn op sedimentopname en de voortplanting van de stroming. Bodemruwheid en materiaaltype kunnen de vorming van flocs zowel bevorderen als onderdrukken, waardoor de mobiliteit van de troebelheidsstroom verandert. Deze bevindingen zijn direct relevant voor operationele strategieën binnen de bagger- en mijnbouwsector, waar de zeebodem herhaaldelijk

wordt verstoord.

Naast de fysische processen onderzoekt dit onderzoek ook in hoeverre meetinstrumenten in staat zijn eigenschappen van troebelheidsstromen te detecteren, met name deeltjesgrootte en concentratie. Hiervoor werden Optical Backscatter Sensors (OBS), een Acoustic Doppler Velocimeter (ADV) en een Laser In-Situ Scattering and Transmissometry (LISST) gebruikt binnen de lock-exchange-opstelling. Daarnaast werden een Malvern Mastersizer en FlocCAM ingezet om monsters, genomen op verschillende locaties in de opstelling, verder te karakteriseren. De resultaten laten zien dat de respons van sensoren sterk afhankelijk is van het type sediment en dat geen enkel instrument afzonderlijk in staat is om in situ betrouwbaar onderscheid te maken tussen primaire (niet-geflocculeerde) deeltjes en aggregaten. Daarom wordt een combinatie van laboratoriummetingen en in-situ sensortechnieken aanbevolen voor onderzoek naar flocculatie.

Samenvattend biedt dit proefschrift nieuwe experimentele inzichten in de koppeling tussen de aggregatie van deeltjes en de dynamica van troebelheidsstromen. Het laat zien dat flocculatie, interacties met de bodem en beperkingen van sensoren allemaal in beschouwing moeten worden genomen bij het voorspellen van het gedrag van sedimentpluimen. De resultaten dragen bij aan een betrouwbaardere beoordeling en monitoring van milieueffecten die samenhangen met offshore-ingenieursactiviteiten en bieden handvatten voor toekomstige veldmetingen. Daarmee versterkt dit onderzoek de wetenschappelijke basis voor een verantwoorde en duurzame uitvoering van diepzeemijnbouw- en baggeractiviteiten.

1

INTRODUCTION

This chapter presents the fundamental concepts of deep-sea mining, turbidity currents, and flocculation. It provides the foundation for the thesis, along with a literature review, and defines the research questions that have been addressed in this thesis work. This chapter also outlines the structure of the thesis and summarizes the content of the subsequent chapters.

1

1.1. BACKGROUND

1.1.1. DEEP-SEA MINING

With the global population on the rise, it is expected to reach over 9 billion people by 2050 (Drexhage et al., 2017), leading to a surge in energy demand worldwide. To meet this demand, a transition from fossil fuels to clean energy is crucial while aiming for a low-carbon future. With growing demand for renewable energy technologies such as electric vehicles, energy storage systems, solar photovoltaics, and wind turbines, the need for raw minerals has surged, leading to significant environmental concerns and an accelerated rate of extraction.

Recycling and reuse of metals are important for supporting clean energy technologies and are often less energy-intensive than primary production. However, recycling alone is insufficient due to variable recycling rates, technical and economic constraints, limited recyclable stock, and dependence on product end-of-life (Drexhage et al., 2017). As a result, mineral mining will remain essential to meet demand for low-carbon technologies, even under high recycling scenarios (Kirsten Hund et al., 2020, Ojiambo and Adachi, 2023).

At present, the global metal supply relies mainly on terrestrial mining which is a mature industry with significant environmental and socio-economic impacts such as deforestation, toxic waste generation, community displacement, declining ore grades, and resource depletion (Sharma, 2015). Growing mineral demand has therefore driven the search for alternative sources, leading to interest in ecologically sensitive deep-sea environments. Deep-sea mining is an emerging industry aimed at extracting metals such as copper, nickel, and cobalt, materials that are key for electric vehicles and for the transition towards a low-carbon future. It is a rapidly emerging industry focused on extracting marine minerals primarily targeting polymetallic nodules, seafloor massive sulphides, and cobalt-rich crusts distributed across the world's oceans.

Polymetallic nodules are found scattered across the abyssal plains of the oceans, typically at depths ranging from 4000-6000 m. These are potato-shaped nodules measuring around 4-10 cm in diameter, rich in valuable metals such as nickel, copper, manganese, cobalt, and various earth metals (Figure1.1). The nodule deposits are mostly found in the Clarion Clipperton Fracture Zone (CCFZ/CCZ) in the north-central Pacific Ocean, the Penrhyn Basin in the south-central Pacific Ocean, the Peru Basin in the southeast Pacific, and the central part of the northern Indian Ocean (Miller et al., 2018).

The polymetallic nodules contain several valuable metals within the same ore, with the potential to lessen environmental impacts by reducing carbon dioxide emissions and waste generation. The nodules present in the CCZ region contain greater quantities of nickel and cobalt on their own than all known terrestrial reserves of these metals (Hein et al., 2013).

The other type of deposit is Seafloor Massive Sulphides (SMS), which occur near hydrothermal vent systems at depths typically ranging from 1500 to 2000 m (Miller et al., 2018) found in the Indian Ocean, the Bismarck Sea, and the Northeast Pacific Rise (Boschen et al., 2013). These deposits are desirable to mining companies due to their high metal grades and concentrations (Boschen et al., 2013).

The third and the last type of deposit is the Cobalt-rich crusts (CRC) found at depths of 600-7000 m on top of flanks and seamounts. They are distributed across knolls, ridges,

Figure 1.1: A polymetallic nodule (Adapted from J. Lee, 2024)

and plateaus. They include trace metals such as cobalt, nickel, and copper, and rare earth metals such as cerium and lanthanum (Hein and Petersen, 2013). Among the three principal deep-sea mineral resources, polymetallic nodules have emerged as the primary focus of current exploration and technological development. This is mainly because they rest unattached on the seabed, unlike other resources, which need to be extracted from around hydrothermal vents (SMS) and from seamounts (CRC). They are by far the most abundant resources found in the deep sea. The process of retrieving nodules from the Clarion Clipperton Fracture Zone, located at depths of 4000-6000 m, presents major engineering and environmental challenges. Despite the contrasting seabed morphologies across all three deposits, the overall mining system configuration remains broadly similar (Helmons et al., 2022). It generally comprises three main stages: excavation and collection of ore, followed by vertical transport and dewatering (Figure1.2).

Deep-sea nodule mining involves three key components: the Seafloor Mining Tool (SMT), the Vertical Transport System (VTS), and the Production Support Vessel (PSV). The SMT operates on the abyssal plains, collecting nodules using a hydraulic or mechanical collector along with sediment and excess water. Inside the collector, nodules are separated from the slurry, while the excess water and fine sediments are discharged from the rear of the SMT in the form of a sediment plume (Helmons et al., 2022) (Figure1.3). The nodules are then transported through the Vertical Transport System, which typically consists of a riser pipe equipped with pumps or lifts. Upon arrival at the Production Support Vessel, the nodules undergo dewatering, and the return water with sediment and nodules fines are discharged back either in the midwater column or near the bed (Figure1.2).

Deep-sea mining comes with uncertainties regarding its potential consequences. It is therefore crucial to assess at this stage the extent to which deep-sea ecosystems might be impacted by mining activities. The affected areas could potentially extend well beyond the immediate mining sites. A major concern is the formation of sediment plumes generated by the SMT. Gillard et al., 2019 showed that under normal flow conditions, the area of influence extends between 4 and 9 km from the mining location. Under deep-sea conditions, the sediments get disturbed by three primary activities. The first involves the discharge of excess water and sediments collected by the SMT, forming the collector plume, which is the main focus of this study. The second source of disturbance in

1

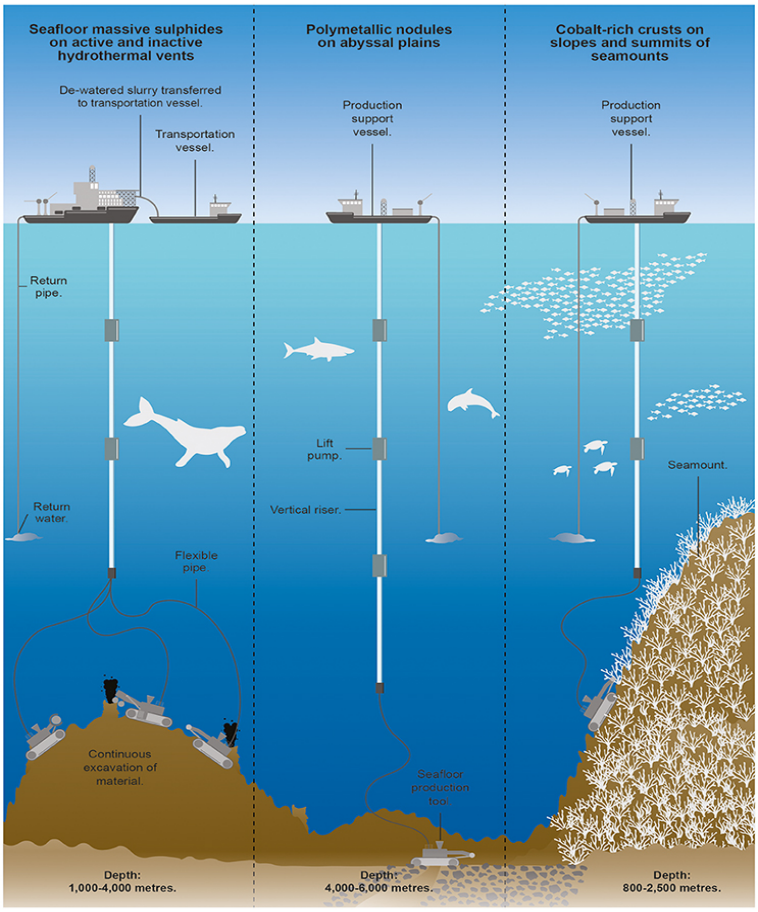

Figure 1.2: A schematic diagram showing the processes involved in deep-sea mining for the three main types of mineral deposits (Miller et al., 2018)

the deep sea arises from the physical movement of the SMT across the seabed, while the third results from sediment spillage occurring around the SMT's inlet.

The spatial extent and environmental significance of these disturbances largely depend on the transport and deposition behavior of the generated sediment plumes. During mining, it is expected that for every 300-400 tons of nodules extracted, a seabed area of the order of 30,000m^2 will be mined per hour, which is equivalent to approximately 200 km^2 per year, yielding 2-3 million tons of ore (Weaver et al., 2022). The discharge of the sediment plume influences the neighboring benthic community. The deep-sea environment may be affected in several ways due to the disturbance of sediments in the area. One of the primary impacts is the direct burial and smothering of benthic organisms as a result of increased sediment deposition (Miller et al., 2018). Suspended particles can also lead to the clogging of the filtering apparatus of filter-feeding organisms, reducing their ability to feed and survive (Global Sea Mineral Resources NV, 2018). Disturbances in the

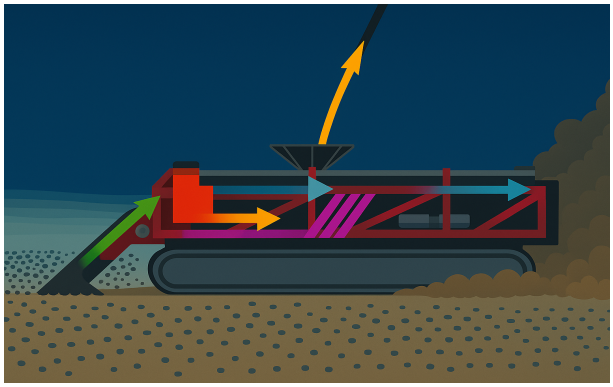

Figure 1.3: A schematic diagram showing the directions of flow of different elements (Adapted from Blue Nodules Summary- Deep Sea Mining, 2020)

environment can also result in modifications to nutrient dispersal patterns, potentially affecting biological productivity (Global Sea Mineral Resources NV, 2018). It may also inhibit recolonization processes by disrupting larval dispersal, increasing their mortality, and reducing the success of larval settlement (Gollner et al., 2017). These potential impacts highlight the need for a detailed understanding of sediment plume dynamics to reliably assess and mitigate the environmental consequences of deep-sea mining. The environmental implications of sediment plumes are not limited to deep-sea mining but are equally relevant to near-shore activities such as dredging.

1.1.2. DREDGING

In recent years, the growing global economic and societal demands have made dredging essential for maintaining the effective functioning of coastal zones (CEDA, 2011, P. L. A. Erftemeijer et al., 2012, Victor et al., 2018). During dredging activities, spilled sediment can result in excess turbidity and sedimentation in the surrounding area. Increased turbidity can lead to a negative environmental impact as it reduces light penetration and visibility. It can also clog the filter-feeder organisms and smother benthos. Along with sediments, there is also a possibility that contaminants get dispersed in a dredging plume (de Wit, 2015). Various studies have proved the environmental impacts of dredging, with most of them being the increased turbidity levels and sedimentation (Varriale et al., 1985, M. Nichols et al., 1990, Gilkinson et al., 2003, P. L. Erftemeijer and Lewis III, 2006, P. L. Erftemeijer et al., 2012, Mestres et al., 2014). The environmental impact of a dredging project depends largely on the frequency at which it is conducted, its duration, the intensity of stressors such as turbidity and sedimentation generated during the operation, along with the resilience of the affected ecosystem (P. L. Erftemeijer and Lewis III, 2006, P. L. Erftemeijer et al., 2012). Some ecosystems are resilient enough to cope with sudden changes in turbidity levels and are thereby better able to tolerate such events (de Wit, 2015).

Dredging is a process that is undertaken worldwide, at all scales, to keep the proper functioning of waterways, harbors, and ports. A common type of dredger is the Trailing

Suction Hopper Dredger (TSHD), in which dispersion of sediment plume takes place. The overflow plume flows through the overflow pipe in the TSHD and is the primary source of suspended sediments (Bray, 2008). In order to better understand and predict these impacts, it is essential to understand the fundamental processes that control turbidity currents.

1.2. TURBIDITY CURRENTS

Turbidity currents are a subclass of gravity currents. They are particle-laden gravity-driven underflows where the particles remain suspended due to fluid turbulence. The transport mainly takes place due to the difference in densities between the turbidity current and the ambient (surrounding) fluid. The generation of turbidity currents is an inevitable outcome of most water-related activities. Turbidity can originate in any aquatic environment due to natural processes, such as sediment-laden flows propagating downslope under the influence of gravity (Wells and Dorrell, 2021). They can also arise due to human interventions, such as dredging, deep-sea mining, trawling, land reclamation, and offshore construction. Turbidity currents also play a crucial role in transporting sediments, nutrients, and pollutants from the continental margin to the world's oceans (Wells and Dorrell, 2021). They propagate through reservoirs, lakes, and oceans due to their higher density than the surrounding fluid. When the flow is denser than the surrounding fluid, it becomes negatively buoyant and sinks, whereas the lighter flows are positively buoyant and rise. Turbidity currents are dilute flows with concentrations less than 10 kg/m^3. They are fully turbulent with a Reynolds number greater than 10000 and contain poorly sorted sediments (Parsons et al., 2007). A turbidity current has three main parts, namely the head, body, and tail (Figure 1.4). The head of the turbidity current exhibits distinctive properties when compared to its body and tail. The head has significantly different mass and momentum from its body and tail (Sequeiros et al., 2018). It has the highest concentration. While propagating, it displaces the ambient fluid, and this causes frictional resistance. At the back of the head, vortices known as Kelvin-Helmholtz billows are formed due to the effect of velocity shear and turbulence in the ambient fluid. This area is known as the body of the turbidity current. As the turbidity current head progresses, the materials towards the end of the current start to deposit, and is known as the tail area (Figure 1.4). These internal flow structures ultimately determine how much material remains in suspension and is transported beyond the area.

The suspended sediment concentration in the area increases, and it propagates as a plume. The area close to any anthropogenic activity (such as deep-sea mining or dredging) is considered the near field zone (up to a few hundred meters). Here, local turbulence, density difference, the sediment release method, and the maneuvering of the equipment influence the sediment plume spread. On the other hand, the far-field zone extends up to tens of kilometers in the sea, river, or estuarine environment surrounding any activity. The effects from the above-mentioned factors no longer influence this zone. The plume behavior in the far field zone is governed by the ambient currents, waves, and settling behavior of sediments in the plume (de Wit et al., 2025). At this stage, the plume is known as the turbidity current (Elerian et al., 2021). Over the past decade, deep-sea mining has emerged as a promising method for extracting met-

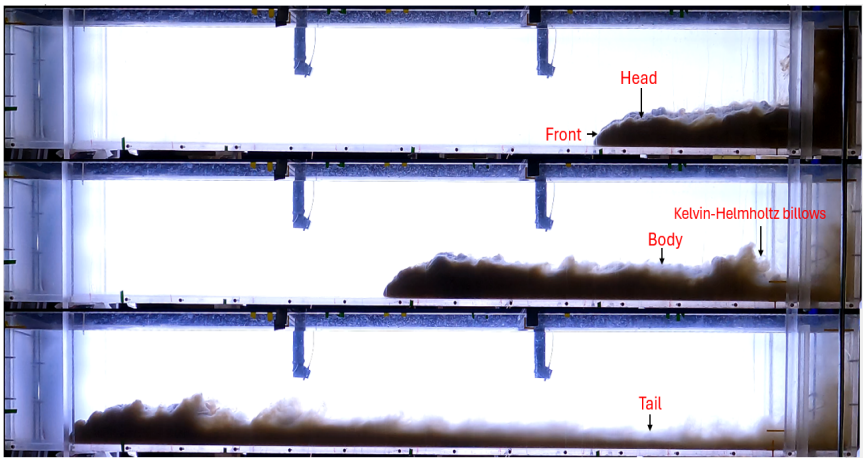

Figure 1.4: Different parts of a turbidity current (head, body, and tail)

als from the ocean floor. During the mining process, there is a generation of turbidity plumes around the Sea-floor Mining Tool (SMT), which propagate as turbidity currents. While hydrodynamic processes govern the large-scale transport of sediment plumes, the behavior of individual particles within the plume is equally important. Interactions between suspended particles can lead to aggregation through the process of flocculation. It can significantly modify particle settling velocities and, consequently, the overall spread of turbidity plumes. Enhanced settling of flocculated particles reduces the amount of sediment remaining in suspension, thereby decreasing both the excess density and the momentum that drive the turbidity current. As a result, plume propagation and spreading are expected to be reduced, potentially limiting the spatial extent of environmental impacts.

1.3. FLOCCULATION

Various lab and in situ studies have observed that flocculation does play a role in reducing the spread of turbidity plumes generated due to deep-sea mining (Gillard et al., 2019, Spearman et al., 2019, Spearman et al., 2020, Muñoz-Royo et al., 2022, Gazis et al., 2025, Li et al., 2026). Most natural sediments contain organic matter, which has the propensity to form flocs. Due to ambient flow conditions, particles in suspension containing organic matter collide and adhere to one another, forming larger particles known as flocs. The rate at which flocs grow or disintegrate depends on several factors, including hydrodynamic shear, residence time, particle size, sediment mineralogy, pH, and salinity (Kiørboe, 2001, Mietta, 2010, Deng et al., 2019, Safar et al., 2019, Chassagne, 2021). Turbulence and gravity both act on flocs, where turbulence drives aggregation, breakup, and erosion, whereas gravity leads to particle settling (Mietta, 2010). The resulting floc characteristics, such as structure, strength, and settling velocity, depend strongly on these interactions. The shape and morphology of flocs can vary widely depending on shear conditions. According to Eisma, 1986, flocs tend to be compact and spherical under

high shear rates, while at lower shear rates, their structure is influenced by the ambient conditions. In the marine environment, both elongated, chain-like and spherical aggregates were observed (Manning, 2001). With an increase in organic matter content, flocs become more irregular, although they are assumed to be spherical in most modeling and laboratory works (Mietta, 2010).

Floc strength governs the resistance to breakup and it depends on floc composition and the type of bonds. Aggregation is controlled by particle surface properties, such as surface charge and ζ potential. Flocs are subjected to gravitational, buoyancy, drag, and turbulent forces, including wake effects during differential settling. While hydrodynamic processes (shear, differential settling, Brownian motion) promote particle collisions, cohesion is provided by biological polymers that enhance stickiness and stability. Denser flocs settle faster, accelerating plume deposition, making flocculation a key process in turbidity plume re-settlement (Eisma, 1986).

1.3.1. FLOCCULATION IN TURBID FLOWS

Flocculation is regulated by a dynamic balance between aggregation and breakup of flocs. It leads to particle aggregation, which increases the settling velocity and promotes faster sediment deposition. This, in turn, could reduce the spread of plumes and lower turbidity levels in both near-field and far-field regions, potentially minimizing environmental impacts. Smith and Friedrichs, 2011 investigated the impact of flocculation on dredging plumes and reported a gradual increase in both settling velocity and floc size over time. They also noticed that higher suspended sediment concentrations were favorable for the formation of larger flocs. Similar studies related to deep-sea mining operations conducted by Gillard et al., 2019, Spearman et al., 2019, Spearman et al., 2020, and Gazis et al., 2025 showed that sediment aggregation can increase the settling potential of suspended materials generated during a deep-sea mining activity. The critical elements that influence flocculation in clayey suspension are organic matter, salinity, and hydrodynamic conditions (Deng, 2022, Ho et al., 2022, Safar et al., 2023). These parameters have proven to play a role in flocculation in the case of deep-sea mining sediments (Gillard et al., 2019, Helmons et al., 2022). Thus, flocculation in turbidity plumes can be viewed as a potential natural mitigation mechanism that limits plume dispersion by promoting the formation of larger particles that settle more rapidly.

Laboratory-scale experiments have further demonstrated the occurrence and significance of flocculation. A preliminary study conducted by Ali et al., 2022a confirmed the formation of flocs under controlled hydrodynamic conditions during the turbidity current propagation.

1.4. SCOPE

The sediments, after being released from a Seafloor Mining Tool or a dredging vessel, travel in the form of a turbidity current. In this thesis, the behavior of such a turbidity current is experimentally investigated, with a focus on the role of flocculation in turbidity current dynamics. Since various factors come into play in in situ measurements, laboratory experiments were designed to replicate and analyze those factors. Flocculation is expected to occur while the turbidity current is propagating, potentially leading

to an earlier settlement of the plume.

As it is very challenging to study the processes involved in a turbidity current propagation in situ, laboratory lock-exchange experiments were conducted. A previous study of Ali et al., 2022a has shown the propagation of flocculated sediments in such an environment. In that case, the flocculated material was in the mixing compartment of the lock-exchange, and its propagation was compared with the propagation of unflocculated material. However, in the marine environment, organic matter is present throughout the water column. When it interacts with suspended sediments within the turbidity current, flocculation will occur, but the influence of flocculation on the current propagation remains an open research question. In addition to examining the role of organic matter in the water column, this study also investigates how a previously disturbed bed and its age (stage of consolidation) influence the propagation of turbidity currents. In situ seabeds vary widely in composition, and it is important to understand how these differences affect turbidity current and flocculation processes, as some beds contain flocculated and unflocculated materials on their surface. Three types of bed conditions were tested to determine which one would have the greatest impact on turbidity current propagation. The role of bed-induced roughness due to the presence of materials on its surface on the front velocity and aggregation process is studied here. Although the findings are relevant to any dredging operations, the focus of the study is on deep-sea mining, and therefore, sediments from a deep-sea mining location were used. The result of this study will enable us to decide whether deep-sea mining operations should be conducted shortly after the material has settled or after a longer period when the bed has consolidated.

The ability to quantify plume properties (concentration, particle size in time and space) has been studied using a large range of measurement techniques. The performance of the optical and acoustic sensors used for monitoring suspended sediments is discussed. In particular, the research aims to establish concentration thresholds for reliable sensor readings and validate accurate interpretation of sediment monitoring data across varying sediment types. Understanding whether optical or acoustic sensors provide more robust and reliable performance for monitoring sediment-laden flows is critical for the effective monitoring of dredging and (deep-sea mining-induced) plumes.

1.5. RESEARCH QUESTIONS

The behavior of turbidity currents as they interact with organic matter suspended in the water column and with a bed over which they propagate is studied here. The main hypothesis is that flocculation, which is promoted by the presence of organic matter and bed interactions, plays a significant role in reducing the turbidity current front velocity. The work presented in this thesis is structured around four key research questions, which are:

1. How does the presence of organic matter in the water column influence flocculation and the propagation of turbidity currents?

2. How does the presence of a bed and its age influence flocculation dynamics and propagation behavior of the turbidity current?

3. What is the role of bed composition on flocculation dynamics and the propagation

behavior of turbidity currents?

4. How effectively can different sensing methods provide quantitative parameters regarding plume properties (concentration and particle size)?

1.6. THESIS OUTLINE

This section outlines the structure of the thesis. Chapter 2 presents the experimental methods and equipment employed in this study, including basic working principles of the instruments used. It also details the experimental setup and procedures followed to prepare and carry out the experiments.

Chapter 3 investigates the role of organic matter present in the water column on flocculation and turbidity current propagation. Using controlled laboratory experiments, the chapter examines floc formation, particle size evolution, and settling behavior under different types and dosages of organic matter and evaluates their influence on flow dynamics.

Chapter 4 examines the influence of bed and its age on flocculation and turbidity current dynamics. Through lock-exchange experiments with pre-existing beds constructed with CCZ sediments, the chapter investigates the role of beds in affecting flow propagation, sediment resuspension, and floc evolution.

Chapter 5 investigates the influence of bed composition on turbidity current propagation and flocculation behavior. Using controlled lock-exchange experiments over different bed types, the chapter analyzes how variations in bed types affect flow dynamics, sediment resuspension, entrainment, and floc characteristics.

Chapter 6 evaluates the performance of optical and acoustic sensing methods for monitoring turbidity and flocculation under controlled laboratory conditions. By comparing sensor responses across different sediment types and concentrations, the chapter assesses sensor sensitivity, calibration behavior, saturation limits, and the ability of a multi-sensor array to distinguish between primary particles and aggregated flocs during turbidity current propagation.

Chapter 7 presents the main findings of the thesis and addresses the research questions by integrating results from Chapters 3, 4, 5, and 6. It shows the implications of flocculation, bed effects, and sensor performance in identifying flocculation in a turbidity current. It also states the recommendations for future research and monitoring strategies.

The schematic outline of this thesis is presented in Figure 1.5.

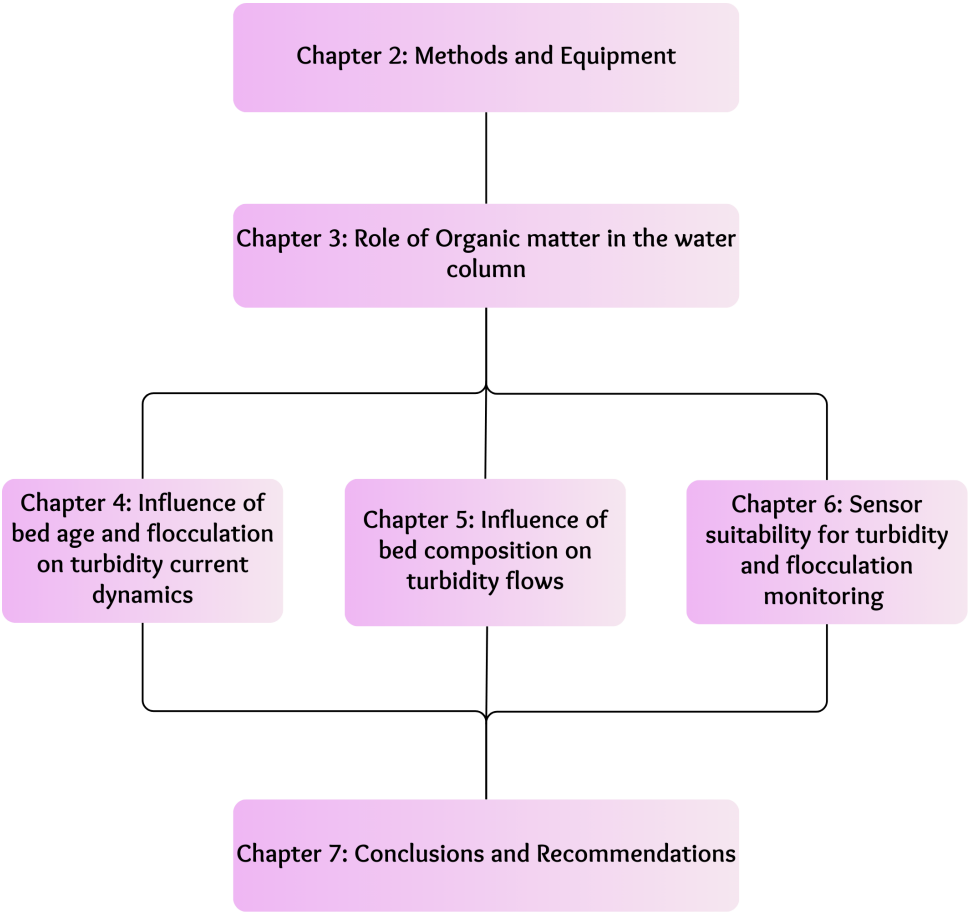

Figure 1.5: Thesis Outline

2

METHODS AND EQUIPMENT

This chapter presents a comprehensive overview of the experimental framework used in the study. It outlines the configurations of the experimental setup, measurement equipment, and the materials used in all the experiments. Experiment-specific protocols and setup configurations are described in the corresponding chapters. Furthermore, the functionality and operating principles of the instruments, such as the Optical Backscatter Sensor (OBS), Acoustic Doppler Velocimeter (ADV), Laser In-Situ Scattering and Transmissometry (LISST), and the Ultrasonic Velocity Profiler (UVP), are introduced.

2.1. LOCK EXCHANGE SETUP

Turbidity currents have been widely studied in laboratory settings using lock-exchange flumes (Nogueira et al., 2013b, Baker et al., 2017a, Craig et al., 2020, Serra et al., 2025). It consists of a lock or gate that separates sediment suspensions from the ambient fluid. Once opened, the gate releases the sediment suspension, which propagates into the outflow compartment of the flume. The experiments conducted in this thesis were also carried out in such a flume. The flume is 3 m long, 0.4 m high, and 0.2 m wide. The mixing section or the lock section is 0.2 m long. Figure 2.1 (a) shows a schematic diagram of the lock exchange flume along with an image of the actual setup (Figure 2.1 (b)). The lock exchange flume has been equipped with siphons (S) and bottom outlets (BO) to collect sediment samples from the turbidity current. An overhead stirrer was also used in the mixing section to form a homogeneous suspension. Four different concentrations were tested: 10, 5, 2.5, and 0.5g/L.

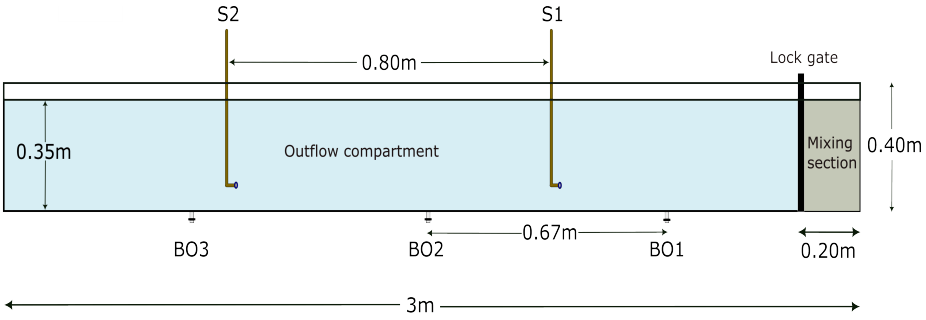

(a) Schematic diagram of the lock exchange flume

(b) Lock exchange flume during propagation of turbidity current

Figure 2.1: Experimental setup for lock exchange turbidity current experiments

2.2. EQUIPMENT

2.2.1. FLOCCAM

The flocs were analyzed using an in-house device known as the FlocCAM (Figure 2.2 (a)). It can measure floc size and settling velocities of flocs greater than 20 μm (Manning et al., 2007, Ye et al., 2020, Shakeel et al., 2021). It consists of a settling column of dimension 10 cm x 10 cm x 30 cm, and a 5MP CMOS camera with a 2592 x 2048 pixels resolution, and a Global Shutter was used to capture flocs in high-resolution images. The sampled flocs were gently transferred into the settling column using a pipette. Videos were recorded at

24 fps during floc settling and analyzed with the Safas software package, which gives the floc sizes and settling velocities (M.Ryan MacIver, 2019). Figure 2.2(b) shows the flocs recorded during their settling through the settling column.

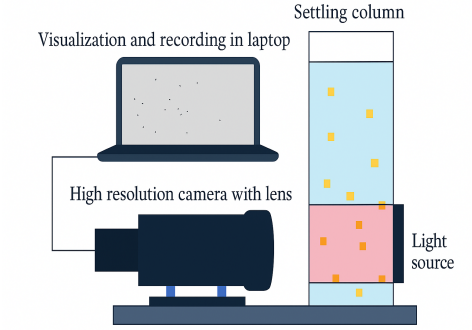

(a) Schematic diagram of FlocCAM (adapted from Ali et al., 2022a

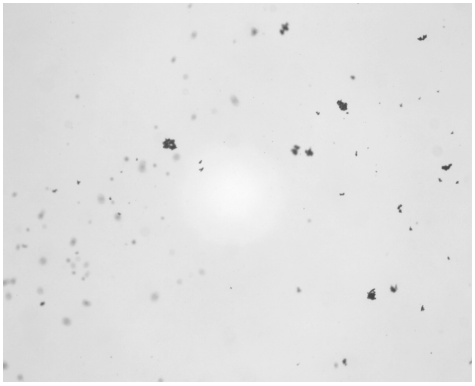

(b) Snapshot from flocCAM video

Figure 2.2: FlocCAM setup and snapshot from FlocCAM video

2.2.2. JAR TEST APPARATUS

The jar test apparatus was used to promote floc growth under a controlled shear rate of $50s^{-1}$. Flocs were formed in cylindrical jars with a diameter of 9.5 cm and a height of 11 cm. The jar test apparatus, JLT6, VELP Scientifica, used in these experiments, consisted of mixing units, beneath which the jars were placed (Figure 2.3). Each jar was continuously stirred by a rectangular paddle positioned 1 cm above the base. The system was coupled to a particle size analyser (Malvern mastersizer) for real-time monitoring of floc evolution with the help of a peristaltic pump (Figure 2.4). The pump continuously recirculated flocs from the jar to the Malvern mastersizer.

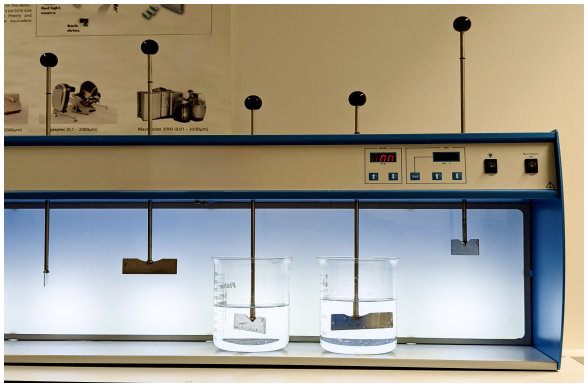

Figure 2.3: Jar test apparatus.

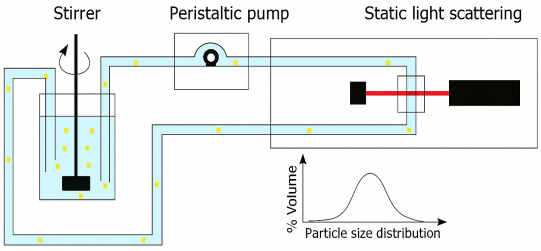

Figure 2.4: Schematic diagram of mixing jar coupled with a particle size analyzer (Adapted from Ali et al., 2022a)

2.2.3. MALVERN MASTERSIZER

The Malvern mastersizer is a laser diffraction-based particle size analyzer developed by Malvern Panalytical. It measures the particle size distribution ranging from 10 nm to 3.5 mm. The instrument consists of an optical unit, a dispersion unit, and a measurement cell. It uses red and blue laser beams that pass through the sample, where the particles scatter the light at various angles. The detector array then captures the scattering pattern, which depends on the particle size and refractive index of the material. The Malvern mastersizer software uses Mie theory to convert scattering data into particle size distributions (Malvern Panalytical, 2024).

In the experiments, the Malvern mastersizer was used to analyze the particle size of sediment samples. The flocs were carefully pumped from the jar test apparatus to the Malvern mastersizer and then back to the jar test apparatus with the help of a peristaltic pump (Figure 2.4). The tubes were 4 mm in diameter. The jar test apparatus was only used in the experiments stated in Chapter 3. In the rest of the experiments, a jar was used, placed on top of a magnetic stirrer to keep the flocs in suspension, and pumped using the peristaltic pump. Both Malvern mastersizer 2000 and 3000 versions were used in experiments throughout this thesis.

2.2.4. ULTRASONIC VELOCITY PROFILER (UVP)

The UVP is an ultrasound-based instrument that measures instantaneous velocity profiles in liquid flows (Figure 2.5). It uses Doppler shift frequency of the echoed ultrasound as a function of time. In this study, a Metflow UVP Duo device was used. A 4 MHz transducer (based on the primary particle size of the sediments, ranging between 5-26 μm) was used to measure the velocity profiles of particles inside the turbidity current. It was mounted at an angle of 20 degrees relative to the vertical and oriented in the flow direction to record 1-D particle velocities along the flow direction (Met-Flow SA, 2024).

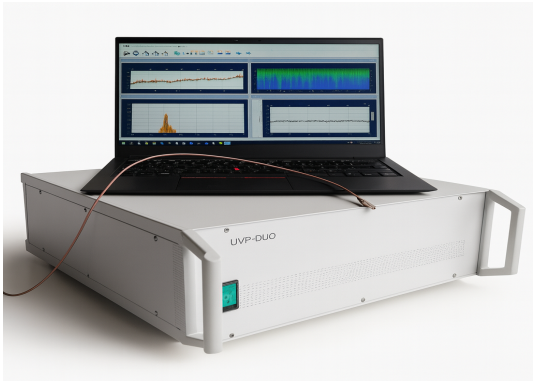

Figure 2.5: Ultrasonic Velocity Profiler (Adapted from Dantec Dynamics A/S & Met-Flow SA, 2025).

2.2.5. OPTICAL BACKSCATTER SENSOR (OBS)

Optical Backscatter Sensors (OBS) are commonly used for turbidity measurements (Figure 2.6). In this study, logger-type deep-sea OBS units (ATUD-OBS, JFE Advantech) were employed. These sensors are specifically designed for long-term turbidity monitoring in deep-sea environments and are equipped with large-capacity SD card storage and commercially available batteries. Although these sensors were originally developed for field applications, deep-sea OBS units were used in the experiments to evaluate their performance under controlled laboratory conditions. This allows an analysis of sensor sensitivity, noise characteristics, and saturation behavior across known sediment concentrations and flocculation states, which is difficult to achieve in natural environments.

These sensors can be used in a variety of applications, including vertical observations when mounted on a deep-sea CTD, monitoring marine snow with sediment traps, measuring turbidity during seabed drilling, and observing hydrothermal deposits (JFE Advantech Co., Ltd., 2025). Here, the OBSs were used to quantify turbidity within turbidity currents in FTU.

Figure 2.6: Optical Backscatter Sensor (Adapted from JFE Advantech Co., Ltd., 2025)

2.2.6. LASER IN-SITU SCATTERING AND TRANSMISSOMETRY (LISST)

The LISST is a laser diffraction instrument used to measure particle size distributions (1-500 μm) in water (Figure 2.7). It works by transmitting a laser beam through the sample, where the suspended particles scatter light at different angles. The scattered light is collected on a 36-ring silicon photodetector array, with each ring representing a specific scattering angle. The resulting angular scattering pattern is then mathematically inverted using the Mie theory or an irregular particle model to obtain the particle size distributions. The LISST instrument can operate autonomously with external battery packs or in real-time via CTD integration, applicable to both field and laboratory use. The LISST used here is from Sequoia and is commercially known as the LISST 200X (Sequoia Scientific, Inc., 2018).

Figure 2.7: Laser In-Situ Scattering and Transmissometry (Adapted from Sequoia Scientific, Inc., 2016).

2.2.7. ACOUSTIC DOPPLER VELOCIMETER (ADV)

An ADV is a device that uses the Doppler shift to primarily measure three-dimensional flow velocity. It consists of four receiver probes and a central transmitter (Figure 2.8) (Nortek AS, 2018). In addition to velocity, the ADV records acoustic signal strength as signal-to-noise ratio (SNR), which depends on the concentration of sediments in the water. Although it is not designed for concentration measurements, it can also be used to compute concentrations after after calibration against known values.

2.3. MATERIALS: SEDIMENTS

The sediments used in the experiments were illite, sediments from the Clarion Clipperton Fracture Zone (referred to as CCZ sediments), and quartz. For the experiments carried out in this thesis, four different concentrations were used throughout: 0.5g/L, 2.5g/L, 5g/L, and 10g/L.

For the lock-exchange experiments in Chapters 4, 5, and 6, the 0.5 g/L concentration was excluded due to practical limitations. At such low concentrations, particularly in the presence of a pre-existing bed, the turbidity currents propagated very slowly and

Figure 2.8: Acoustic Doppler Velocimeter (Adapted from Nortek AS, 2018).

often ceased before meaningful measurements could be obtained. The selected concentrations were chosen based on material availability, the operational measurement range of the sensors, and concentration levels considered representative of deep-sea mining sediment plumes.

2.3.1. ILLITE

Some experiments were carried out with illite as it is readily available and has stable properties, such as particle size, which helps ensure repeatability and comparability between experimental runs. This material has also been used in the previous work of Ali et al., 2022a. It is also the primary mineral component in the Clarion Clipperton Zone sediment, making 39-54 % of the uppermost layer (International Seabed Authority (ISA), 2010, Helmons et al., 2022). The illite used here is "Granulated green clay for poultice and plaster" purchased from Agriletz Laboratories. It has a d_{50} of 6.4 μm when measured using static light scattering technique in Malvern mastersizer 2000 (Wahab et al., 2024). It has a density of 2750 kg/m^3.

2.3.2. QUARTZ

Quartz flour, commercially known as M10 (Sibelco), was used to construct a bed on the flume bottom that was non-flocculating. The flour has a d_{50} of 23 μm and a density of 2650 kg/m^3. The particle size distribution is shown in Figure 2.10. The material is milled, resulting in highly angular, broken grains.

2.3.3. CCZ

The clay used here was from the Clarion-Clipperton Fracture Zone in the Pacific Ocean, specifically from the NORI-D license area. The density of the material was found to be 1166 kg/m^3. The d_{50} obtained from Malvern mastersizer 3000 was found to be 26.3 μm. The particle size distribution shown in Figure 2.11 shows a bimodal distribution, with a large number of particles in the range of 4-5 μm, with the peak at 80-90 μm. The

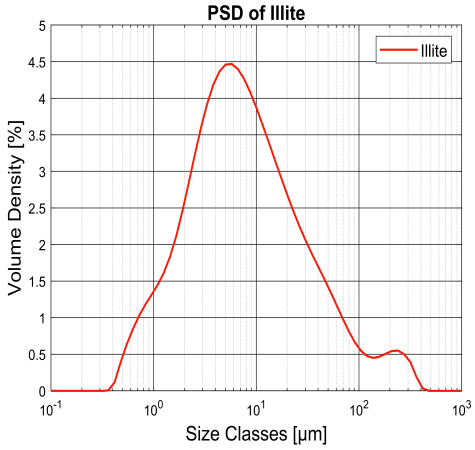

Figure 2.9: Particle Size Distribution of Illite measured using Malvern mastersizer 2000

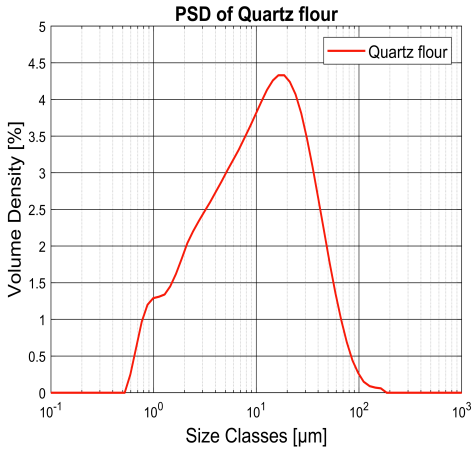

Figure 2.10: Particle Size Distribution of Quartz clay (Sibelco M10) measured using Malvern mastersizer 3000)

clay was obtained from the top 30 cm of the bed, collected with box cores. However, it is worth mentioning that the top few centimeters of the bed were unavailable for this study. The loss of the topmost layer also resulted in the loss of the highest concentration of organic matter, with the subsequent layers having a comparatively lower amount of organic matter. The water depth at which the sediment was sampled was approximately 4000 m. It was then stored in a 150 L barrel under wet, dark, and room temperature conditions.

All the particle size distributions shown in Figures 2.9, 2.10, and 2.11 are the average of 10 measurements, carried out using dried materials, except for CCZ, which was in wet form, dispersed in fresh water.

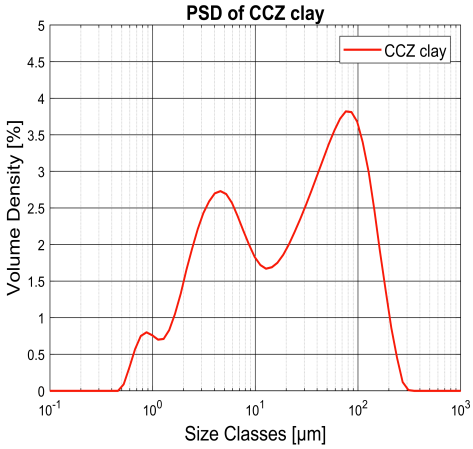

Figure 2.11: Particle Size Distribution of CCZ sediment measured using Malvern mastersizer 3000

2.4. MATERIALS: WATER

2.4.1. SALTWATER

The experiments were conducted in saltwater, which was used to simulate deep-sea conditions. Additionally, the study by Ali et al., 2022a demonstrated that saltwater enhances the flocculation behavior of clay. The salt used here was sodium chloride (NaCl) purchased from Boom Laboratories. The electrical conductivity of the saltwater was kept at 34.7mS/cm, similar to that of seawater.

2.5. FLOCCULANTS

2.5.1. ZETAG

Sediments in general contain organic matter which is present everywhere in the water column. However, the material used here (illite) is devoid of any organic matter and, therefore, does not form flocs on its own. In order to study the nature and behavior of flocs that were formed inside the body of the turbidity current during its propagation, as studied in Chapter 3 (Wahab et al., 2024) and Chapter 5 (Wahab et al., 2025) , it was crucial to add a flocculant that would form flocs within the time scale of lock exchange experiments (here, 30s-4 mins). Two types of flocculants were used in Chapter 3, anionic and cationic, used one at a time. In Chapter 5, only anionic flocculant (Zetag 4120) was used. The anionic flocculant is a polymer referred to as Zetag 4120 (BASF). It has a medium charge and high molecular weight. The other flocculant used is Zetag 7587 (BASF), which is a cationic polymer. It has a high charge and medium molecular weight. These flocculants are in the form of dry powder and are mixed with water to form a stock solution. Polyacrylamide-based polyelectrolytes such as the ones from the Zetag line are comparable to Exopolysaccharides (EPS), which are high-molecular weight carbohydrate polymers produced by marine bacteria or microalgae (C. M. Nichols et al., 2005, Deng et al., 2019). These EPS are the building materials for microbial aggregates like

biofilms and flocs (Flemming and Wingender, 2001).

A flocculant dosage of 2.5mg/g of clay was used in all the experiments, as this was sufficient to promote rapid floc formation within the short duration of the lock exchange experiments. This ensured consistent aggregation conditions across experimental runs and minimized variability associated with incomplete or delayed flocculation.

2.5.2. STANDARD PROTOCOL

The protocol followed across all the lock-exchange experiments is discussed here. The subsequent steps, which vary depending on the experiments, are described in each chapter specifically.

1. The salt water was prepared, and the salinity was adjusted to 34.7 mS/cm
2. The flume was cleaned and gradually filled with saltwater, except for experiments where a bed was needed to be constructed.
3. The lock gate was positioned at its designated place.
4. The sediment was then added to the mixing container (pre-filled with water) and mixed for approximately 20 minutes, to ensure a homogeneous suspension.

Various other equipment and experimental conditions were used. Table 2.1 shows the equipment used in Chapters 3, 4, 5, and 6.

Table 2.1: Equipment used in each chapter

Chapter/Equipment	Mastersizer	FlocCAM	UVP	OBS	LISST	ADV
3	✓	✓				
4	✓	✓	✓			
5	✓	✓	✓			
6	✓	✓	✓	✓	✓	✓

3

ROLE OF ORGANIC MATTER PRESENT IN THE WATER COLUMN

This chapter presents a detailed study on the role of organic matter on turbidity current propagation relevant to dredging and deep-sea mining. Here, synthetic (anionic or cationic) organic matter or flocculant was added to the water column. Even though the added flocculant produced negligible changes in the water density, the turbidity currents propagated with higher front velocities when flocculant was present. The study demonstrated that flocs formed within the short propagation time of 30-60s, and produce larger flocs at higher dosages. Moreover, the flocs sampled from the body of the flow were larger and more open than those sampled near the bed when flocculant dosage was higher. These observations highlight the significance of sediment-flocculant interactions on turbidity current propagation, offering new insight into the role of organic matter in turbidity current dynamics.

This chapter has been published in Journal of Marine Science and Engineering, **Wahab et al., 2024**

3.1. INTRODUCTION

The spreading of sediment plumes and the generation of turbidity currents are a consequence of human interventions, such as dredging or (deep-) sea mining. Dredging is a crucial activity for the construction and maintenance of ports and waterways, land reclamation, and flood and storm protection, to name a few (CEDA, 2011, P. L. A. Erftemeijer et al., 2012, Victor et al., 2018). Dredging is also carried out to excavate contaminated sediments, thereby improving water quality and aquatic ecosystems (Bruun et al., 2005). With the global population on the rise, deep-sea mining has appeared in recent years as an alternative source for rare metals. A significant amount of these high-grade metals are present in potato-shaped deposits known as polymetallic nodules at a depth of 4000–6000 m in the Pacific Ocean in an area known as the Clarion Clipperton Fracture Zone (CCFZ/CCZ).

During the process of extracting polymetallic nodules, the dispersion of sediment plumes behind the Sea-floor Mining Tool (SMT) is one of the main concerns that the deep-sea mining industry has to deal with. The excess water along with sediment that is discharged from the SMT travels through different regimes during the course of its release, as it propagates and eventually settles (Elerian et al., 2021).

For any of these dredging or mining activities, the creation of turbidity plumes is an inevitable part. It leads to an increase in suspended solids concentration, which can further propagate. The spread of a turbidity plume depends on the settling velocities of the suspended material, the technology and operation control used for dredging or excavating, and the ambient water characteristics. Sediment plumes can be quite localized, having a minimal direct impact on marine mammals living in a marine environment (Todd et al., 2014). However, in certain types of activity, such as deep-sea mining, sediment plume dispersion modeling results showed that the area of influence ranged from 4 to 9 km under normal flow conditions and when an eddy had passed through the study site (Gillard et al., 2019). The discharge of the sediment plume has a direct influence on the habitat. It can lead to limited light penetration, smothered organisms, reduced visibility and food, and also to a disruption in reproduction patterns. Turbidity currents have a potential impact on the local ecosystem, but the effect is species- and location-specific (Todd et al., 2014). In the case of an environment such as the deep sea, any change in the environment could be significantly large (Gausepohl et al., 2020). Limiting the spread of turbidity flows is, therefore, a key objective of deep-sea mining activities.

Creation of turbidity currents in deep-sea mining activities

Turbidity currents are a subclass of gravity currents. Their transport mainly takes place due to the difference in density between the turbidity current and the ambient fluid. According to Elerian et al., 2021 and van Grunsven et al., 2018 the horizontal discharge of sediments can typically be divided into several stages for a near-field scenario. After being discharged from the SMT itself, the flow behaves as a turbulent jet (Elerian et al., 2021, van Grunsven et al., 2018). The jet then loses its momentum and the entrainment of ambient fluid takes place. The jet is mainly driven by the density difference and is defined as a plume (van Grunsven et al., 2018). The density difference causes the plume to sink. At the impingement area, there is the possibility of sea-bed erosion and deposition (Elerian et al., 2021). The last stage is the turbidity current stage, where the flow

propagates as a turbidity current, moving along the seabed, away from the SMT's path (Elerian et al., 2021).

The deep-sea sediments found at the top of the sea floor consist of mineral particles and organic matter. When this material is resuspended, it has been found that there is an occurrence of flocculation (Gillard et al., 2019, Spearman et al., 2020). Flocculation is the process where organic materials, under various hydrodynamic conditions, bind the sediment particles together, leading to the formation of larger particles, known as flocs. According to Spearman et al., 2020, it has been seen that the formation of flocs lead to an early settlement of plume, thus reducing its spread. The process of flocculation has been widely studied in various environments such as in rivers and estuaries (Eisma, 1986), where organic matter is the main driver for flocculation, and also in the field of sanitary engineering (Droppo and Ongley, 1994), where synthetic flocculants (usually polyacrylamide-based polyelectrolytes) are used. The mechanisms and the controlling factors involved in these environments are generally well known (Droppo and Ongley, 1994). However, studies on flocculation in turbidity flows in open water are limited. A model with calibrated flocculation parameters using the existing experimental work of Gillard et al., 2019 was set up that included flocculation. Although the effect of flocculation is already clearly present in the near field, its effect on the propagation of the turbidity current is likely to take place in the far field (Elerian et al., 2023a).

To study the importance of the different variables in the system (clay and organic matter concentration in particular) on the propagation of the turbidity flows, laboratory-scale experiments in the form of lock-exchange experiments are usually performed (Nogueira et al., 2013a, Baker et al., 2017b, Craig et al., 2019).

The propagation of flocculated sediment/synthetic organic matter (polyacrylamide flocculant) slurries in lock-exchange experiments by Ali et al., 2022a and Ali et al., 2022b enabled to study the changes occurring in floc size and structure during turbidity current propagation. It was in particular found that additional flocculation takes place during the turbidity current propagation. In the marine environment, organic matter is found everywhere in the water column. One unanswered research question, targeted in the present chapter, is whether the presence of this organic matter (unbounded to clay) in the flow compartment of a lock-exchange will or will not affect the turbidity current propagation. To mimic the action of organic matter two synthetic flocculants (polyacrylamide-based) were used (Shakeel et al., 2020), as they are well-characterized polyelectrolytes that are representative of the action of polysaccharides (polysaccharides are produced by microorganisms in situ and constitute a large class of natural flocculant).

3.2. METHODS

The jar test experiments were carried out using a sediment concentration of 0.5 g/L. The protocol that was adopted for these experiments is as follows. Details of the set-ups are found in Chapter 2.

1. Two samples (one for Malvern analysis and the other for FlocCAM analysis) of the chosen concentration (0.5 g/L) of illite and saltwater were prepared using a volumetric flask.

2. Each of the illite saltwater suspensions was then mixed separately at 800 rpm using an overhead stirrer for 5 min in order to ensure a homogeneous suspension.

3. A stock solution of Zetag 4120 with water was prepared. Four different dosages of Zetag 4120 (milligram per gram of dry mass of clay) (0.35 mg/g, 0.25 mg/g, 0.2 mg/g, and 0.1 mg/g of clay) were chosen for the jar tests.

4. The samples (illite and a chosen dosage of Zetag 4120) were then mixed for 30 s at 75 rpm (which corresponds to a 50/s shear rate) using the JLT6 jar test apparatus setup.

5. One sample was immediately measured in FlocCAM and videos were recorded.

6. For the other sample, a clean jar with saltwater was placed under the JLT6 jar test apparatus and constantly mixed at 75 rpm. The flocs were then scooped from the illite-saltwater suspension containing Zetag 4120 with the help of a pipette and were put into the jar under the JLT6 jar test apparatus.

7. The jar was connected through a peristaltic pump to the Malvern Mastersizer 2000. The pumping speed was kept at 88 rpm, which was just sufficient to pump the flocs to and out of Malvern Mastersizer 2000, minimizing the shear that might affect the floc structure.

8. The floc size was then obtained from Malvern Mastersizer 2000. The time difference between adding Zetag 4120 and obtaining the first floc size measurement would be at least 90 s.

The standard protocol that was followed for the lock-exchange experiments has been stated in Chapter 2, Section 2.5.2. After the tank had been filled and a designated mass of sediment had been added to the missing section of the flume, the following steps, specific to this set of experiments, were followed:

1. In case of runs with flocculant, a weighed mass of Zetag 4120 or Zetag 7587 (according to the dosage) was added to the outflow section of the flume and mixed with a hand mixer for 30 s. The lock gate was opened after the water level in the outflow compartment was stable.

2. The propagation of turbidity currents was recorded using a GoPro Hero 9 camera for analysis of the front position using Tracker software (Version 6.1.3) (Brown et al., 2008).

3. To collect samples from the turbidity current, a duplicate experiment was performed in each case, following the above-mentioned steps. The samples were taken from two siphons located at the same height but at two different positions in the flume. Bottom outlets were also used to collect samples at three different positions in the flume (See Figure 2.1(a)).

4. The collected samples were then analyzed using the particle sizer and FlocCAM setup described in Chapter 2.

3.3. RESULTS

The results of the experiments that were performed are presented in this section.

3.3.1. PARTICLE SIZE MEASUREMENTS USING THE MALVERN MASTERSIZER

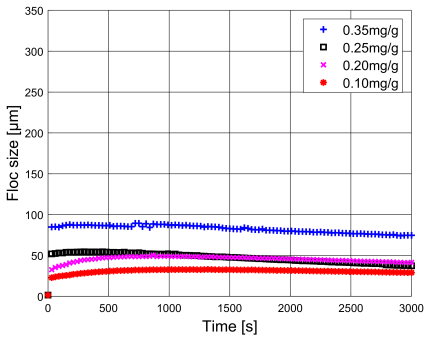

(a) d_{10}

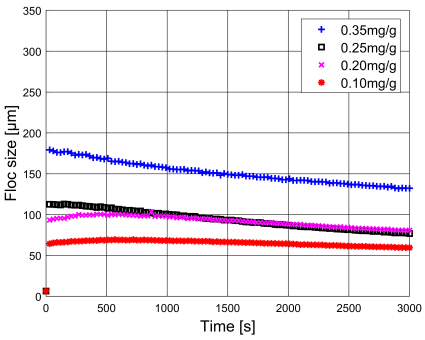

(b) d_{50}

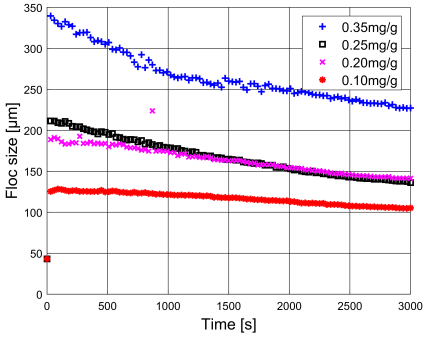

(c) d_{90}

Figure 3.1: Comparison of floc sizes obtained from Malvern Mastersizer using different dosages (mg of added flocculant per gram of clay) of Zetag 4120 as indicated in the legends. The red square at $t = 0$ indicates the size of unflocculated illite clay.

The evolution of floc sizes over time, formed with four different dosages of Zetag 4120, are shown in Figure 3.1. Floc sizes were recorded using the static light scattering technique as described in (Chapter 2, Section 2.2.3). The d_{10}, d_{50} and d_{90} of illite clay (unflocculated) were found to be 1.56 µm, 6.4 µm, and 43 µm, respectively, and are indicated by the red squares in the figures. The flocculant was added just after t = 0. The corresponding particle size distributions are shown in Figure 3.2.

For all measured sizes (d_{10}, d_{50} and d_{90}), a very rapid increase in particle size occurred (within a few minutes) after the addition of flocculant. After reaching maximum size, these d_{10}, d_{50} and d_{90} floc sizes are observed to decrease as a function of time (Figure 3.1), and the PSD peak shifted to the left (Figure 3.2). The position of the maximum floc size shifted to smaller times when increasing the flocculant dosage. This behavior

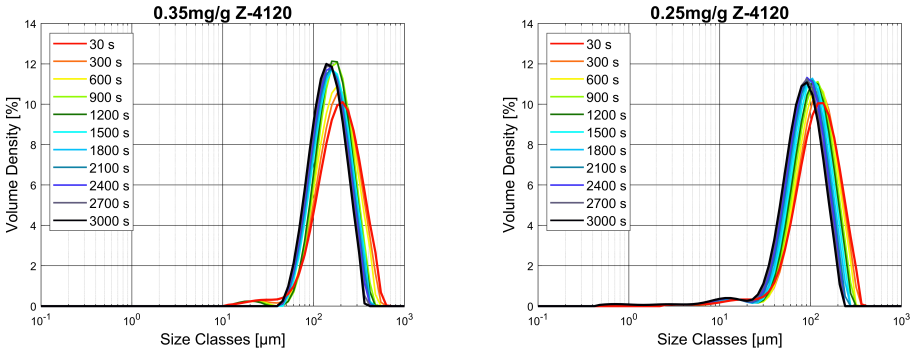

(a) 0.35 g/L (b) 0.25 g/L

(c) 0.20 g/L (d) 0.10 g/L

Figure 3.2: Particle size distributions obtained from static light scattering measurements using the Malvern Mastersizer 2000 for different sediment concentrations.

indicates that there is a competition between the aggregation of polyelectrolyte and clay and the action of shear. It is known that flocs, under the action of shear, are prone to reconform and, hence, become denser (Shakeel et al., 2020) and rounder in shape. Indeed, the PSD peaks are observed to sharpen over time, indicating that flocs become more monodisperse. At the same time, the d_{90} of flocs decreases substantially, and the d_{50} similarly decreases (Figure 3.1). The d_{10} does not vary much (Figure 3.1), and the relative amount of fine particles does not increase in time, see Figure 3.2, which confirms that flocs are not eroding or breaking. For 0.35 mg/g, at t = 30 s, a small peak was observed between 10 and 50 µm. This peak represents small, unflocculated materials (Zetag and illite). At t = 3000 s, the primary peak sharpened and the smaller peak disappeared, leading to the conclusion that all smaller particles have now been incorporated in flocs. This would imply that 0.35 mg/g is close to the optimal flocculant dosage, which is in line with the fact that flocs at this dosage are the largest.

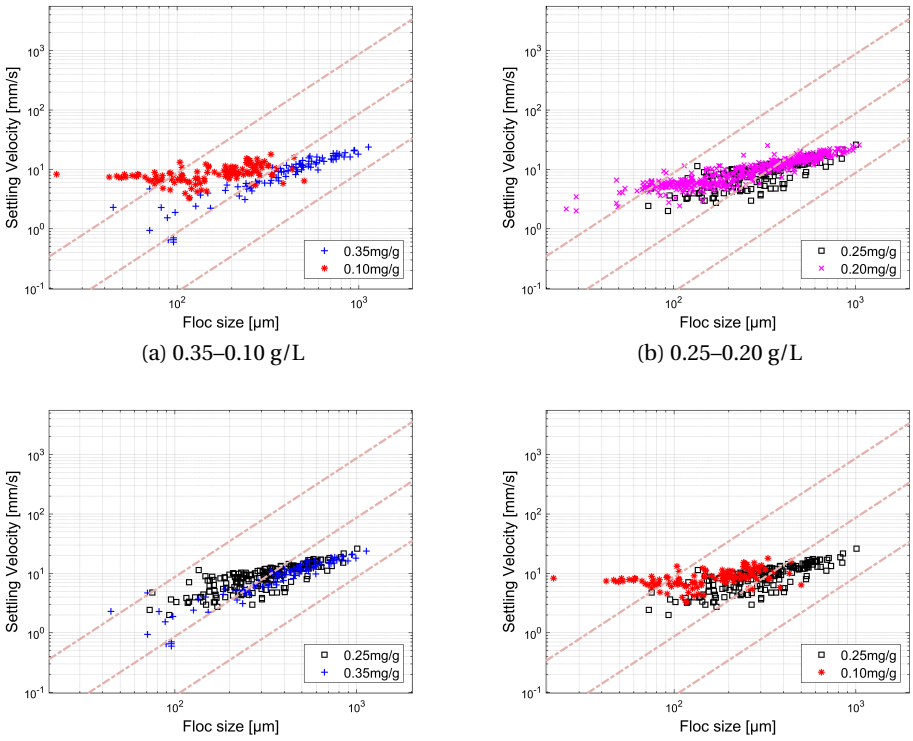

(a) 0.35–0.10 g/L

(b) 0.25–0.20 g/L

(c) 0.25–0.35 g/L

(d) 0.25–0.10 g/L

Figure 3.3: Comparison of floc size and settling velocity using different dosages of Zetag 4120. The lines represent isodensity values of 1160, 160, and 16 kg m^{-3}.

3.3.2. PARTICLE SIZE DISTRIBUTIONS AND SETTLING VELOCITIES OBTAINED FROM FLOCCAM

Figure 3.3 shows floc size and settling velocities obtained from FlocCAM video analysis. It is quite striking that the settling velocities obtained in all cases, for all particle sizes, are quite similar. This behavior can be linked to the influence of hydrodynamics resulting from the collective motion of the sampled flocs, see Ali et al., 2023, whereby flocs are entrained in the wake of the surrounding ones. Nonetheless, some features are apparent when comparing the distributions. In figure 3.3 (a), it is seen that flocs formed with a 0.35 mg/g dosage are larger than that of the lowest dosage of 0.10 mg/g. However, the settling velocities of the flocs (below 300 µm) formed with 0.10 mg/g dosage are (on average) higher. One of the reasons could be that there were more flocs in that size range at 0.10 mg/g, leading to higher settling velocities due to collective motion. It has indeed been found that collective motion can lead to individual settling velocities 10 or 100 times higher than individual settling velocities measured by sampling single flocs (Ali et al., 2023). On the other hand, it is not excluded that another reason could be that the flocs formed at 0.10 mg/g contained more sediment particles than flocs formed with

0.35 mg/g. The floc sizes and settling velocities of flocs formed with 0.25 mg/g and 0.20 mg/g (Figure 3.3(b)) do not differ much from the ones observed for 0.35 mg/g.

In Appendix A, figure (A.1), snapshots from FlocCAM videos are shown. The size of the formed flocs is governed by the clay-to-Zetag 4120 dosage ratio used.

3.3.3. COMPARISON BETWEEN MALVERN AND FLOCCAM RESULTS

Particle Size Distributions (PSD) obtained from the Malvern and the FlocCAM are compared in Appendix A, figure (A.2), using the bin sizes of the Malvern. In all cases, it is found that the peak in floc size obtained from the FlocCAM measurements is shifted to the right (indicating larger particle sizes) compared to the peak found by Malvern measurements. This implies that the d_{50} found by the FlocCAM are higher than the ones found using Malvern. There are several reasons for these differences: (1) particles measured by FlocCAM can experience differential settling, and hence aggregate while settling (though this reason is most probably not the main one), (2) flocs measured by Malvern are sheared in the tubes (of diameter 4 mm) in which the samples were pumped from the jars to the measurement chamber, leading to reconformation in the floc structure and (3) the software producing the PSD found by Malvern smoothen the data to produce bell-shaped curves, which leads to an underestimation of the larger sizes, see Sanz, 2018.

3.3.4. LOCK-EXCHANGE EXPERIMENTS

To study the influence of the presence of (synthetic) organic matter in the flow compartment on the turbidity current, a relatively high dosage of flocculant was chosen (corresponding to a flocculant to clay ratio of 2.5 mg/g). In order to achieve a 2.5 mg/g of clay dosage, it was necessary to use a flocculant concentration of 1.785 g/L. This amount of flocculant changes the water density by a small percent only and is therefore not expected to play a significant role in the propagation of a density-driven flow.

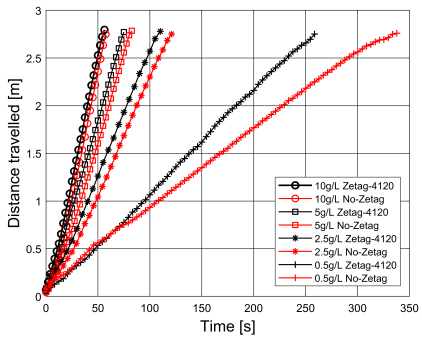

(a) Zetag 4120 and no Zetag

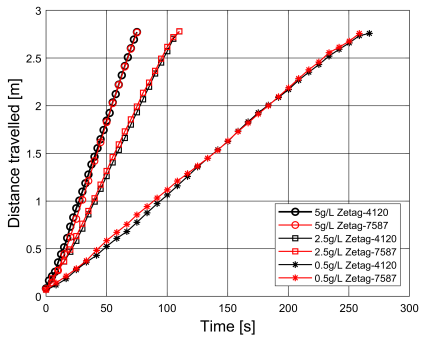

(b) Zetag 4120 and Zetag 7587

Figure 3.4: Front positions of turbidity currents for different flocculant types at identical sediment concentrations.

3.3.5. WITH ANIONIC POLYELECTROLYTE ZETAG 4120

Front positions of turbidity currents as a function of time for different sediment concentrations with and without Zetag 4120 are compared in figure 3.4 (a). The associated velocities are shown in figure 3.5 (a). The velocity values were obtained from video recordings (recorded at 24 fps) using a moving average point of 5 to smoothen the velocity fluctuations. The velocities in the Zetag 4120 cases were always higher than in the No-Zetag cases. For the 0.5 g/L case, it is seen that the initial velocity for the No-Zetag case was higher than its Zetag counterpart. From the video recording for 0.5 g/L sediment concentration, it was observed that the materials did not entirely come out of the mixing section of the lock-exchange flume. Thus, the momentum and density difference of the turbidity current was reduced. For all sediment concentrations, the front positions of turbidity currents with Zetag 4120 reached the end of the flume faster than their No-Zetag counterpart. The hypothesis behind this is that the polymer (Zetag 4120) acts as a lubricant, lowering the friction between water and the traveling current. In particular, the bottom surface of the flume becomes lubricated by the unflocculated polymer, thus allowing the turbidity current to travel faster.

3.3.6. WITH CATIONIC POLYELECTROLYTE ZETAG 7587

In figures 3.4 (b) and 3.5 (b), the front positions of turbidity currents and their corresponding velocities in the presence of cationic polyelectrolyte Zetag 7587 are compared with the fronts created with the anionic flocculant, Zetag 4120. It is clear that the front propagation is not affected by the type of flocculant used, as both the flocculant cases have similar front velocities. However, the floc size varies in both the cases. The flocs formed with cationic flocculant are smaller in size when compared to the ones formed with anionic flocculant, which is due to the difference in the binding mechanism of flocculant to the sediment particle (Figures 3.6 and 3.7).

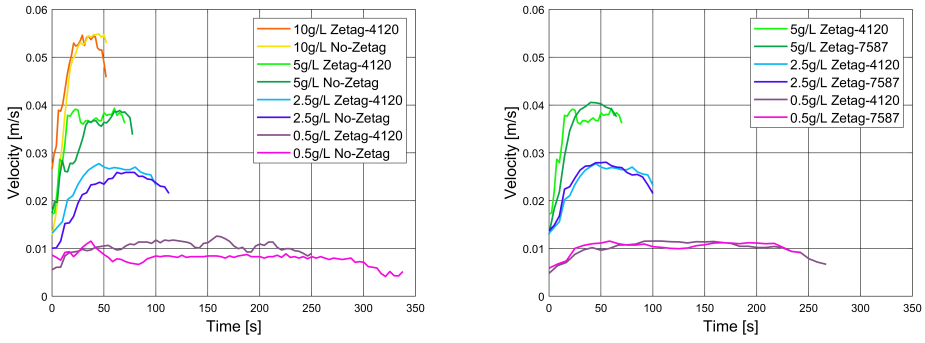

(a) Zetag 4120 and no zetag

(b) Zetag 4120 and Zetag 7587

Figure 3.5: Velocity of the turbidity current front as a function of time for different flocculant types.

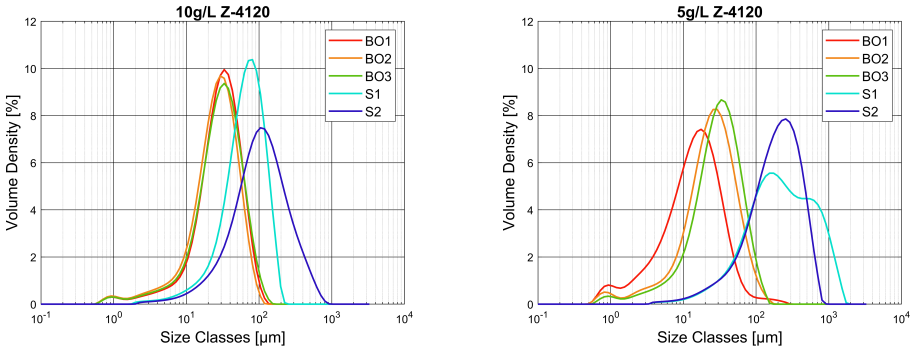

(a) 10 g/L (b) 5 g/L

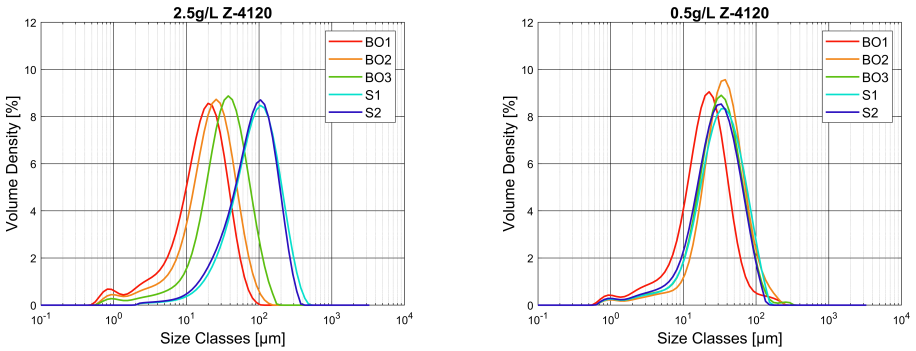

(c) 2.5 g/L (d) 0.5 g/L

Figure 3.6: Particle size distributions of samples collected from turbidity currents generated using Zetag 4120 at different sediment concentrations.

3.3.7. PARTICLE SIZE ANALYSIS AS A FUNCTION OF POSITION IN THE CURRENT

There are in total five samples (three bottom outlets and two siphons) taken from the turbidity current. The first bottom outlet (BO) is located at a distance of 67 cm from the lock gate. The other two BOs are located at a distance of 67 cm from each other. The siphons (S) are placed at a distance of 80 cm from each other and at a height of 3 cm from the flume bottom, as this was found to be the optimum position to collect samples from the body of the turbidity current and not from the bottom or bed. (Figure 2.1). The PSDs of these samples were obtained from the particle sizer (Malvern Mastersizer 2000), and the displayed PSDs (Figures 3.6 and 3.7) are the ones obtained from the first measurement of the machine (30 s after injection of the sample), to minimize the effect of shearing in the tubes.

From PSD graphs of samples obtained from bottom outlets and siphons (Figures 3.6 and 3.7), it is observed that the particle (floc) sizes in the siphon samples are generally larger than those collected from the bottom outlets. Due to the convective motion of particles in the turbidity current, it is expected that open-structure flocs will be formed

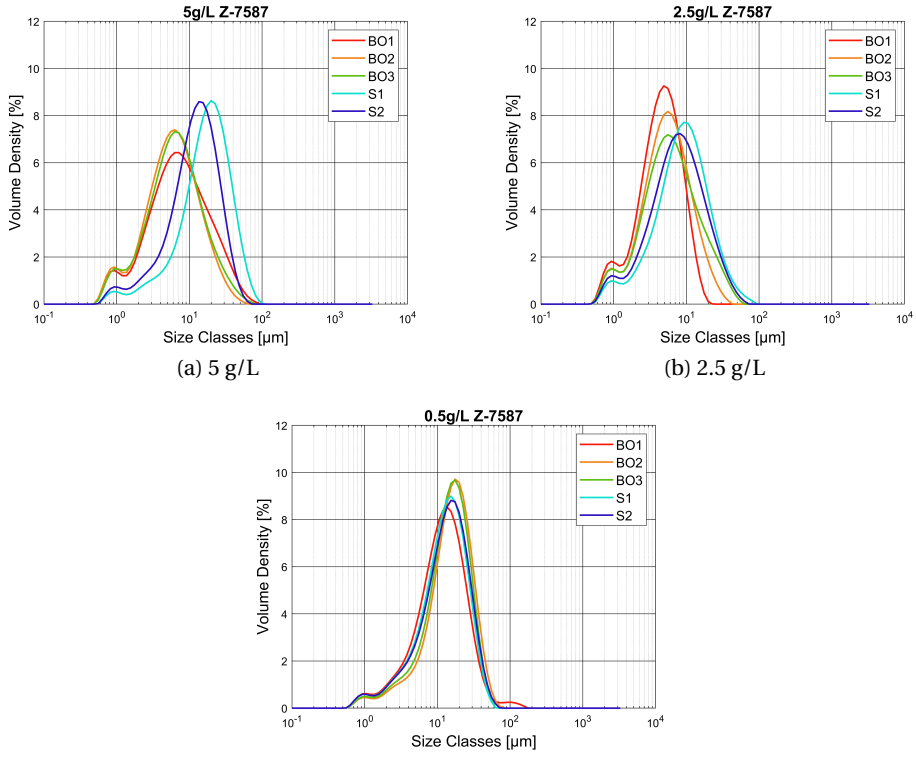

(a) 5 g/L

(b) 2.5 g/L

(c) 0.5 g/L

Figure 3.7: Particle size distributions of samples collected from turbidity currents generated using the cationic flocculant Zetag 7587 at different sediment concentrations.

by contact between clay and flocculant in the water column. The smaller sizes observed in the bottom samples may indicate that, after settling, flocs underwent reconformation of the polymeric tails, resulting in smaller aggregates. This interpretation does not imply a continuous decrease in floc size along the turbidity current path; as Figure 3.6 (a) and (b) show, floc sizes can increase during transport as aggregation proceeds. Rather, the differences between siphon and bottom samples likely reflect the distinct hydrodynamic and settling environments experienced by the flocs before sampling.

The sampled cationic flocs (created with illite clay and Zetag 7587) from the siphons are found to be smaller on average than the anionic flocs (created with illite clay and Zetag 4120) by at least one order of magnitude. In the case of cationic flocs, electrostatic attraction is the main driving mechanism (Goodwin, 2009). Here, polymer bridging takes place, which leads to the formation of strong aggregates. The breakage of these flocs is irreversible and flocculation is very sensitive to applied mixing conditions (Barany et al., 2009, Barany et al., 2010, Bárány et al., 2011). In the case of anionic flocs, a cationic agent is required to bind the polymer to the sediment (Shakeel et al., 2020, B. J. Lee et al., 2012). The cations here are the Na+ ions from the dissolved inorganic salt. Due to the

high affinity of the cationic polyelectrolyte with the clay, it is assumed that in a turbulent environment, this polymer will lead to more compact aggregates than an anionic polymer, which might be the reason for this large difference in size in suspended flocs (collected from the siphons). The flocs sampled at the bottom outlets and siphons were further investigated using the setups described in Chapter 2. The evolution of d_{50} of flocs collected from the siphons as a function of clay concentration in the flume is given in Figure A.5. One can see that the flocs created using the anionic flocculant (Zetag 4120) are significantly larger than the flocs created by the cationic flocculant (Zetag 7587) (see Figures A.3 and A.4) and that the d_{50} sizes for the flocs created using the anionic flocculant are shear sensitive as the anionic flocs are more open-structured and the cationic ones are compact. The anionic flocs collected from the siphons have their d_{50} size decreased roughly by half in 300 s, after being measured several times in the particle sizer. Flocs collected from the bottom outlets, on the other hand (see Figure A.3), do not change significantly in size over that period. This size dependence evolution as a function of time holds for 2.5 g/L, 5 g/L, and 10 g/L. For 0.5 g/L, it is found that flocs in Figures A.1 and A.2 are quite small compared to the other cases, as flocculation barely occurs in that case. Cationic flocs collected from the siphons (Figure A.5) or collected from the bottom samples (Figure A.4), on the other hand, did not exhibit significant changes upon shear, hereby confirming our hypothesis of these flocs being denser than anionic flocs. Some snapshots of the collected flocs, recorded using the FlocCAM, are given in Figures A.8-A.11.

3.4. DISCUSSION

In the present article, the action of two different polyelectrolytes (one anionic and one cationic) on the flocculation ability of illite clay was investigated in a lock-exchange environment. In contrast to what has been conducted in previous work, see Ali et al., 2022a. In these experiments, unflocculated illite clay was stored in the mixing compartment, whereas the flocculant was added in the outflow section.

Influence of flocculation on turbidity current propagation

The study aimed to verify whether flocculation would or would not occur during the turbidity current propagation and whether the velocity of the turbidity current would be affected. All experiments were carried out in saltwater. According to Mietta, 2010, salt-induced flocculation of mineral clay is of the order of 15 to 20 min. It was already shown in Ali et al., 2022a that there is no effect on the propagating turbidity current due to the presence of salt within the short duration of time (<1 min) of the density current propagation in the lock-exchange flume, in the case that flocs are released from the mixing compartment. Nevertheless, salt ions do have a significant effect on flocculation when it is conducted in the presence of an anionic polyelectrolyte (in the outflow compartment), as the salt cations are required to bind the polymer to the sediment. It was found that, indeed, turbidity currents are affected by the presence of flocculant in the (salt)water. Sampling at different positions in the lock showed that the illite clay indeed had bound to the flocculant (irrespective of the flocculant charge, i.e., the flocculant being anionic or cationic).

Behavior of flocs obtained from different locations of turbidity currents

The size of the flocs was recorded using two setups. The first one, the SLS particle

sizer (Malvern MasterSizer 2000), requires particles to pass through tubes to access the measurement chamber. This results in the fact that floc size was found to decrease as a function of measurement time, due to the continuous shearing in the tubes. This peculiarity of the measurement system was used to our advantage to confirm that flocs created by anionic polyelectrolyte sampled from the siphons were rather open in structure, as their sizes were found to decrease by half in some cases, after shearing for 300 s. Flocs obtained from the BOs, on the other hand, were found to be rather unaffected by shearing due to the shorter length of the sampling tube of the BOs compared to the siphons (1 m). This led us to conclude that flocs collected at the bottom of the flume probably had a longer residence time in the flow, and hence they became denser over time, due to the collapse of the polymeric hairs on the flocs.

Behavior of flocs analysed with Malvern Mastersizer 2000 and FlocCAM

The results obtained from the FlocCAM were first compared with the results from the particle sizer. It was found that the mean floc size of flocs obtained from the FlocCAM experiments was always higher than the ones obtained from the particle sizer. Several reasons were given to explain this observation. The two most important ones are, the first, related to the shearing in the tubes already described above, and the second, linked to the software of the particle sizer. It was also shown in the first part of the chapter that the settling velocities recorded using the FlocCAM are not representative of the individual settling velocity (Stokes settling) of flocs. It would therefore be inadequate to use the settling velocity results to try to estimate the particle density. Nevertheless, the FlocCAM provided some visual confirmation of the creation of flocs in the flume.

Behavior of flocs created with two different types of flocculant

Although flocs created by anionic flocculant and cationic flocculant were found to be very different in size, it was found that the turbidity currents in both cases propagated with the same velocity. It was also found that their front velocity was larger compared to the case where no flocculant was present in the outflow compartment. The hypothesis for this difference is due to the lubrication action of the (unflocculated) polymer, especially at the bottom of the flume.

By varying sediment concentration and flocculant concentration (using Zetag 4120), it was also found, by performing jar tests coupled with particle size measurements using the Malvern set-up, that a higher dosage (mg/g of clay) of flocculant leads to the formation of larger flocs. In the lock-exchange experiments, only one (high) flocculant dosage was used to verify whether flocculation would or not impact the turbidity current propagation. In future studies, it would be interesting to check the dependence of the front on the dosage of flocculant. In this study, particular attention should be paid to the interaction between the bed of the flume and the turbidity current. In natural systems, as in the CCZ region, but also most marine environments, the seabed floor is composed of organic matter in the form of biofilms or flocculated debris. It would be interesting to know how the composition of such a bed influences plume propagation as seen in the work of Gillard et al., 2019 and Spearman et al., 2020, where there was the occurrence of flocculation. The influence of a bed, formed from sediment collected at the sea-floor, will be discussed in the next chapter.

3.5. CONCLUSIONS

Based on the findings of this experimental study, the behavior of flocs was observed to vary with different flocculant dosages and types. A higher dosage led to the formation of larger flocs. The flocs formed with anionic Zetag were larger in size than the ones formed with cationic Zetag. Additionally, changes in floc size were analyzed depending on the sampling location with more compact flocs obtained from bottom outlets when compared to those from siphons. The role of flocculants within the water column was also discussed, as well as how flocculation takes places inside of the turbidity current when it propagates. This knowledge can be useful in understanding floc characteristics for controlling sediment plume dispersion in case of dredging activities and as well as in mining operations.

4

INFLUENCE OF BED AGE AND FLOCCULATION ON TURBIDITY CURRENT DYNAMICS

.

This chapter investigates the influence of seabed conditions on turbidity current propagation and flocculation dynamics in a lock-exchange setup. Experiments were conducted in saltwater with sediments collected from a deep-sea mining location in the Clarion Clipperton Zone. The results show that the presence of a bed significantly influenced the turbidity current front propagation, leading to reduced front velocities compared to a no-bed case. Additionally, larger and denser flocs were formed in the presence of a bed. This study also sheds light on the role of the age of the bed on turbidity current propagation, with (freshly) formed beds being efficient in reducing sediment spread. These findings are important for predicting the spread of a turbidity current during deep-sea mining activities.

This chapter has been published in Frontiers in Earth Science, **Wahab et al., 2026**

4.1. INTRODUCTION

The growing demand for clean energy technologies has increased the need for metals such as manganese, nickel, copper, and cobalt that are essential for producing wind turbines, solar panels, and electric vehicles. A significant amount of these metals is present in potato- shaped deposits known as polymetallic nodules found in the vast abyssal plains in the deep- sea. They are found at a depth of 4000-6000 m in the Pacific Ocean in an area known as the Clarion Clipperton Fracture Zone (CCFZ/CCZ).

One of the main concerns during the extraction process of polymetallic nodules is the dispersion of sediment and suspended matter beyond the Sea-floor Mining Tool (SMT) trajectory, as sideways propagating turbidity currents (Elerian et al., 2021). Turbidity currents are a subclass of gravity currents (also known as density currents). The transport, driven by gravity, primarily takes place due to the difference in density between the turbidity current and the surrounding fluid (Middleton, 1993). The difference in density, in shallow waters, may arise due to variations in temperature (between the turbidity current and the ambient water) or solute concentrations. In this chapter, we concentrate on turbidity currents which originate from the density difference between the suspended sediment and ambient water. In the case of turbidity currents, the sediment is held in suspension by fluid turbulence (Middleton, 1993).

During a deep-sea mining operation, excess water and sediment discharged from the SMT move through various flow stages before settling (Elerian et al., 2021; van Grunsven et al., 2018). Initially, the discharge behaves as a turbulent jet (Stage 1). It then entrains more water, thus increasing in mass and reducing in velocity, where it enters stage 2. At this point, the jet is known as a plume and is driven mainly due to the density difference between the plume and the ambient fluid, which sinks and impinges and might result in seabed erosion and deposition (Stage 3). In the final stage, the flow evolves into a turbidity current (Stage 4) moving along the seafloor. Results obtained from sediment plume dispersion modeling showed that the area of influence varied between 4 and 9 km, depending on whether normal conditions prevailed or an eddy had passed through the study location (Gillard et al., 2019).

Mousadik et al., 2024 conducted in situ measurements on turbidity flows caused by an SMT. They showed that the particle size and settling velocity distribution were influenced by the kind of disturbance to which the sediments were exposed. This disturbance was a function of various factors such as the SMT's operations, hydrodynamic processes, and the time elapsed after discharge. It was found that in a certain type of maneuver (selfie), the Particle size distribution (PSD) was different for the detrained sediment from the gravity current compared to that from the turbulent wake. The PSD is also influenced by the position within the plume and the time elapsed since its discharge, but most significantly by the subsequent fluid dynamic processes. Their results indicate that flocculation is likely to occur, especially close to the SMT where the turbidity flow is still at a higher sediment concentration.

PSD in the water column is expected to decrease due to deposition of heavier particles as a function of distance from the SMT. However, Gazis et al., 2025 showed that flocculation occurred during deep-sea sediment plume propagation as they found an increase in median particle size with distance. These results were based on measurements taken at further distances from the same vehicle disturbance as described by Mousadik

et al. Gillard et al., 2019 also proved that flocculation occurred in laboratory experiments using deep-sea sediments, which similarly changed the PSD and median particle size. In this case, the author used a fixed volume of sediment and water, mixed at a constant rate. The conditions in this case are steadier and do not account for the rapid dilution of sediment concentration as in the case of a turbidity current, which is more dynamic.

Elerian et al., 2023b developed a numerical near field model that included flocculation. The flocculation parameters were calibrated with the flocculation parameters based on the laboratory work of Gillard et al., 2019. From the numerical evaluation, it was clear that flocculation readily occurs (within the first 100 m from the SMT), forming larger particles and thus higher settling velocities at distances beyond the first 100 m from the SMT. Although the hydrodynamics in the near-field are not yet affected by the generation of flocs, the PSDs of the sediment and hence their settling velocities changed, compared to the initial discharge concentration.

Sea-floor sediment typically consists of clay, sand, fragments of rock, and organic material (BGR, 2019; Lang et al., 2019; Zawadzki et al., 2020.) This organic material comes from aggregates of organic detritus that sink through the water column. The aggregates are altered on their way down by grazing, microbial degradation, and chemical processes (Karl et al., 1988). The ones larger than 500 μm are called marine snow (Alldredge and Silver, 1988). The leftover materials that make it to the deep-sea floor include less degradable substances such as cellulose, chitin, and other proteinaceous structural compounds (Boetius and Lochte, 1994).

In the work of Ali et al., 2024b, the flocculation between organic matter and mineral sediment coming from deep-sea clay has been studied in detail. The CCZ sediments sampled from two different regions were studied as a function of mixing time, shear, and sediment concentration. It was found that the organic matter had amphiphilic properties, which are in line with the composition of deep-sea organic matter. The results showed that flocculation occurred in all situations in less than 2.5 minutes and that sizes could increase by 3-6 times compared to unflocculated materials.

In a previous study, detailed in chapter 3 and Wahab et al., 2024, it was shown that flocculation occurred in a propagating turbidity current using illite clay and an anionic polyacrylamide flocculant, which similarly flocculates within seconds. These experiments were performed in a lock exchange flume, where the turbidity current propagated on the plexiglass bottom in the absence of a bed. Turbidity current lock exchange experiments conducted by Nogueira et al., 2013b investigated the role of roughness on the front propagation velocity. The roughness imparted by the freshly deposited bed reduces the turbidity current propagation.

Apart from flocculation, which has proven to reduce sediment spread, it thus remains to be investigated whether the presence of a (disturbed) bed would or would not reduce sediment spread.

For any deep-sea mining activity, the first run would take place on an undisturbed ocean bed. The propagation of turbidity currents will likely differ between an undisturbed bed and the one that has already undergone mining and the materials have settled. In this chapter, the difference in propagation between turbidity currents under different bed scenarios were studied. Experiments were performed using deep-sea sediments in saltwater, first using a plexiglass bottom, then a 1-day old bed and finally a

3-day old bed. The bed was made by leaving the materials from a turbidity run on the plexiglass bottom.

It is crucial to understand the role of the bed, specifically how an older bed or one formed by newly deposited materials influences the front propagation velocity of the turbidity currents. In deep-sea mining activities, the sediments disturbed by the SMT or the discharged materials will be deposited in the vicinity, with a chance to interact with passing turbidity currents. This newly created bed will influence the current's propagation. Additionally, flocculation will also be influenced due to loose materials being picked up during the turbidity current propagation. Simultaneously, materials will also be dropped along the way due to the influence of the roughness of the freshly formed bed. Understanding how changes in bed properties affect a turbidity current propagation will hence help to better design the pathway of the mining vehicles

4.2. METHODS

The materials and the equipment used in the experiments are described in Chapter 2. Here, the new experimental conditions and protocol that are specific to these experiments are described.

4.2.1. PRE-EXISTING BED

Three types of beds were used in these experiments.

1. No bed: The turbidity current directly propagated on the plexiglass bottom of the flume. This case was used as the controlled condition.
2. 1-day bed: This type of bed was constructed by leaving the sediments at rest overnight from a previous run for approximately 16-18 hours (Figure 4.1).
3. 3-day bed: This bed was constructed by leaving sediments at rest over the weekend for approximately 68 hours. The durations of beds (16h/ 68h) were chosen to ensure the practicality of the experiments. The construction of both beds is described in Section 4.2.2.

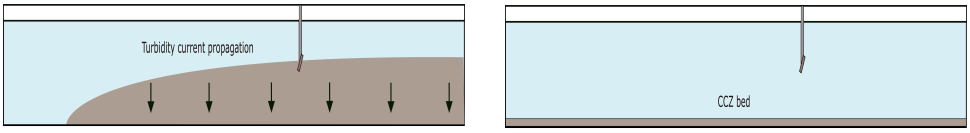

(a) Turbidity current propagation (b) CCZ bed

Figure 4.1: Schematic diagram showing (a) the propagation of the turbidity current (from right to left) with arrows symbolizing sediment settling (b) and the formed CCZ bed

The lock exchange experiments were carried out using three different initial concentrations of CCZ sediments (2.5, 5, and 10g/L) in the mixing compartment. The setup was similar to what was used in the previous works of Wahab et al., 2024 and Wahab et al., 2025.

The experimental matrix for the lock exchange experiments is shown here.

Type of beds	Concentration [g/L]
No bed	2.5, 5, 10
1-day bed	2.5, 5, 10
3-day bed	2.5, 5, 10

Table 4.1: Experimental matrix with different bed types and concentrations

4.2.2. EXPERIMENTAL PROTOCOL

The following protocol was adopted for these experiments.

1. The lock exchange flume was prepared and filled with saltwater as mentioned in Section 2.5.2.
2. The volume of CCZ sediment was measured by first determining the dry mass fraction in 100 mL of the sediment sample. Depending on the target concentration, the required mass of dry sediment was calculated, and then the corresponding volume of sediment suspension was measured accordingly to be added to the mixing section of the flume. The mixture was then mixed for 20 minutes using an overhead stirrer.
3. In case of the "No bed" scenario, upon release of the lock gate, the sediment was released into the outflow compartment. Thus, leading to the formation of a turbidity current that propagated on the plexiglass bottom until it reached the end of the flume.
4. After the experiment had ended, the sediment and water were left undisturbed in the flume for 16-18 hours or 68 hours, depending on whether a "1-day bed" or a "3-day bed" was desired.
5. The next day(s), the flume bottom was lined with a layer of sediment, which is referred to as the "1-day bed/ 3-day bed".
6. The lock gate was placed back in position, and the lock section was filled with sediments and then released. The turbidity current, in this case, propagated on top of a bed.
7. The propagation was recorded using a GoPro Hero 11 camera. The videos were then analyzed to obtain the front velocity using Tracker software (Version 6.1.3) (Brown et al., 2008).
8. The particle velocity inside the turbidity current was recorded by a 4 MHz UVP transducer mounted in the flume. The transducer was kept at a fixed position throughout all the experiments. The velocity data was collected from the head of the turbidity current when it reached a distance of 120 cm from the lock gate.
9. The experimental matrix was repeated following the same procedure (Steps 1-6) to collect samples via siphons. The sample collection began when the head of the turbidity current was at 100 cm from the lock gate, i.e. at 10 cm from the siphon position. The collected samples were then analyzed using FlocCAM.

4.3. RESULTS

The results of the experiments that were conducted are presented in this section.

4.3.1. FRONT PROPAGATION ANALYSIS OF TURBIDITY CURRENTS

Figure 4.2(a) shows the front positions of turbidity currents with CCZ sediments for different initial sediment concentrations (2.5, 5, and 10g/L), considering three different bed scenarios. The associated velocities are shown in Figure 4.2(b). The results indicate that the front velocity reduces due to the presence of the bed. The effect of the 1-day bed is especially pronounced at lower concentrations, where the momentum generated by the turbidity current is lower. In contrast, at higher concentrations, where the momentum is higher, the presence of a bed does not affect the front velocity. It was observed that the front velocity increased by 3 and 4 % for 1-day and 3-day beds, respectively, relative to the no bed condition (for 10g/L). In the presence of the 3-day bed, it is seen that the velocity is higher than that of the 1-day bed. As the beds age, the turbidity current velocity increases. One of the possible explanations could be that the organic matter in the water column takes longer to settle. In the case of the 3-day bed, this extended settling time allowed more organic matter (from the sediments in the water column) to accumulate, leading to changes in the biofilm covering the bed, resulting in a smoother bed. Moreover, over time, it is expected that these changes lead to a more compact bed, difficult to erode.

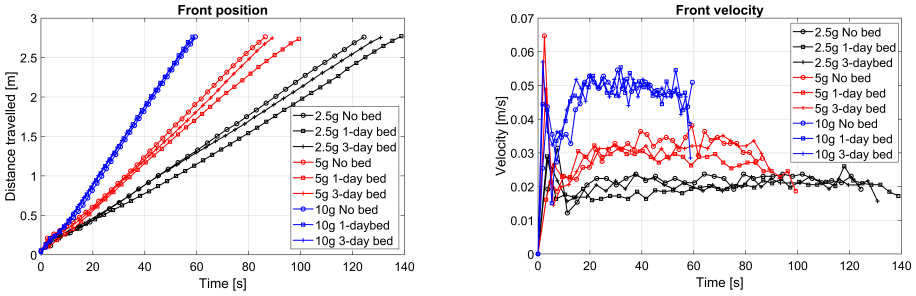

(a) Front position (b) Front velocity

Figure 4.2: Front position and front velocity of the turbidity current as a function of time.

4.3.2. ULTRASONIC VELOCITY PROFILER (UVP)

Figure 4.3 shows velocity profiles recorded using a 4MHz UVP transducer. The data presented here were extracted when the head of the current reached 120 cm from the lock gate (at 30 cm from the transducer). For 10g/L and 5g/L, the instantaneous velocity profiles for "No bed" condition started with a higher velocity when compared to the 1 and 3-day bed cases. The velocity profiles for 2.5g/L were comprised of noise due to fewer seeding materials being available. From the UVP data, it is seen that the turbidity current height was between 8 and 11 cm from the flume bottom for 2.5g/L, whereas it was in the range of 10-12 cm for 5g/L and 10g/L concentrations. The presented data is from the "head" position of the turbidity current as defined in Sequeiros et al., 2018 when

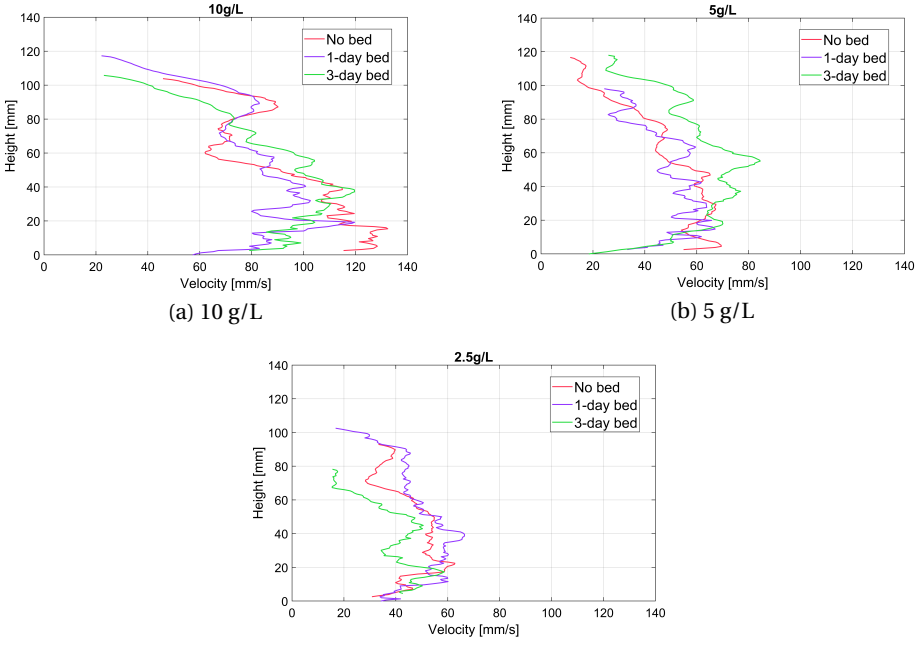

(a) 10 g/L

(b) 5 g/L

(c) 2.5 g/L

Figure 4.3: Instantaneous velocity profiles measured using the Ultrasonic Velocity Profiler (UVP) for different sediment concentrations and bed conditions.

the head height is the maximum. The transducer also recorded the particle velocity at the body and tail of the turbidity current. The data was comprised of noise due to low seeding materials being left at those parts of the turbidity current.

4.4. FLOCCAM

The sediment samples were collected via siphon and analyzed using the FlocCAM. The floc data obtained from video analysis using SAFAS software are presented here. Two types of beds are considered here: no bed and a 1-day bed, as described in Section 4.2.1.

The data in Figure 4.4 represent the settling velocities of particles as a function of their size, for three different sample concentrations. The isodensity lines indicate a relative density in the range of 1600-16 kg/m^3. Particles usually do not settle under Stokesian conditions in the FlocCAM experiments. As has been demonstrated in Ali et al., 2024a, Stokesian settling velocities can be observed when the distance between a particle and its closest neighbor is high. Particles falling under these conditions are termed "individual" in the legend. Particles falling in the vicinity of others are termed "collective". As expected, collective settling velocities are generally one decade higher than individual settling velocities. From Figure 4.4(a), note that the particle's settling velocity range is substantially wider than in Figure 4.4(c).

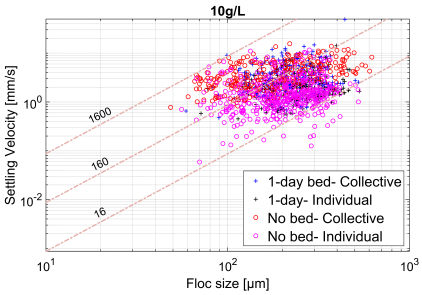

(a) 10 g/L

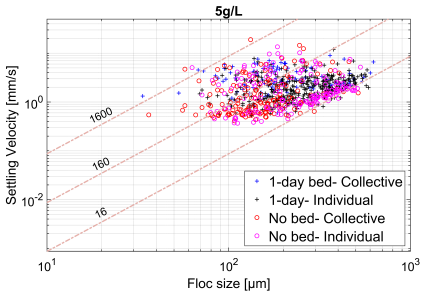

(b) 5 g/L

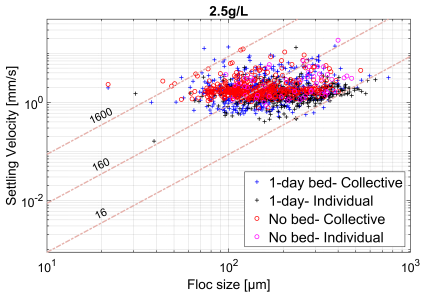

(c) 2.5 g/L

Figure 4.4: Floc size versus settling velocity of CCZ flocs. Isodensity lines (1600, 160, and 16 kg/m^3) represent relative floc densities calculated from measured floc sizes and settling velocities using Stokes' law, assuming primary particle densities of 2600, 1160, and 1016 kg/m^3. These lines serve as reference guides for interpreting how floc density varies with floc size.

Figure 4.5 presents the box plots for settling velocities under two different bed scenarios: no bed and 1-day bed. The flocs are categorized into "individual flocs" and "individual and collective flocs", as defined above. It is observed that the median settling velocities for the 1-day bed cases are higher when compared to their counterparts, the "No bed" cases.

The presence of a bed leads to larger flocs, which is evident from the median floc sizes shown in Figure 4.6. Median floc sizes were found to be 225, 220, and 190 μm for 10g/L, 5g/L, and 2.5g/L, respectively, which is higher than the "No bed" cases. The flocs, in both the cases, were found to be more open-structured.

4.5. DISCUSSION

In this study, how a pre-existing sediment bed influences the dynamics of turbidity currents and the associated flocculation processes has been investigated in a lock exchange environment using sediments from the Clarion Clipperton Zone (CCZ). The findings from this study shed light on the influence of the underlying bed on the hydrodynamics of the current.

In the study conducted by Wahab et al., 2024, flocs were formed with different flocculant dosages. A synthetic flocculant was added to a suspension of illite clay. The

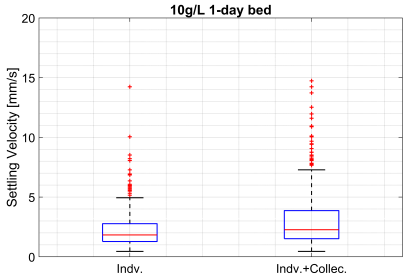

(a) 1-day bed (10 g/L)

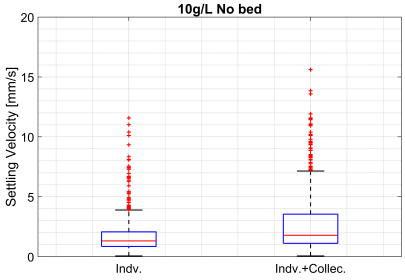

(b) No bed (10 g/L)

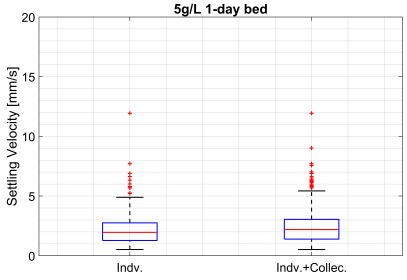

(c) 1-day bed (5 g/L)

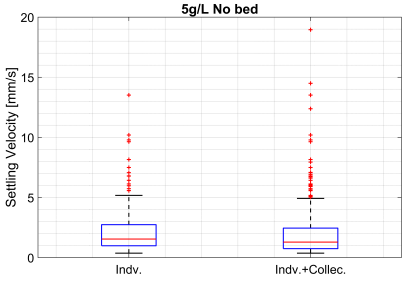

(d) No bed (5 g/L)

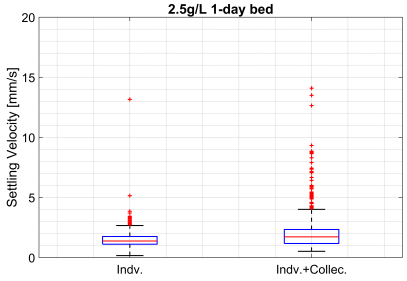

(e) 1-day bed (2.5 g/L)

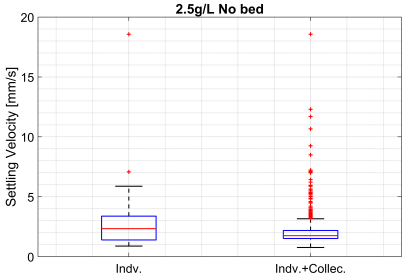

(f) No bed (2.5 g/L)

Figure 4.5: Box plots of settling velocity of CCZ flocs for different sediment concentrations and bed conditions.

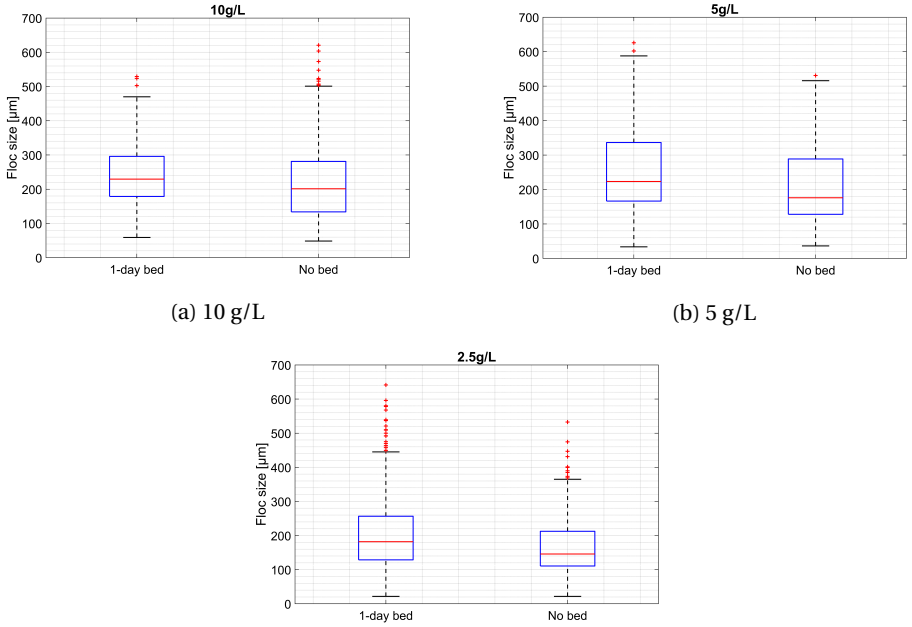

(a) 10 g/L

(b) 5 g/L

(c) 2.5 g/L

Figure 4.6: Box plots of floc sizes of flocs sampled from different types of beds. The data were obtained from FlocCAM measurements.

sediment concentration was kept constant with varying flocculant dosages. The flocs formed with a lower dosage of flocculant had higher settling velocities when compared to the flocs formed with a higher flocculant dosage. Due to the abundance of flocculant being available, larger, open flocs were formed compared to the case where flocculant was scarce. This caused the flocs to contain more sediment particles bound by a lesser amount of flocculant. Additionally, the particles that were smaller in size (less than 100 μm) were observed to have higher settling velocities. This could be attributed to the flocs falling in the wake of larger flocs, thus ending up having larger settling velocities (Ali et al., 2024a).

With more materials being available in the presence of a bed, as in the present study, denser flocs were being formed. Sediment particles from the bed were picked up during the turbidity current propagation, which led to these denser flocs. It was also observed that the "Individual and collective flocs" had higher settling velocities in comparison to the "individual" flocs alone, in line with the findings of Ali et al., 2024b.

In the article of Ali et al., 2024b, experiments were performed whereby flocs were left to rest in jars. Flocs were then carefully sampled over time and their size measured. It was observed that the floc sizes gradually increased over time (until day 10), followed by a decrease. Minimal disturbance was found to promote the growth of flocs that were previously not in contact. Additionally, after 10 days, flocs were breaking and/or reconforming. In the case of a 1-day bed, the flocs within the turbidity current during propagation

came into contact with the flocs lying on the bed, leading to an increase in size.

Influence of a bed on turbidity current propagation

Studies conducted earlier explored a bed's influence on turbidity current propagation (Adduce et al., 2009; Peters and Venart, 2000; Özgökmen and Fischer, 2008). It was found that the roughness of a bed influences the propagating velocity of a turbidity current. In the present study the behavior of the turbidity current mechanism in the presence of a bed was investigated for different sediment concentrations. In line with previous studies, it was found that the presence of a bed significantly alters the front velocity. In case of 2.5g/L and 5g/L, the presence of a 1-day bed, reduced the front velocity by 9 % and a 3-day bed by 3 %. From instantaneous velocities recorded by a UVP transducer, the velocity near the flume bottom was found to be around 12 cm/s for 10 g/L, 6 cm/s for 5 g/L, and 3cm/s for 2.5 g/L for no-bed condition. The variation in the initial velocities is due to the momentum of the turbidity currents.

According to the EIA report of The Metals Company (Gillard and Thomson, 2022), it was stated that erosion of the blanketing layer (newly formed bed) occurred at 9-10 cm/s velocities. The erosion was further increased at flow velocities of 15 cm/s. This was in the case when the blanketing layer was thin, formed with 0.5g/L and 0.25g/L sediment concentration. In case of a blanketing layer formed with 1g/L (Gillard and Thomson, 2022), no sediment resuspension was observed in the velocity range of 4-15 cm/s. So if the turbidity current flows with velocities in the range of 10-15 cm/s, there is a chance of erosion, where the materials will be incorporated in the propagating turbidity current, thus adding more materials and influencing flocculation. However, in this case, this velocity is not sufficient to cause erosion of the blanketing layer.

Influence of age of bed in turbidity current propagation

The results of this study show that the age of the bed plays a significant role in turbidity current propagation. The front velocities show that the 1-day bed has a stronger influence on the propagating turbidity current compared to the 3-day bed. This indicates that freshly deposited beds impart greater roughness and resistance to flow. As the bed ages, the flocs undergo reconformation Ali et al., 2024b, and the surface becomes smoother, leading to a reduction in frictional resistance to flow. This behavior was also observed in the previous works of Nogueira et al., 2013b and Adduce et al., 2009, where the presence of a rough bed resulted in velocity reductions. The 3-day beds in this study have been smoothed due to deposition of materials over time, which yielded higher front velocities (Baghalian and Ghodsian, 2022; Maggi et al., 2022). In our study, two beds were examined, and the results clearly showed a shift in turbidity current behavior. The findings imply that as the bed undergoes further aging beyond the timescales investigated here, its influence on front velocity may diminish once the bed surface reaches a more stable state.

Jar tests were conducted (described in Appendix B, Section B.3.1) to confirm the erodibility of beds. The 3-day bed eroded faster compared to the 1-day bed. A similar behavior has been reported by Ali et al., 2024b. In this study, flocculation experiments on CCZ clay were performed in jars under mild stirring. When the stirring was stopped, flocs settled at the bottom of the jar and were left to age. It was found in line with the present study, that the median floc size decreased over time. The peculiar behavior was ascribed to the specific type of organic matter in the sample: because of the hydrophobic

nature of the organic matter, flocs on top of the 3-day bed have reconformed, become smaller in size, and hence are easily mobilized.

Influence of bed on flocculation

The settling velocity range of particles at higher concentration is larger than that at lower concentration (Figure 4.4). This can be interpreted by the fact that at higher sediment concentration, particles have a larger collision frequency with both clay and organic matter, hence forming flocs that settle faster. At the same time, the turbidity current will propagate faster because of the higher momentum than at lower concentrations. Flocs formed at lower concentrations, on the other hand, will have a lower collision frequency, will travel for a longer period before reaching the siphon. Therefore, they are expected to have a more coiled (compact) structure, resulting in the elimination of flocs with low settling velocities, which exhibit a loose, organic-matter rich structure. One of the interesting mechanisms observed here was the characteristics of flocs changing upon the introduction of a bed. The settling velocities of flocs increased, which implied that denser flocs were formed. The initial concentrations were kept the same in both cases: no bed and 1-day bed. The increase in floc density and settling velocity in the presence of a bed indicates that materials were being picked up when the turbidity current was propagating on top of it. The floc sizes also increased. In deep-sea operations, it will prove in favor, as a freshly disturbed bed would enhance flocculation, thus leading to an early settlement of the plume. Also, the floc sizes depended on the sediment concentration, as found earlier in the work of Ali et al., 2024a. The snapshots presented in Figure B.1, B.2, and B.3 (Appendix B) also confirm that larger flocs were being formed in the presence of a bed. These larger flocs have an influence on the propagation velocity of the turbidity currents.

4.6. CONCLUSION

New insights were gained through this study on the role of bed on turbidity current propagation, considering flocculation. It also pointed out the significance of the duration of beds, with freshly deposited beds imparting roughness to current propagation. The interaction of turbidity currents and sediment beds not only affected transport dynamics but also altered the floc behavior. The increase in floc size and density in the presence of a bed suggested that sediment resuspension and erosion play a crucial role in flocculation. These findings are particularly relevant for deep-sea mining operations, where freshly deposited sediments may enhance or hinder turbidity current spread. Future studies should explore a broader range of bed ages. These findings ultimately contribute to a better understanding of deep-sea sediment plume behavior and its spread.

5

INFLUENCE OF BED COMPOSITION ON TURBIDITY FLOWS

This study investigated the impact of various types of bed composition on turbidity current propagation in relation to flocculation. A lock-exchange setup was used, comprising a mixing section and an outflow compartment. The bed types investigated were a quartz bed, a quartz bed topped with (unflocculated) illite clay, and a quartz bed with flocculated illite. The findings confirmed that the presence of a bed influenced the turbidity current propagation. In particular, it was found that the propagation velocity was strongly reduced when the bed was composed of freshly made flocs compared to the case where the bed was made of quartz alone, which does not form flocs. While propagating on a clay bed, either illite clay or flocs were picked up and aggregated into larger flocs. These larger flocs were then deposited further downstream during propagation. Moreover, the propagation velocity was higher over a quartz bed when no flocculant was added to the outflow compartment water than when flocculant was present. This confirms that flocculation occurs in the water column during propagation.

This chapter has been published in Frontiers in Marine Science, **Wahab et al., 2025**

5.1. INTRODUCTION

Turbidity can originate in any aquatic environment due to natural processes, such as sediment-laden flows propagating downslope under the influence of gravity. It can also arise due to any anthropogenic activities such as dredging, deep-sea mining, trawling, land reclamation, and offshore construction. Such activities can resuspend and release sediments into the water column, leading to the formation of turbidity flows. Among these activities, dredging has been extensively studied due to its importance in maintaining the effective functioning of coastal zones (CEDA, 2011; P. L. A. Erftemeijer et al., 2012; Victor et al., 2018). Sediment spilled during a dredging activity could result in excess turbidity and sedimentation around the dredging area (Bray, 2008; Laboyrie et al., 2018). In contrast to plume propagating in a slope, turbidity currents generated by human activities can also occur on a flat bed. Turbidity currents affect the surrounding environment, with an immediate impact on the marine ecosystem. It can alter species population and shift food webs depending on severity and duration of the exposure and the sensitivity of the ecosystem (Lunt and Smee, 2020; Riza et al., 2023). They also play a crucial role in transporting sediments, nutrients, and pollutants from the continental margin to the world's oceans

Turbidity currents are dilute sediment-laden flows with concentrations less than 10 kg/m^3 (Parsons et al., 2007). They are fully turbulent with a Reynolds number greater than 10000 and contain poorly sorted sediments (Parsons et al., 2007). A turbidity current has three main parts, namely the head, body, and tail. The head of the turbidity current exhibits distinctive properties when compared to its body and tail. The head has significantly different mass and momentum from its body and tail. It has the highest concentration. While propagating, it displaces the ambient fluid, and this causes frictional resistance.

The presence of a bed affects the turbidity current propagation. The roughness of the bed plays a significant role in influencing the current kinematics, by reducing the front velocity due to more drag (Nogueira et al., 2013b). In the case of a non-erodible bed, no additional material is picked up during the propagation. However, in an erodible bed, materials can be eroded, while some materials can be deposited, which will in turn affect the dynamics of the turbidity current (Parker et al., 1987). The turbidity currents can contribute to active sediment transport and rapid bed deformation, processes that contribute to erosion of various submarine canyons (Hu and Cao, 2009).

Studies have confirmed the occurrence of flocculation in the dredging plume (de Wit et al., 2025; Ali et al., 2022a). In Chapter 3 (Wahab et al., 2024) and Chapter 4 (Wahab et al., 2026), the role of organic matter distributed in the water column on turbidity current propagation on a flat bed was studied. Together, these studies highlight how organic matter (flocculant) promotes flocculation, which in turn affects the turbidity current propagation. It was found that flocculation within turbidity flows is influenced not only due to the presence of suspended organic matter but also due to bed interactions. Hydrodynamics such as mixing rate inside the turbidity current (influenced by concentration) and residence times, i.e., for how long the sediment and organic matter were mixed, influenced the density and settling velocity of flocs.

The age of a bed also plays a vital role in flocculation dynamics. A previous study by Wahab et al., 2026 showed that the turbidity current front velocity decreased in the pres-

ence of 1-day old bed (made with sediments from the Clarion Clipperton Zone, located between Hawaii and Mexico) but increased for a 3-day bed. In a study conducted by Ali et al., 2024b on the same material, flocs were created in a jar by mixing and left to rest on the bottom of the jar. Floc sizes were observed to gradually increase over time until resting day 10, after which a decline in size occurred. This reduction in size was attributed to the reconformation of organic matter inside the floc due to the amphiphilic property of the organic matter found in the Clarion Clipperton Zone.

The main goal of this research is to investigate the underlying mechanism by which a bed with loose materials influences flocculation and turbidity current dynamics. Laboratory experiments simplify the complex nature of real-world deep-sea turbidity currents. They were designed to isolate and study the governing mechanisms of particle aggregation and their impact on current propagation under transitional-turbulent conditions (here, Re=2878, Fr=0.15). This study specifically examines how bed roughness imparted by freshly deposited sediments affects floc formation and settling behavior. To ensure repeatability of the experiments, as natural sediments tend to have variability in their properties depending on their geographic origin and focus on the driving mechanism, illite clay (devoid of organic matter) was combined with an anionic polyacrylamide flocculant previously applied in related studies Wahab et al., 2024. By using sediments with consistent behavior, the study could focus on the fundamental mechanisms that influence turbidity current dynamics due to the presence of a bed rather than any site-specific sediment characteristics. Furthermore, the use of illite and flocculants ensured sufficient materials were available throughout the experiments.

5.2. METHODS

The protocol that was followed while conducting these experiments is as follows:

1. Quartz bed
    - Dry quartz flour was distributed on the flume bottom to make the bed.
    - The quartz flour was moistened and allowed to rest for a minimum of 1 hour.
2. Lock-exchange flume
    - 210 liters of saltwater was gradually pumped into the flume with minimal disturbance up to a height of 35 cm.
3. Mixing section
    - Three different concentrations were used (Table 5.1). A weighed mass of illite based on the desired concentration was added to the mixing section of the flume, which contained 14 litres of saltwater. It was then mixed for 20 minutes.
4. Outflow compartment
    - Different types of beds and saltwater, which were used in the experiments in the outflow compartment, are described in Section 5.2.1.

5. Turbidity current propagation
    - The lock gate was then opened, allowing the sediment mixture out and travel along the length of the flume.
    - A UVP transducer was also installed at a fixed position in the setup to measure the velocity of particles within the turbidity current. The sampling frequency was set at 8 profiles per second.
    - A GoPro Hero 11 camera was used to record videos, which were later analyzed with Tracker software (Brown et al., 2008).
6. Experimental matrix
    - The experimental matrix was repeated as per the protocol (Steps 1-3), where sediment samples were collected from the body of the turbidity current using a siphon.
7. Floc analysis
    - The collected samples were then analyzed with FlocCAM.

5.2.1. TYPES OF BEDS

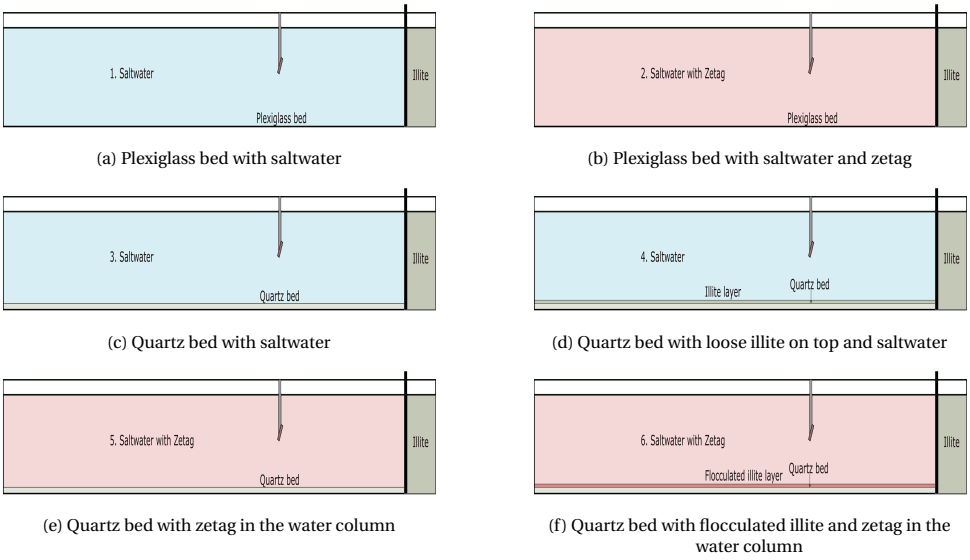

(a) Plexiglass bed with saltwater

(b) Plexiglass bed with saltwater and zetag

(c) Quartz bed with saltwater

(d) Quartz bed with loose illite on top and saltwater

(e) Quartz bed with zetag in the water column

(f) Quartz bed with flocculated illite and zetag in the water column

Figure 5.1: Formation of different types of beds. Here, blue represents the absence of Zetag, while pink denotes its presence in the water column.

The bed construction is described in this section. The primary objective is to investigate how the presence of a bed affects the front velocity of turbidity currents. This is particularly relevant in scenarios like dredging or marine mining, where consecutive operations occur, leading to successive turbidity currents.

For two experiments, the flume bottom (made of plexiglass) was used. A bed was then prepared for the remaining experiments by layering quartz flour on the plexiglass flume bottom to mimic an existing (sea) bed. The bed was approximately 5 mm thick. The flume tank was then carefully filled with saltwater with the least disturbance.

Six different kinds of experimental conditions (bed and saltwater) were prepared for these experiments, which are shown schematically in Figure 5.1.

1. Plexiglass bed: The turbidity current in this case propagated on the plexiglass bottom of the flume. The water in this case was pure saltwater with no zetag.

2. Plexiglass bed with zetag: The turbidity current propagated on top of the plexiglass. The saltwater in the flume contained zetag in this case.

3. Quartz bed (Q.B): This bed was constructed by laying quartz flour on the flume bottom and leveling it. The flume was then carefully filled with saltwater to the required height.

4. Quartz bed with illite (Q.B+Illite): This bed was prepared using a consistent protocol, where freshly flocculated illite was allowed to settle on top of the quartz bed from a preceding run, thus naturally creating a uniform layer of illite. The previous study of Wahab et al., 2026 showed that the age of the bed has a role to play in the consolidation of the bed, with an older being more consolidated and smoother compared to a freshly deposited bed. Here in these experiments, the duration in between runs was kept consistent (15 minutes), ensuring that the bed had a similar age before each run. In this way, the variability in bed roughness was minimized, ensuring consistency in preparation.

5. Quartz bed with zetag (Q.B+Zetag): This bed was prepared similarly to the quartz bed, but with zetag homogeneously suspended in the water column. A specified dosage of zetag was added to the outflow compartment of the flume and gently mixed before the experiment.

6. Quartz bed with zetag and illite (Q.B+Zetag+Illite): This bed was prepared in a similar way to the "Quartz bed with illite". The only difference was that the water used here had zetag in it.

Table 5.1 shows the matrix for the experiments performed in the lock-exchange.

Type of beds	**Concentration [g/L]**
Plexiglass bed	2.5, 5, 10
Plexiglass bed with zetag	2.5, 5, 10
Quartz bed	2.5, 5, 10
Quartz bed with illite	2.5, 5, 10
Quartz bed with zetag	2.5, 5, 10
Quartz bed with zetag and illite	2.5, 5, 10

Table 5.1: Experimental matrix with different bed types and concentrations

5.3. RESULTS

The results of the experiments that were conducted are presented here.

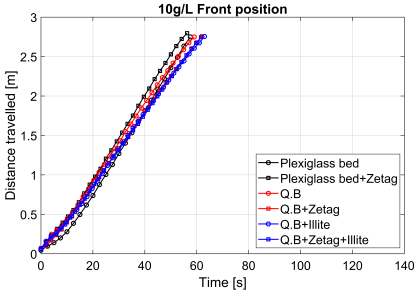

(a) Front position (10 g/L)

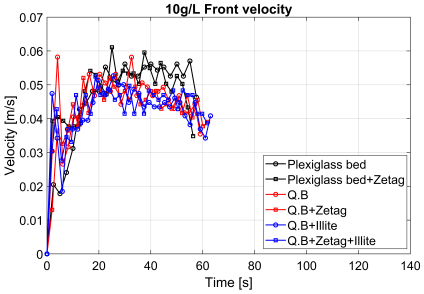

(b) Front velocity (10 g/L)

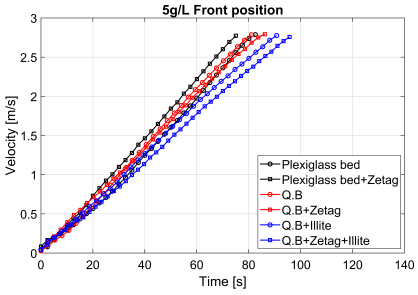

(c) Front position (5 g/L)

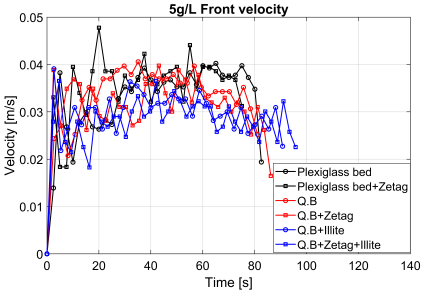

(d) Front velocity (5 g/L)

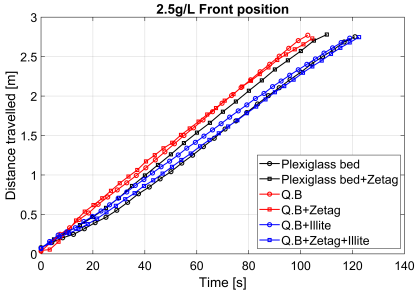

(e) Front position (2.5 g/L)

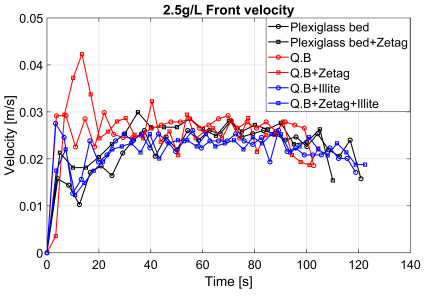

(f) Front velocity (2.5 g/L)

Figure 5.2: Front position and front velocity of turbidity currents for different initial sediment concentrations.

5.3.1. FRONT PROPAGATION ANALYSIS OF TURBIDITY CURRENTS

Here, the front positions of turbidity currents are analyzed. A similar pattern as seen in Wahab et al., 2026 has also been observed in these experiments. The videos recorded with Go Pro camera were analysed using the Tracker software, where the front position was recorded with respect to time.

Across all three concentrations, the presence of a bed was found to reduce the front

velocity of the turbidity current compared to a plexiglass bed (no bed condition). This finding supports the hypothesis that flocculants in the ambient water act as a lubricant, reducing bed roughness and thereby promoting faster current propagation (Wahab et al., 2024). In contrast, when loose bed materials (from a previous run) were introduced in combination with the flocculant, the front velocity showed the greatest reduction, indicating that the enhanced surface roughness counteracted the lubricating effect of the flocculant.

Figure 5.2 shows that the presence of a bed delays the turbidity current front compared to the case without a bed. For a plexiglass bed, with no quartz bed or zetag in the water column, the front positions at 10g/L and 5g/L were similar to those observed for the quartz bed, with front velocities of approximately 0.057 m/s and 0.040 m/s, respectively. However, for 2.5g/L concentration, the velocity matches the ones of Q.B+Illite and Q.B+Zetag+Illite cases (0.025 m/s).

When zetag was added to the water column over a plexiglass bed, the turbidity current front reached the end of the flume fastest at 10g/L and 5g/L, with maximum velocities of 0.061 m/s and 0.047 m/s, respectively. This corresponds to an increase in approximately 11% compared to the case with no zetag in the water column, for the plexiglass bed case. The front positions are shown in (Figure 5.2 (a), (c), (e)), while their corresponding velocities in (Figure 5.2 (b), (d), (f)).

In the case of quartz bed, for all three concentrations studied, the introduction of the quartz bed influenced the front position, which is comparable to "Plexiglass bed" cases (for 10g/L and 5g/L). For the Quartz bed with illite case, when compared to the quartz bed alone, the introduction of illite clay on top of the bed reduces the front velocity further by 1 and 3% respectively for 10g/L and 5g/L. In case of Quartz bed with zetag, the turbidity current front velocity has been observed to be lower than in the case without zetag suspended. For the Quartz bed with zetag and illite in all three concentrations studied, the turbidity current propagating on this type of bed is the slowest compared to the other bed types. The maximum velocities were 0.052 m/s for 10 g/L, 0.036 m/s for 5g/L and 0.025 m/s for 2.5g/L.

5.3.2. UVP VELOCITY PROFILES

The instantaneous velocity profiles obtained from the UVP transducer are shown here in Figure 5.3.

The velocity profiles represent the horizontal component of particle velocity within the turbidity current. The data shown here were extracted when the head of the current reached 120 cm from the lock gate (30 cm from the transducer). To capture the head region, a time window of 45-60 seconds was selected around the arrival of the front at 120 cm from the lock gate. The velocity data were collected only from the head and not from the body, as it contained more noise due to a reduction in the amount of seeding materials, which produced more noise than readable data.

Various processes take place inside a turbidity current. Thereby, the particles inside the current may not be representative of the front velocity. For the Q.B+Zetag+Illite bed cases, the initial velocities were generally the lowest, except at 5 g/L, where the velocities remained lowest across the entire height of the current. Also, the velocity of particles in the case of a quartz bed was found to be relatively higher across all three concentrations.

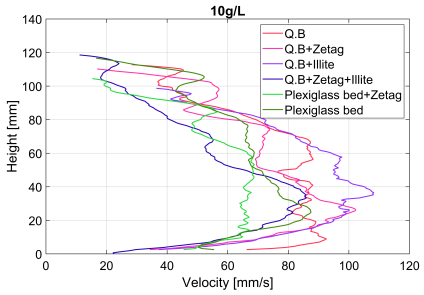

(a) 10 g/L

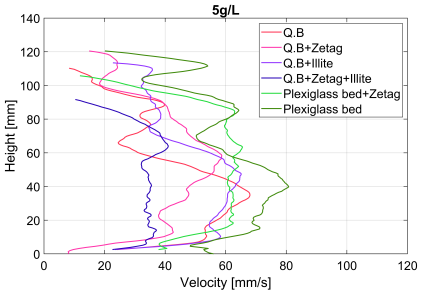

(b) 5 g/L

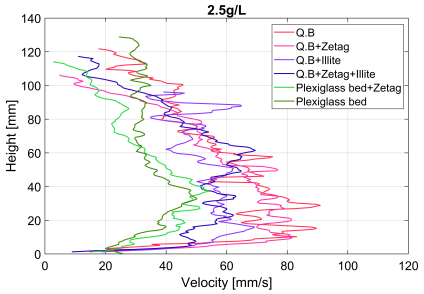

(c) 2.5 g/L

Figure 5.3: Instantaneous velocity profiles obtained from UVP measurements for different initial sediment concentrations.

5.3.3. FLOCCAM

Samples were collected from the body of the turbidity current via a siphon located 2cm above the bed and 90cm from the mixing section. They were then analyzed using the FlocCAM using Safas software. The flocs formed with zetag present in the outflow compartment for two types of bed scenarios are shown here: Quartz bed with zetag (Q.B+Zetag) and Quartz bed with zetag and illite (Q.B+Zetag+Illite).

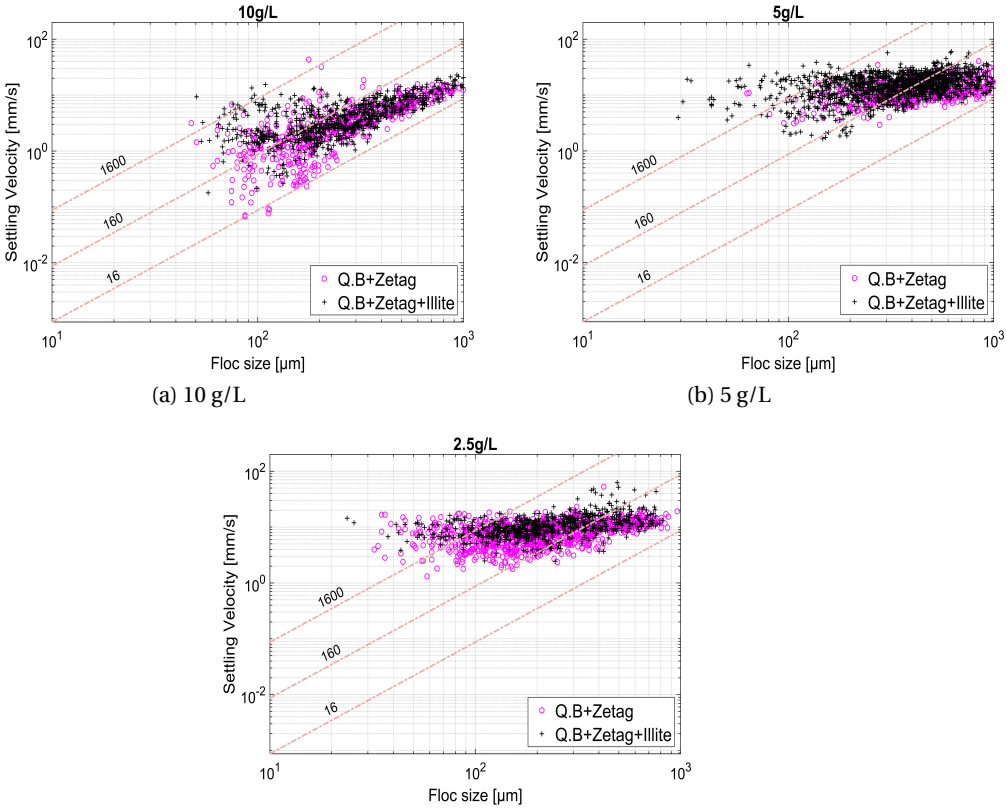

(a) 10 g/L

(b) 5 g/L

(c) 2.5 g/L

Figure 5.4: Floc size vs settling velocity of illite flocs. The isodensity lines (1600, 160, and 16 kg/m^3) indicate relative floc densities. The relative densities were derived from Stokes' settling velocity considering three different particle densities (2600, 1160, and 1016 kg/m^3), where densities of the formed flocs were calculated from their measured sizes and settling velocities. These lines serve as reference guides to interpret the density ranges of the formed flocs with respect to their sizes.

It is seen that for all three concentrations, the flocs formed with an illite layer on top had higher settling velocity than those formed with a quartz bed alone. The quartz bed with illite had loose particles on its surface, which were picked up when a turbidity current passed over it. This led to the formation of denser flocs (Floc images are shown in C). Additionally, the settling velocity distribution was observed to be narrower within a specific range of 3-30 mm/s for 5g/L and 2-20 mm/s for 2.5g/L. On the other hand, it

was widespread in the case of 10g/L, ranging between 0.1-10 mm/s (Figure 5.4).

SETTLING VELOCITY

Figure 5.5 shows the settling velocities of the flocs formed with three different sediment concentrations: 10g/L, 5g/L, and 2.5g/L.

Here, the median settling velocities indicate that the flocs formed with illite on the bed surface led to the formation of denser flocs compared to those formed with a quartz bed alone. The settling velocities of flocs formed with 10g/L has lower settling velocities when compared to that of 5g/L and 2.5g/L. After analyzing the video recordings of flocs, it was found that the 10g/L sediment concentration flocs fell individually, following Stokes' settling velocity. They also comprise of a large number of smaller flocs in the range of 100 μm. On the contrary, the flocs in the case of 5g/L sediment concentration fell as a stream collectively (also known as collective settling). Their settling velocities are in the comparable range (Figure 5.4) between 5-62 mm/s for 2.5g/L and 5-60 mm/s for 5g/L. For 2.5g/L concentration, the maximum settling velocities for d10, d50, and d90 for Q.B+Zetag+Illite flocs were 16, 17, and 62 mm/s, respectively. In case of 5g/L concentration, the maximum settling velocities for d10, d50, and d90 for Q.B+Zetag+Illite flocs were 38, 5,7 and 60 mm/s, respectively.

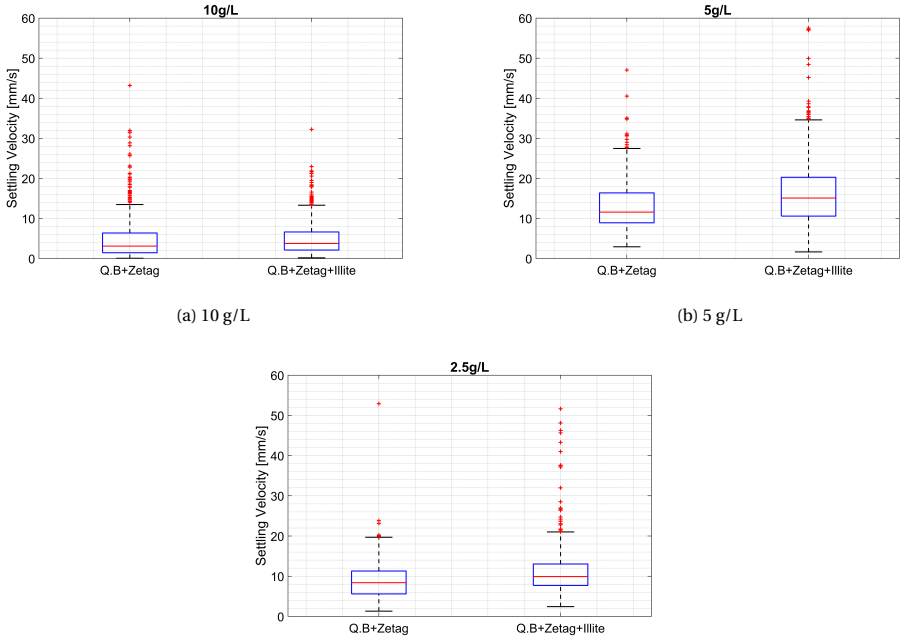

(a) 10 g/L

(b) 5 g/L

(c) 2.5 g/L

Figure 5.5: Settling velocity of flocs under different bed conditions for initial sediment concentrations of 10, 5, and 2.5 g/L.

FLOC SIZE

Figure 5.6 shows the floc size distributions formed under two different bed conditions: Quartz bed with Zetag and Quartz bed with Zetag combined with illite. The median floc size for Q.B+Zetag was consistently larger than that observed for Q.B+Zetag+Illite. Video recordings further revealed distinct differences in floc morphology. Flocs generated with Q.B+Zetag appeared fluffier, with visible voids and a looser structure, whereas those formed with Q.B+Zetag+Illite were darker and more compact (Appendix C). This difference can be attributed to the amount of material bound during floc formation, where fewer particles were incorporated in Q.B+Zetag case, resulting in looser flocs with voids. Whereas, in the case of Q.B+Zetag+Illite, the presence of illite on the bed provided additional fine materials that enhanced binding, resulting in the formation of compact flocs.

The composition of the bed material also influences the differences in floc density. In the Q.B+Zetag case, the absence of illite on top of the quartz bed allowed quartz particles to be incorporated into the flocs. Since quartz has a lower density than illite, this likely contributed to the formation of less dense flocs. In contrast, flocs formed with Q.B+Zetag+Illite were developed exclusively with illite present on the bed surface, with no exposure to the Quartz bed, resulting in higher overall floc density.

The flocs as seen from FlocCAM video recordings are shown in Appendix C.

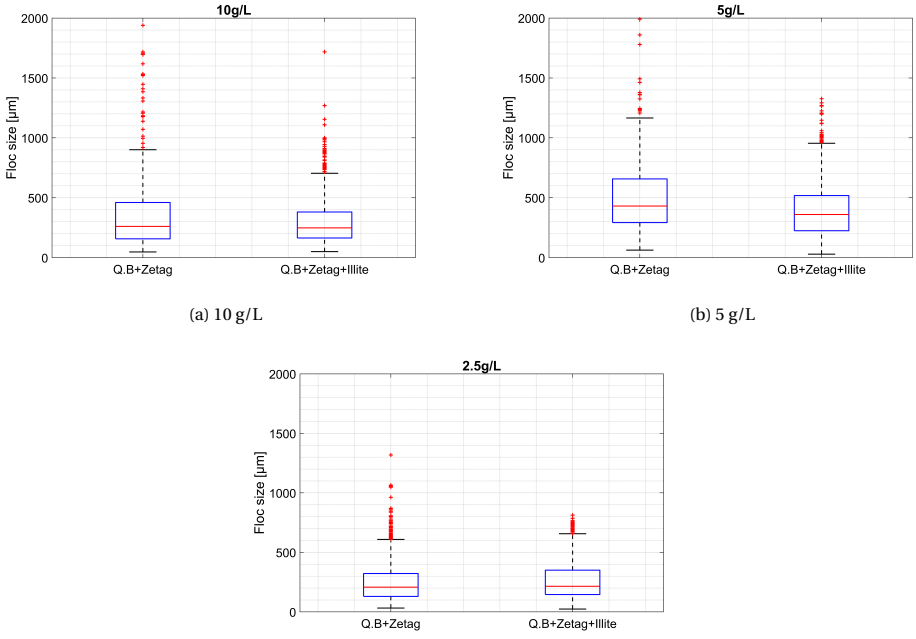

(a) 10 g/L

(b) 5 g/L

(c) 2.5 g/L

Figure 5.6: Floc size of illite flocs under different bed conditions for initial sediment concentrations of 10, 5, and 2.5 g/L.

5.4. DISCUSSION AND CONCLUSION

The effect of different types of beds and saltwater compositions on the velocity of propagating turbidity currents in relation to flocculation has been studied in this chapter.

This study showed that the presence of a bed influences the front velocity of turbidity currents. In the case of a rougher bed surface, the resistance offered is greater, which decelerates the turbidity current, leading to sediment deposition along the way. It can also lead to sediment re-suspension depending on the erosion velocity of the turbidity current. On the other hand, for a smoother or consolidated older bed, the sediment particles are not easily eroded, hence reducing the likelihood of re-suspension. The frictional resistance offered by such a bed is lower, allowing the current to travel longer distances. The bed roughness adds complexity to the flow dynamics (Maggi et al., 2022), influencing the hydrodynamic conditions under which sediment transport and deposition occur.

Influence of a bed on turbidity current propagation

Figures 5.2 (a), (c), and (e), show that the front propagation of turbidity currents at concentrations of 5g/L and 10g/L over a plexiglass bed was similar to that over a quartz bed. However, at 2.5g/L, the propagation was similar to that observed in the Q.B+Zetag and Q.B+Zetag+Illite cases. For the 5g/L and 10g/L turbidity currents, the higher sediment concentration provided greater mass and momentum, allowing the flow to propagate faster and remain largely unaffected by the roughness of the quartz bed.

During the propagation of a turbidity current, entrainment of ambient water takes place. This entrainment of water increases the mass of the turbidity current, leading to a reduction in its front velocity, thus conserving momentum. It was observed that when the instantaneous velocity falls below the range of 2.6cm/s, as in the case of 2.5g/L, the turbidity current flow enters a transitional regime (Re=1800), indicating that it is not fully turbulent. Moreover, due to its lower sediment concentration, flocculation was also limited.

In case of 10g/L and 5g/L sediment concentration, the turbidity currents propagating on the plexiglass bed with zetag homogeneously distributed in the water column, have been observed to be the fastest. This was due to the lubrication effect of the polyacrylamide flocculant, where the flume bottom becomes lubricated, enabling the turbidity current to travel faster (Wahab et al., 2024). Although flocculation was expected to promote settling and thereby reduce the propagation velocity of the turbidity current, this effect was not dominant under the laboratory conditions investigated here. The reduction in bottom friction caused by the polyacrylamide flocculant outweighed the potential decrease in front propagation resulting from floc settling. In contrast, for turbidity currents propagating over a quartz bed, the increased bed roughness provided additional flow resistance, resulting in lower front velocities despite the presence of Zetag. A possible mechanism is that, in the plexiglass experiments, the flocs formed within the current rolled and glided smoothly over the smooth lubricated surface, allowing the current to retain momentum and propagate more rapidly. Whereas in the absence of Zetag, the current mainly consisted of unflocculated fine particles suspended in the water column and did not benefit from this lubricating effect.

Influence of a bed on flocculation

In figure 5.2, it is seen that the presence of a flocculated illite bed significantly reduced the front velocity of the turbidity currents. The quartz bed with zetag case was

slower compared to the case that had no zetag. This could be due to the fact that the materials were coming in contact with zetag that was homogeneously distributed in the water column, which led to flocculation on the way. However, the case with a flocculated illite layer on top with zetag in the water column was the slowest. This was due to flocs that were already formed from the previous run and were lying on the bed. These flocs with a minimum median size of 250 μm (Figure 5.6) added considerable resistance to the flow.

According to Köllner et al., 2020, the bottom friction is moderate when the particles are smaller than or roughly equal to the viscous sublayer (thickness=250 μm, whereas median particle size=250-400 μm). However, it increases significantly when the particles are protruding from the viscous sublayer, making it hydraulically rough, resulting in a more rapid deceleration of the flow. In this case, the minimum median floc size is 250 μm, with most of the flocs protruding beyond the viscous sublayer, which has a thickness of 250 μm. As a result, these flocs provide friction to the flow, causing fluctuations to the front velocity (Figure 5.2 (b), (d), (f)). In contrast, cases with lower or moderate friction involved illite particles (d_{50}=6.4 μm) that remained fully embedded within the viscous sublayer (250 μm).

Influence of flocculation on particle velocity inside the turbidity current

UVP data revealed that at concentrations of 10g/L and 5g/L, the turbidity currents over quartz beds and plexiglass beds exhibited higher velocities near the bottom compared to those that were lined with an illite layer. This observation supports the hypothesis that flocculation occurs, accompanied by the pickup and deposition of heavier particles near the bottom (Wahab et al., 2024). Such processes alter the hydrodynamics of the turbidity currents, leading to a reduction in flow velocity.

Influence of bed on settling velocity

In case of 10g/L, the flocs lie within the isodensity lines, indicating a relative density range of 1600-16 kg/m^3. On the contrary, flocs formed at 5g/L and 2.5g/L exhibit higher densities and correspondingly higher median settling velocities. Across all experiments, the zetag-to-clay ratio was kept constant. Therefore, at higher clay concentrations, distance between clay particles is reduced, promoting faster aggregation with illite, as the flocculation rate is approximately linearly proportional to concentration, see Ali and Chassagne, 2022. The settling velocities were higher in the case of Q.B+Zetag+Illite compared to Q.B+Zetag, even though their sizes were smaller when compared to Q.B+Zetag flocs. This implies that the flocs were reconforming or folding rather than breaking. Floc breakup is a mechanism that typically occurs in turbulent conditions. In the lock-exchange environment, the relatively low shear rates combined with the short propagation time (60-120 s) of the turbidity current are not expected to cause significant floc disintegration. FlocCAM video recordings further confirmed the presence of stable flocs with no signs of fragmentation. If floc breakup had occurred, the settling velocities would have been lesser compared to cases where there was floc reconformation or folding.

Influence of bed on floc size

It was observed that flocs formed on quartz beds that had an illite layer (Q.B+Zetag+Illite) on top with zetag in the water column were smaller in size than the ones that had no illite (Q.B+Zetag). The newly formed flocs aggregated either with flocculated illite present on

the bed or with new illite inside the turbidity current. The median floc size in these cases ranged from 250-400 μm. Given that the d_{50} of illite is 6.4 μm and that of quartz is 23 μm, flocs formed directly on the quartz beds were generally larger than those formed on illite-topped quartz beds. Thus, across all concentrations, the floc size was consistently larger in the Q.B+Zetag cases compared to the Q.B+Zetag+illite cases. The floc images are shown in Appendix C, where larger flocs were formed in Q.B+Zetag case.

The bed has a critical role to play in turbidity current propagation. It has also been proven to influence flocculation. The roughness of the bed imparted due to materials lying on top significantly influences the flow dynamics of the turbidity current. These findings are particularly interesting from a dredging perspective. Additionally, the concentration of clay plays a significant role in floc formation and bed pickup. The sediment properties change during a turbidity current propagation, and for precise modelling, such information is crucial.

6

SENSOR SUITABILITY FOR TURBIDITY AND FLOCCULATION MONITORING

In this chapter, lock-exchange experiments were conducted to investigate the response of optical and acoustic sensors to suspended sediments within a propagating turbidity current under controlled conditions. The results demonstrate that different sensors exhibit distinct sensitivities to particle characteristics, particularly in their ability to detect small primary particles compared to larger aggregates. In addition, sensor responses to increasing concentration varied, with differences in the rate at which signals declined following peak observations. A combined use of OBS, ADV, LISST (in situ), and FlocCAM (in the lab) proved more effective in distinguishing between primary particles and aggregated flocs than any single sensor alone. These findings highlight the importance of multi-sensor approaches for advancing the understanding of flocculation processes in turbid flows, particularly in complex environments such as dredging and deep-sea mining operations.

Manuscript is under preparation

6.1. INTRODUCTION

Monitoring of suspended sediment concentrations is crucial for offshore activities, including both natural processes such as turbidity currents in submarine canyons and human-induced operations such as dredging, offshore construction, or deep-sea mining. Sediment plumes generated from such an activity have the potential to travel far away places depending on the characteristics of the sediment and the ambient water. They can also persist for extended periods of time, potentially affecting light penetration, biogeochemical cycles, and benthic and pelagic ecosystems. As a result, monitoring and estimation of suspended solids concentrations are essential not only for environmental impact assessment but also for understanding sediment pathways, plume evolution due to changes in sediment behavior (flocculation), seabed evolution, and mitigation planning.

In situ, measurement of suspended solids concentration and particle characteristics (primary particles and flocs) is technically challenging. In case of offshore engineering activities, such as dredging or deep-sea mining, the suspended sediment concentration measurements are used to assess plume dispersion and to validate numerical models in order to ensure compliance with environmental thresholds imposed in the area where the activity has been carried out. Turbidity current monitoring processes rely on a combination of acoustic and optical sensors, sediment traps, laser particle sizer mounted on moorings (Lintern and Hill, 2010, Xu, 2011, Khripounoff et al., 2012, Hughes Clarke, 2016, M. A. Clare et al., 2017, M. Clare et al., 2020). Advances in technology, particularly in acoustic devices such as the Acoustic Doppler Current Profiler (ADCP) or Acoustic Doppler Velocimeter (ADV), have facilitated depth-related measurements of flow velocity and acoustic backscatter, which is widely regarded as a proxy for sediment concentration measurements (Thorne and Hanes, 2002, Cacchione et al., 2006, Shih, 2012). Field studies have shown that effective turbidity plume monitoring can be achieved by integrating stationary sensor arrays with mobile platforms such as CTD rosette systems, autonomous underwater vehicles (AUVs), and remotely operated vehicles (ROVs), each providing complementary spatial and temporal coverage (Haalboom et al., 2023). A combination of acoustic profilers mounted close to the seabed, along with optical backscatter sensors (OBS), AUVs, and particle camera were particularly suited for resolving vertical profiles of suspended sediment concentration in the near-bed region (Gazis et al., 2025). In-situ particle size measurements using LISST showed that the mean particle diameter increased during plume passage, which was attributed to flocculation (Diaz et al., 2023). Studies show that the sensor output is not entirely controlled by sediment concentration, but also by particle size distribution, mineral composition of the sediment, and aggregation properties, which vary with environments. This creates additional uncertainty in environments where flocculation occurs, as variations in particle size and structure can substantially modify sensor response even when mass concentration remains unchanged. As a result, the interpretation of sensor data in dynamic environments remains a challenge.

Turbidity currents are transported by the ambient water currents, which increases the suspended solids concentration in an otherwise clear environment. This is particularly evident in the context of deep-sea mining. Field experiments conducted during scaled mining trials have shown that mining-generated plumes consist of fine sediment

particles that undergo flocculation, forming aggregates or flocs, which are larger than the primary particles that were initially suspended (Muñoz-Royo et al., 2022, Haalboom et al., 2023, Mousadik et al., 2024, Gazis et al., 2025). A usual combination of an array of sensors, such as Optical Backscatter Sensors (OBS), acoustic profilers (ADCP), and Laser In-Situ Scattering and Transmissiometry (LISST) are used in the field to measure turbidity, particle concentration, and evolution of particle size. These combined measurement techniques help understand the temporal evolution of particle size distribution and concentration.

Despite major advances in sensor technology and deployment strategies, there lies a lot of uncertainties on how the sensors would respond to different sediment types and concentration levels. Sensor signals are influenced not only by the suspended sediment concentrations but also by the variations in particle size distribution, flow conditions (turbulent or laminar) and the aggregation properties of the sediments, which would lead to their flocculation. However, studies that isolate and quantify these effects under controlled conditions remain limited (Gillard et al., 2019).

Based on this background context, the objective of this study is to assess how well the selected sensing methods combined can provide crucial information on suspended sediment concentration and particle size distribution in a controlled environment (laboratory setup). This leads to a series of related aspects, which are described here. The study focuses on the following subtopics:

1. The calibration process and its robustness and saturation limits of optical and acoustic sensors.

2. The sensitivity of the sensors to different sediment types, opacity, and particle size distributions

3. The capability of multi-sensor array to distinguish between primary and aggregated flocs during a turbidity current propagation

4. Comparison between in situ observations and ex situ measurements in a laboratory setup.

6.2. METHODS

The experiments were carried out in a modified lock-exchange flume, which is explained in the following section.

6.2.1. MODIFIED LOCK-EXCHANGE FLUME

The lock-exchange flume was modified to hold three optical backscatter sensors (OBS), which are commonly used field turbidity sensors, at 50 cm, 110 cm, and 200 cm from the lock gate. The OBSs were fixed into the flume in such a way that the sensor bodies were supported outside the tank, while their measurement heads were positioned inside the flume through watertight seals, ensuring direct exposure to the flow without leakage. Another hole was drilled at 140 cm from the lock gate to hold the LISST (a field-deployed laser particle sizer widely used for in-situ particle size and concentration measurements) at the center of the flume. Similar to the OBS configuration, the LISST body

was mounted externally, and only the optical measurement section was inserted into the flume through a sealed port.

The ADV was suspended into the flume with the help of a holder and placed near the first OBS at 55 cm from the lock gate. An ADV was selected instead of an ADCP because the measurement volume of an ADCP is considerably larger than the dimensions of the experimental setup and would not provide sufficient measurement volume within the confined flume. The ADV, with its small sampling volume and high temporal resolution, was therefore more suitable for laboratory-scale measurements in this study. The OBSs and LISST were placed perpendicular to the direction of flow at the side wall of the flume, whereas the ADV points at the flow from above. Sediment samples were also collected from the turbidity current with the help of a siphon, placed between OBS 1 and 2 (Figure 6.1).

The ADV and OBS were positioned close to the lock gate, whereas the LISST was located further downstream. The reason behind this was that as flocculation is a time-dependent process, particles reaching the LISST had experienced a longer residence time and potentially greater aggregation than those measured upstream. As the ADV was primarily used to estimate suspended sediment concentration, it was positioned close to the lock gate to capture the sediment-laden flow before significant settling or flocculation could occur. In contrast, the availability of three OBS sensors provided greater flexibility in sensor placement, allowing turbidity measurements to be obtained at multiple locations along the flume and enabling the evolution of the turbidity current to be monitored. Consequently, some of the observed differences between sensors may reflect spatial variations in the turbidity current rather than solely differences in sensor performance.

Field sensors were deliberately chosen instead of (adapted) laboratory instruments to replicate, as closely as possible, the sensor responses and practical limitations encountered during real offshore monitoring of dredging and deep-sea mining plumes. Using standard field sensors in an experimental setup provided a better understanding of the behavior of the sensors under controlled conditions, to be relevant for in-situ monitoring applications.

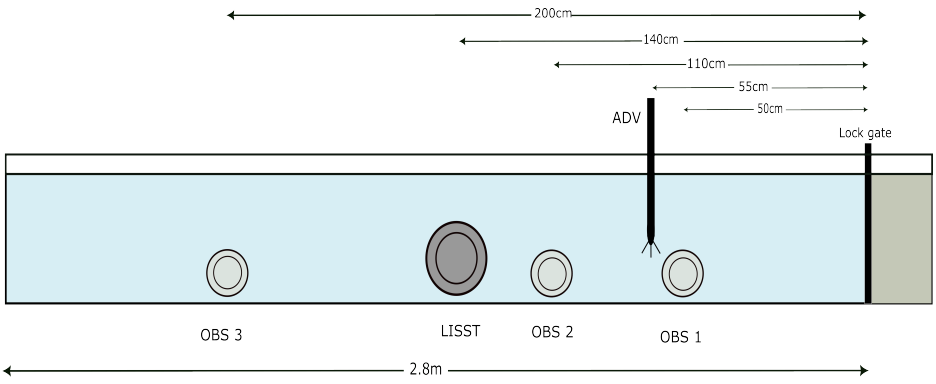

Figure 6.1: Modified Lock-exchange flume with OBS, LISST, and ADV

The following protocol was used to carry out the experiments.

1. The lock-exchange flume, equipped with three OBSs, a LISST, and an ADV was first tested for water-tightness by partially filling it, after which it was filled to the required water depth.

2. The lock gate was placed into the flume, and sediments were mixed in the lock section for approximately 20 minutes in order to ensure homogeneous suspension.

3. For experiments with illite-Zetag, the flocculant Zetag 4120 was added to the outflow compartment of the lock-exchange flume.

4. After the lock gate was released, the sediment-laden flow propagated through the flume. Along its path, it first passed an OBS sensor, followed by the ADV probe, which recorded SNR values. The flow then encountered a second OBS, subsequently the LISST, and finally the third OBS near the downstream end of the flume.

5. The sensors are turned off (LISST and ADV) after the turbidity current has reached the end of the flume. The OBSs, being battery-operated, kept on running and were only dismounted at the end of the day to download the data and change the batteries for the next day.

6. After completion of each experiment, the flume was carefully cleaned, ensuring that there was no sediment from previous runs on the sensors. The flume was then filled with salt water again and prepared for the next experimental run.

7. The same experimental protocol was followed with the sensors in place, however, a siphon was installed between OBS 1 and OBS 2 to collect sediment-water samples for analysis using the Malvern Mastersizer and FlocCAM.

6.2.2. MATERIALS

Table 6.1 presents the experimental matrix. The materials used in these experiments were illite, CCZ sediment, quartz, and Zetag 4120 which have been described in Chapter 2.

Table 6.1: Experimental matrix showing different sediments and concentrations used

Illite [g/L]	CCZ [g/L]	Quartz [g/L]	Illite-Zetag [g/L]
2.5	2.5	2.5	2.5
5	5	5	5
10	10	10	10

6.3. SENSOR CALIBRATION

Calibration curves were established using a range of known sediment concentrations to quantify the relationship between sensor output and suspended sediment concentration under controlled conditions. This enables the raw signal to be reliably translated

to the corresponding concentration values that are specific to a certain sediment type. Here, calibrations were performed only for quartz, CCZ, and illite sediments, as these represent the primary particle types used in the experiments. No separate calibration was conducted for the illite-Zetag mixtures because the addition of flocculant produces time, sediment, and dosage-dependent aggregates, making it impractical to develop a stable and reproducible concentration response relationship.

Calibrations were carried out exclusively for the OBS and ADV sensors, as their signals require conversion to concentration through empirical relationships. The LISST, on the other hand, provides direct measurements of particle size distribution and volumetric concentration based on laser diffraction principles and therefore does not require additional calibration. Similarly, sediment samples collected via siphoning and analyzed using the Malvern mastersizer and FlocCAM are treated as independent measurement techniques. They provide particle size distribution (Malvern mastersizer) and particle (floc) size and settling behavior (FlocCAM) directly from the recorded videos (FlocCAM) or diffraction analysis (Malvern mastersizer) and do not rely on sensor-specific calibration curves.

6.3.1. OPTICAL BACKSCATTER SENSOR

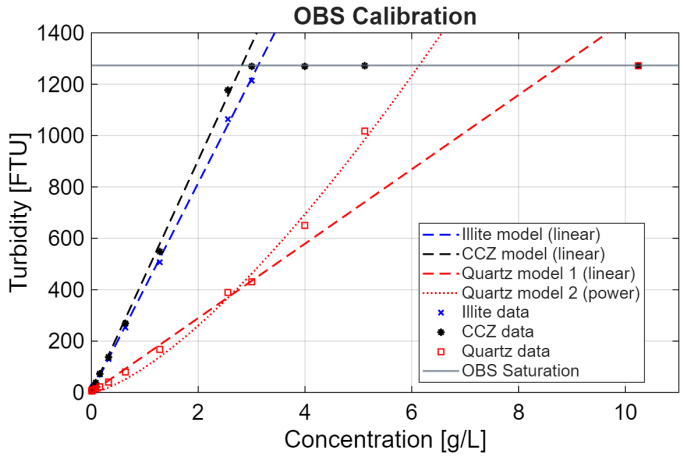

Figure 6.2: Calibration Curve obtained from OBS

Three Optical Backscatter Sensors (OBS) were used in these experiments to perform concentration analysis in a lock exchange setup. All three sensors were calibrated using known concentrations to produce the calibration curve (Figure 6.2). The maximum turbidity that the OBSs can record is 1273 FTU, which corresponds to around 3 g/L for illite and CCZ sediments. Here, a bucket with a volume of water was used in which sediments were added gradually with increasing concentrations. The suspension was continuously stirred using an overhead stirrer in order to ensure a homogeneous mixing. Each of the three OBSs was lowered one at a time, and turbidity values were recorded. The measured FTU values were then subsequently converted to concentration values with the help of calibration curves, including both linear and quadratic fits, depending on the character-

istics of the material. The calibration procedure is important as the sensors measure the intensity of light that is scattered back by the suspended sediment particles instead of sediment concentration directly. The sensor response depends on the type of sediment and its characteristics, such as particle size, shape, composition, etc.

As shown in Figure 6.2, the calibration curves for illite and CCZ sediment show a linear trend between turbidity and concentration over the range of investigated concentrations. However, in the case of quartz, it follows a linear trend up to a concentration of 3 g/L then it switches to a quadratic fit. This difference can be attributed to the sediment's characteristics. Quartz is relatively coarser, angular, and non-flocculating, which causes stronger scattering and optical attenuation at higher concentrations, leading to a non-linear calibration curve. Illite and CCZ, on the other hand, contain finer particles that remain within the optimal sensitivity range of the OBS, resulting in a more consistent scattering behavior and a linear response.

6.3.2. ACOUSTIC DOPPLER VELOCIMETER (ADV)

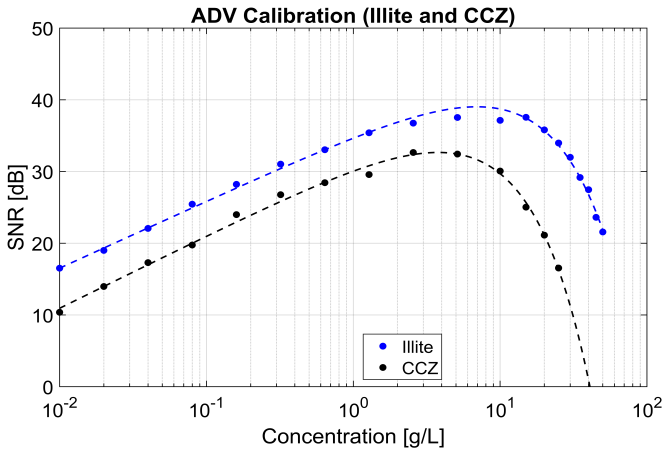

Figure 6.3: Calibration Curve obtained from ADV for Illite and CCZ sediment

For the ADV, a similar procedure was followed, where a series of known sediment concentrations was added to the calibration bucket to record the corresponding Signal-to-Noise Ratio (SNR) values for each concentration. The resulting relationship was then fitted using the Sonar equation (Equation 6.1) (Chmiel et al., 2018).

$$\mathrm{SNR} = \frac{10}{\Pi_1}\left(\log_{10}(AC) - 4\log_{10}(R) + \frac{C_{\mathrm{ADV}}}{10} - \frac{1}{5}R\alpha_w - \frac{2}{10}R\alpha_p\right) \tag{6.1}$$

The Sonar equation contains three unknown parameters: Π_1, Π_2 and C_{ADV}. The particle attenuation coefficient α_p is expressed as $\alpha_p = \Pi_2 Ur_{analyt} C$, where Π_2 acts as an empirical correction factor for the analytical Urick attenuation coefficient Ur_{analyt}. The calibration data with concentration and SNR values were used as an input to calculate the values of these unknown parameters. The values of fixed constants such as analytical

particle attenuation coefficient, Ur =1.727 m^2/kg, water attenuation, α_w=26.9 dB/m and measurement distance, R=0.15 m were adopted from Chmiel et al., 2018. The unknown parameters Π_1, Π_2, and C_{ADV} were estimated by fitting the Sonar equation to the ADV concentration-SNR data using nonlinear least-squares regression with the Levenberg-Marquardt algorithm with robust optimization.

The calibration curves were developed for three sediment types: illite, CCZ sediment, and quartz. The overall shape of the calibration curves for illite and CCZ sediment remained consistent and followed the Sonar equation (Figure 6.3). However, quartz exhibited a different behavior, with few data points in the concentration range of 1-10 g/L deviating from the fitted Sonar equation. This deviation is likely related to the characteristics of the quartz particles used in this study. The quartz consisted of freshly milled, highly angular and irregular grains with rough surfaces, whereas illite and CCZ sediments are finer, platy, and cohesive materials that tend to form flocs (Glé et al., 2013; Vergne et al., 2023). These differences in particle behavior lead to distinct acoustic scattering responses. As a result, the standard calibration relationship may not be directly applicable to quartz. A sensitivity analysis has been performed for quartz in Section 6.3.3. Additionally, it was observed that the concentrations at which the ADV response would reach its saturation point varied depending on the sediment type.

6.3.3. SENSITIVITY ANALYSIS OF ADV CALIBRATION CURVE FOR QUARTZ

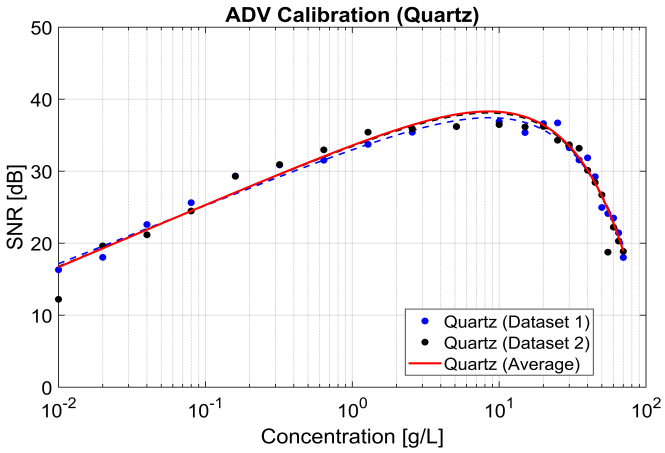

Figure 6.4: Calibration Curve obtained from ADV for Quartz

The calibration curves for quartz are shown here. As mentioned earlier, several data points in the concentration range of 1-10g/L deviate from the fitted Sonar equation. Two independent datasets are presented to construct the calibration curve, along with the averaged dataset. The concentration conversion shown in this study is based on the averaged dataset, as it provides a consistent relationship between the SNR and sediment concentration (Figure 6.4).

When the concentration conversion was performed using either of the individual datasets, the resulting concentrations exceeded the input, which is physically unrealistic

and indicates an overestimation.

The ADV also shows a particularly high sensitivity to quartz particles, compared to illite and CCZ sediment, likely due to their optical and acoustic scattering properties. As a result, sensor saturation occurs at higher concentrations for quartz. This behavior suggests that sediment properties strongly influence acoustic backscatter and should be cautiously accounted for when using this technique.

6.4. RESULTS

This results section is subdivided according to the sensor types in order to evaluate how each measurement technique responds to suspended sediments during turbidity current propagation. The performance of the OBS, ADV, and LISST is therefore presented separately. Within each sensor type, the results are further analyzed for different initial concentrations (2.5, 5, and 10 g/L) and for the four sediment types (illite, quartz, illite-zetag, and CCZ).

6.4.1. OPTICAL BACKSCATTER SENSOR

Here in Figure 6.5, 6.6, and 6.7, the readings from each of the senors for each sediment types and concentrations are shown. In Figure 6.1, the positions where the OBSs were stationed inside the flume are shown.

2.5G/L

In Figure 6.5, the curves show the concentration variations with time obtained from OBS measurements from three different sensors. Due to the gradual propagation of turbidity current, the sensors record the signal at different times. The temporal evolution of concentration (from turbidity) measured for illite and illite-zetag are comparable. Although the initial sediment concentration in the mixing tank was 2.5g/L, the measured concentrations progressively reduced as the flow propagated, owing to dilution and particle settling.

For illite and illite-zetag experiments, the peak concentrations recorded by the sensors were between 1 and 1.5 g/L. This indicates comparable behavior of turbidity currents generated by the materials.

In the case of CCZ sediments, the OBS measurements exhibited stronger signal fluctuations, with peak concentrations reaching up to 1.9 g/L. For OBS 1, a small peak is observed at the beginning at 40 seconds, indicating that the turbidity current is not yet fully developed at this location. This initial peak reflects start-up effects associated with the opening of the lock gate. OBS 2 and 3 provide a more reliable representation of the flow, as they are positioned further away from the lock and hence the start-up effects are already mitigated.

For quartz, the measured signal is comparatively lower, close to 1g/L across all the sensors.

6.4.2. 5G/L

Figure 6.6 presents concentration variations over time obtained from three OBSs, with an initial concentration of 5g/L. For the illite experiments, the sensor signals remain be-

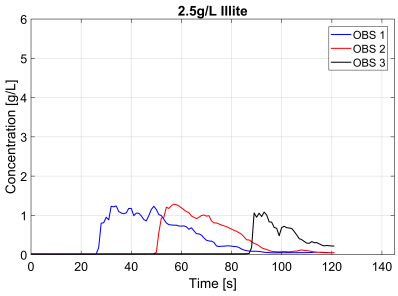

(a) Illite

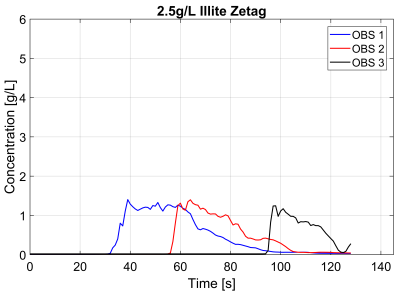

(b) Illite-Zetag

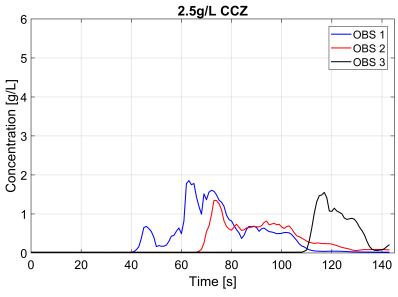

(c) CCZ

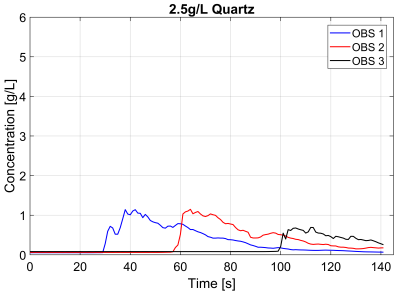

(d) Quartz

Figure 6.5: OBS measurement 2.5g

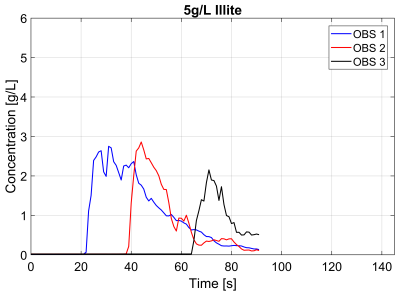

(a) Illite

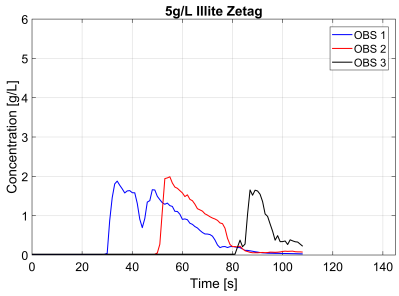

(b) Illite-Zetag

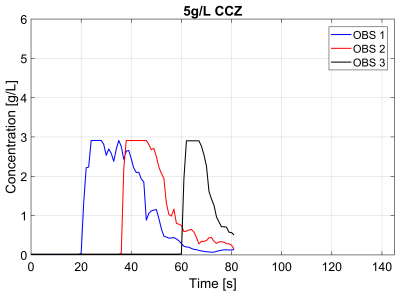

(c) CCZ

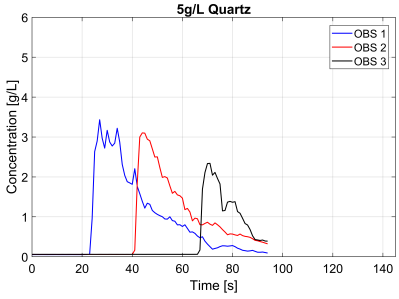

(d) Quartz

Figure 6.6: OBS measurement 5g

Table 6.2: Peak concentration values for 2.5g/L input concentration

	Illite	Illite Zetag	CCZ	Quartz
OBS 1	1.24	1.40	1.85	1.11
OBS 2	1.28	1.39	1.35	1.10
OBS 3	1.08	1.24	1.55	0.63

Table 6.3: Peak concentration values for 5g/L input concentration

	Illite	Illite Zetag	CCZ	Quartz
OBS 1	2.74	1.87	2.91	3.43
OBS 2	2.85	1.98	2.90	3.1
OBS 3	2.15	1.65	2.90	2.3

low the saturation limit, even when saturation occurs, it is only for a brief duration. Following the passage of the turbidity current, the signal then gradually decreased as the sediment settles along the flume.

For illite-zetag experiments, peak concentrations remain below 2g/L and exhibit a smooth decay. In case of CCZ sediment, all three OBSs reached saturation during the passage of the turbidity current.

In contrast, quartz exhibits a pronounced decay in concentration with distance. The materials settled rapidly during propagation, resulting in a significantly lower sediment concentration by the time the turbidity current reached OBS 3. Additionally, it is seen that OBS 1 measured concentration higher than 3g/L, reflecting the delayed saturation threshold for quartz.

6.4.3. 10G/L

Table 6.4: Peak concentration values for 10g/L input concentration

	Illite	Illite Zetag	CCZ	Quartz
OBS 1	3.12	3.12	2.91	4.80
OBS 2	3.12	3.12	2.90	3.66
OBS 3	3.11	3.11	2.90	4.48

Figure 6.7 shows the concentration variations over time for an initial concentration of 10g/L. For most sediment types (illite and CCZ), the measured concentrations reached the sensor limit, indicating a plateau around 3g/L. Although an exception has been observed in the case of quartz experiments.

Quartz particles are lighter in color and exhibit lower opacity compared to illite and CCZ sediments. The output concentrations for quartz have been in the range of 3.5-5g/L, which the sensors measure without getting saturated. This points towards the response of sensors towards different types of sediments.

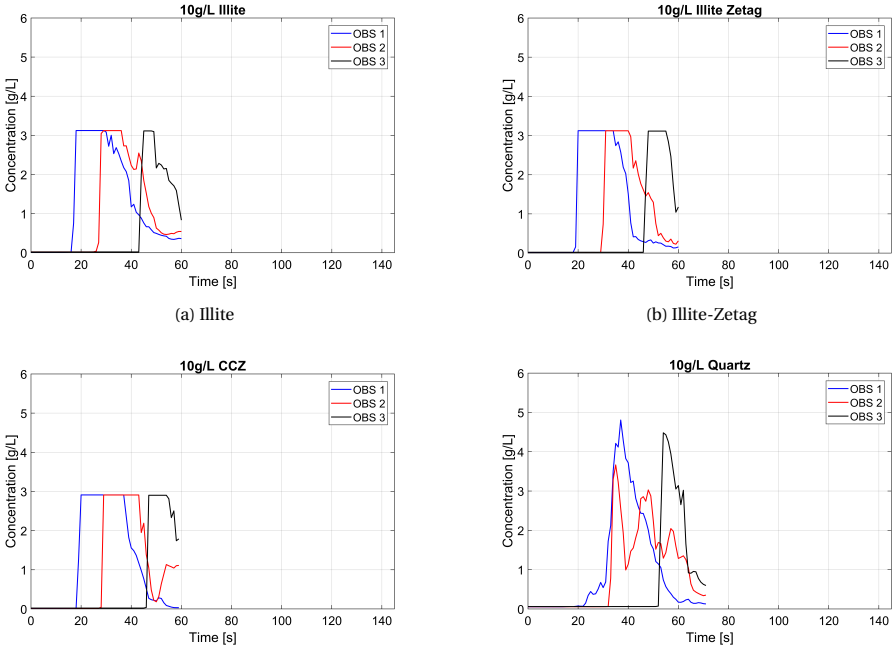

(a) Illite

(b) Illite-Zetag

(c) CCZ

(d) Quartz

Figure 6.7: OBS measurement 10g

6.4.4. ACOUSTIC DOPPLER VELOCIMETER

Figure 6.3 presents the calibration curve for illite and CCZ sediments. Illite reached saturation at concentrations of approximately 10g/L, whereas CCZ sediment exhibits an earlier saturation, with peak SNR values corresponding at around 4g/L. Figure 6.4 shows the quartz calibration. The concentration conversions are shown here.

6.4.5. 2.5G/L

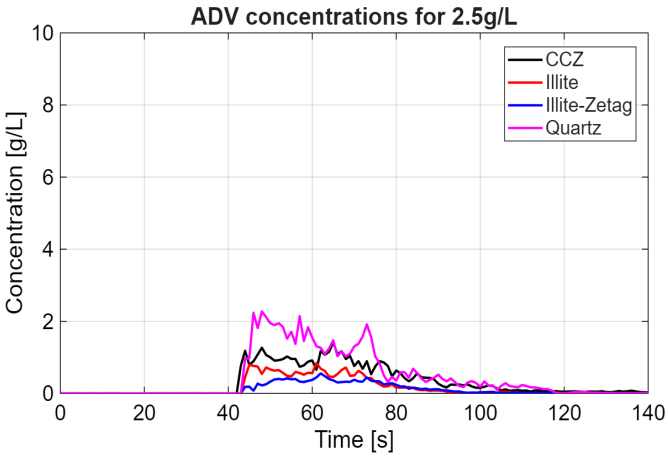

Figure 6.8: Concentrations obtained from ADV for 2.5g/L input concentration

Figure 6.8 presents the sediment concentrations derived from the converted SNR values. The measured concentrations for illite and illite-zetag are comparatively low (approximately 0.75-1g/L), whereas slightly higher concentrations were observed for CCZ sediment (approximately 1.5g/L). As per the ADV measurements, quartz exhibits the highest recorded concentration of around 2.1g/L.

6.4.6. 5G/L

Here it is seen that the measured concentration values for illite, illite-zetag, and CCZ is similar (starting at around 2g/L). In this case as well, the output concentration for quartz was the highest (3g/L), compared to the other concentrations.

6.4.7. 10G/L

In case of 10g/L input concentration, the lowest recorded concentration was for illite-zetag. The measured concentrations for illite and CCZ showed considerable fluctuations, with possible saturation effects observed for CCZ. The highest output concentration values were recorded for quartz at around 6.5g/L, with an indication of sensor saturation.

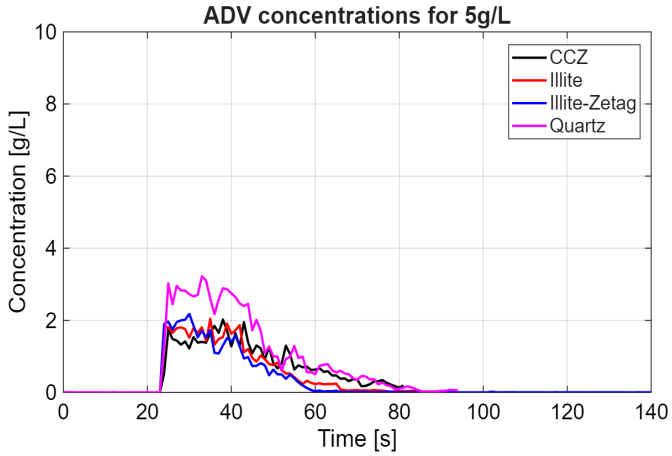

Figure 6.9: Concentrations obtained from ADV for 5g/L input concentration

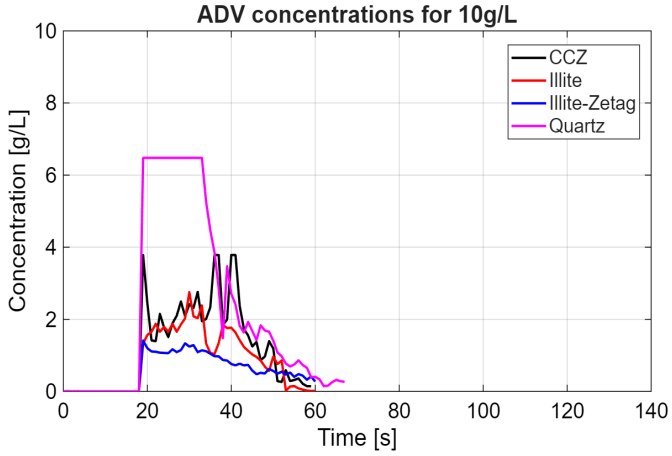

Figure 6.10: Concentrations obtained from ADV for 10g/L input concentration

6.4.8. LISST

The data presented here is from the Laser In-situ Scattering and Transmissometry (LISST) 200X. The primary particle size of each material is shown as a reference in black dashed lines.

6.4.9. 2.5G/L

Figure 6.11 presents the evolution of particle size distribution over time measured using LISST. It shows that both illite and illite-zetag exhibit similar bimodal distributions, characterized by a secondary peak around 3 μm. However, the volume density is higher for illite than for illite-zetag. For CCZ sediments, it is seen that a substantial volume of materials are in the larger size range of 60 μm, indicating the floc formation. The particle

size distribution of quartz remains relatively unchanged over time, suggesting limited aggregation behavior of the material.

Table 6.5: Particle size observed by LISST for 2.5g/L input concentration

	Illite	Illite Zetag	CCZ	Quartz
Primary peak	6	20	60	15
Secondary peak	3	3	3	3

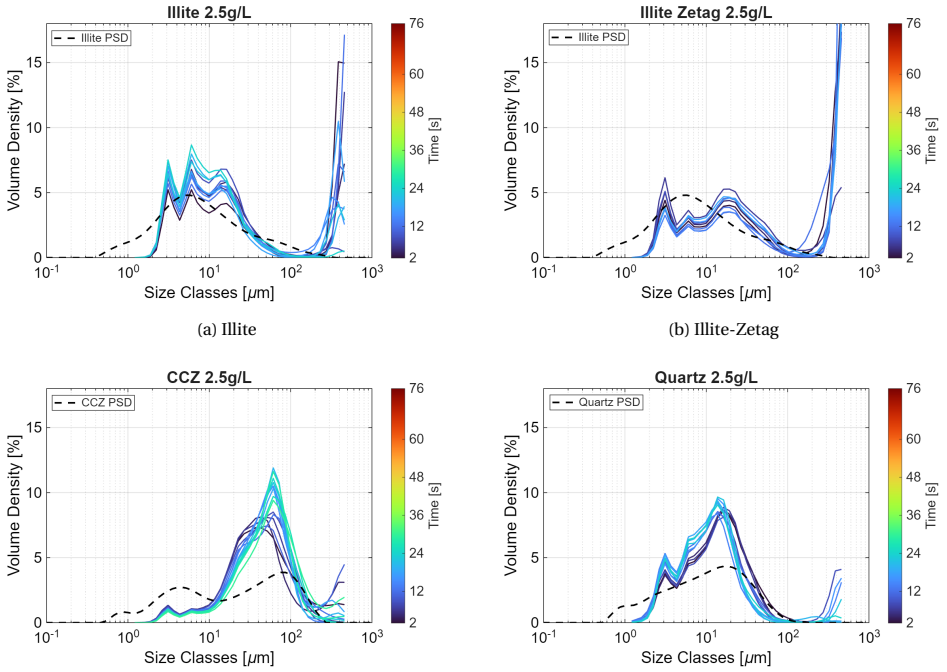

(a) Illite

(b) Illite-Zetag

(c) CCZ

(d) Quartz

Figure 6.11: LISST measurement for 2.5g/L input concentration

6.4.10. 5G/L

Figure 6.12 shows the temporal evolution of PSD for an initial concentration of 5g/L. Both illite and illite-zetag exhibit polymodal distributions characterized by three distinct peaks, with overall curve shapes remaining largely similar throughout the experiment. The illite-zetag case contains more LISST measurements, which can be attributed to the slower propagation of the turbidity current while still being in the measurable range of the device. This prolonged measurement window provided improved temporal resolution of the aggregation process. For CCZ sediments, the PSD is dominated by a higher volume fraction of larger particles in the range of 150 μm. The PSDs shifted slightly towards the right, indicating an increase in particle size with a decrease in volume. In case

of quartz, there is not much variation in terms of particle size and volume over time. The particle size remained constant in the range of 10-20 μm.

Table 6.6: Particle size observed by LISST for 5g/L input concentration

	Illite	Illite Zetag	CCZ	Quartz
Primary peak	15	25	150	15
Secondary peak	3	3	3	3

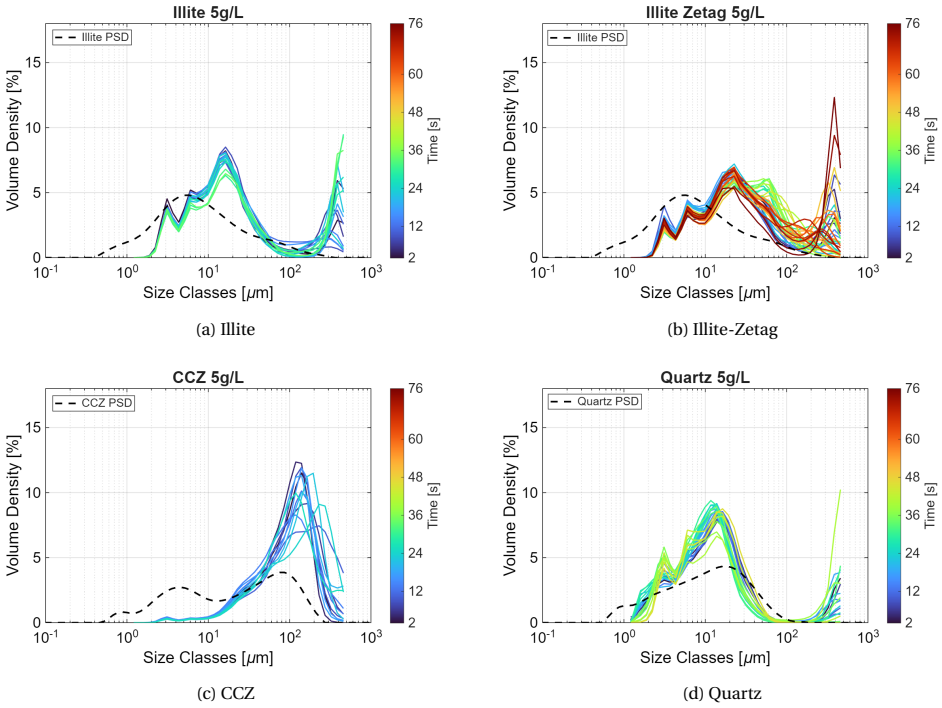

(a) Illite

(b) Illite-Zetag

(c) CCZ

(d) Quartz

Figure 6.12: LISST measurement for 5g/L input concentration

6.4.11. 10G/L

At an initial concentration of 10g/L, illite continues to exhibit a bimodal particle size distribution, with no substantial change in the particle size (approximately 20 μm). However, a gradual reduction in particle volume density was recorded over time. On the contrary, the illite-zetag showed a slight rightward shift in PSD, indicating formation of larger aggregates known as flocs. For CCZ sediments, the PSD is dominated by a pronounced peak around 100 μm, with a slight variation in particle volume throughout the run. The LISST measurements for quartz have been consistent across all the concentrations, with minimal temporal variations in PSD, with particle size remaining in the size range of 10 and 20 μm, with only minor fluctuations in volume density.

Overall, these results highlight how the instrument visualizes different sediment types. Clay-rich sediment, such as illite and CCZ demonstrate floc formation and its evolution over time, whereas non-cohesive material, such as quartz, remains largely unaffected by concentration and time in terms of PSD.

Table 6.7: Particle size observed by LISST for 10g/L input concentration

	Illite	Illite Zetag	CCZ	Quartz
Primary peak	20	100	100	20
Secondary peak	3	3	3	3

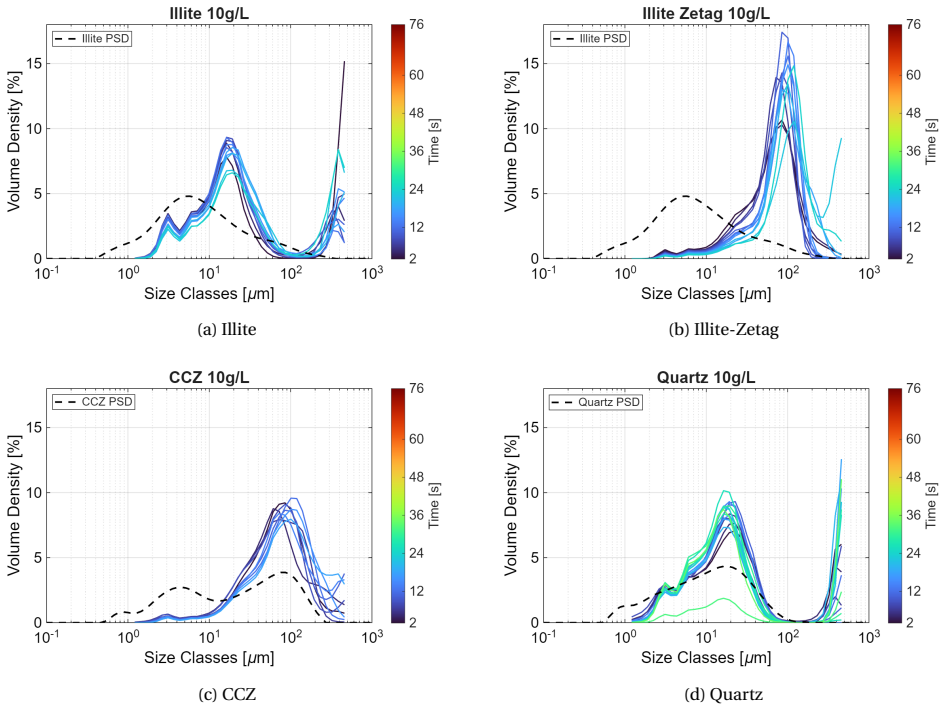

(a) Illite

(b) Illite-Zetag

(c) CCZ

(d) Quartz

Figure 6.13: LISST measurement for 10g/L input concentration

6.4.12. COMPARISON BETWEEN MALVERN MASTERSIZER, LISST, AND FLOC-CAM

LISST measures particle size in situ, whereas Malvern Mastersizer provides ex-situ particle size measurements. For the Malvern analysis, samples were first collected and then analyzed outside the experimental setup. Since particle aggregation and breakup evolve over time, the temporal evolution of PSDs from both the devices is presented here.

For the CCZ sediments, the particle size distribution (PSD) obtained from Malvern Mastersizer exhibits a bimodal distribution, indicating the presence of two dominant

particle size classes with relatively higher volume fractions. This pattern indicates the existence of primary particles and larger aggregates or flocs. On the other hand, the illite-zetag case shows a predominantly monomodal PSD curve with comparatively more stable flocs over time.

The PSDs derived from LISST measurement for CCZ sediments are largely monomodal with only slight temporal shifts over time, indicating limited change in the particle size. However, for the illite-zetag case, the LISST results show a bimodal distribution at initial concentrations of 2.5g/L and 5g/L, reflecting the presence of both primary particles and flocs. At 10g/L, the PSD becomes monomodal, with the peak shifting towards larger particle size along with a higher volume fraction of larger particles.

The PSD obtained from FlocCAM provides floc sizes in their near-natural forms, without being subjected to the shear forces associated with Malvern Mastersizer. The measured floc size range was approximately between 100 and 1000 μm.

While these three techniques provide complementary perspectives on particle size and flocculation behavior, each measurement method has inherent strengths and limitations. LISST measures PSD in situ, providing real-time information, but is limited by its fixed-size detection range and by uncertainties in interpreting what particle structures it "sees," particularly in highly flocculated suspensions.

Malvern Mastersizer measures PSD ex situ over time, offering high-resolution size distributions, but the required sampling and pumping can induce additional aggregation, folding, or break-up of flocs, potentially altering the original structure.

FlocCAM measures ex situ as well, and although sampling and pipetting introduce some disturbance, it likely provides the most realistic representation of floc morphology and size. However, it is labor-intensive and less suited for high-frequency measurements.

6.4.13. FLOCCAM

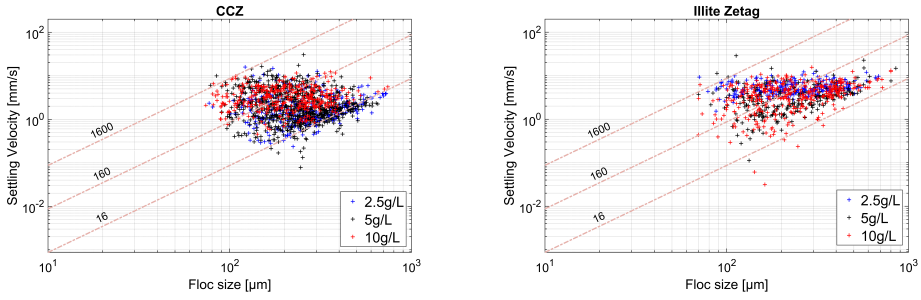

(a) CCZ (b) Illite–Zetag

Figure 6.14: Floc size vs settling velocity of CCZ sediment and illite flocs. The isodensity lines (1600, 160, and 16 kg/m3) indicate relative floc densities. The relative densities were derived from Stokes' settling velocity, considering three different particle densities (2600, 1160, and 1016 kg/m^3), where densities of the formed flocs were calculated from their measured sizes and settling velocities. These lines serve as reference guides to interpret the density ranges of the formed flocs with respect to their sizes

Sediment samples collected from the turbidity currents using a siphon were analysed

with FlocCAM, and the recorded videos were then processed using the SAFAS software for floc size and settling velocity. The results are presented here for two sediment types: CCZ and illite-Zetag. Illite and quartz were not analysed as no particle aggregation is expected to take place. For the CCZ sediment, (Figure 6.14(a)) the floc size distribution exhibits a broader spread, indicating a wider range of settling velocities compared to the illite-zetag case. This points towards the differences in aggregation behavior and floc structure between the two sediment types. The settling velocities of CCZ flocs were found to be in the range of 0.5 and 50 mm/s wheres that for illite-zetag flocs were in the range of 5-45 mm/s (Figure 6.14(b)).

6.4.14. SETTLING VELOCITY

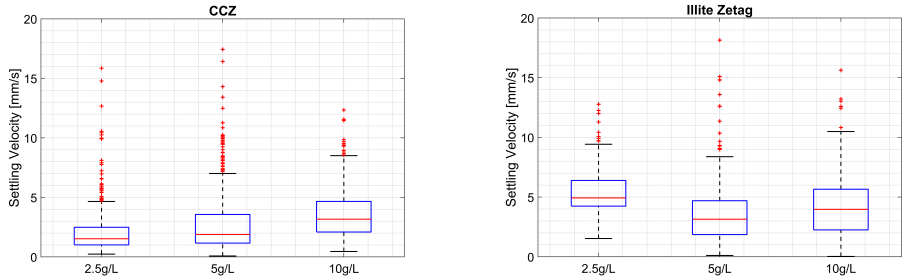

(a) CCZ (b) Illite–Zetag

Figure 6.15: Settling velocity of flocs obtained from FlocCAM

The median settling velocity is shown in Figure 6.15. In case of CCZ sediments, the median settling velocity gradually increases with concentration, indicating heavier particles at higher sediment concentrations. However, in the case of illite-zetag, the flocs formed with 2.5g/L concentration exhibit the highest settling velocity.

6.4.15. FLOC SIZE

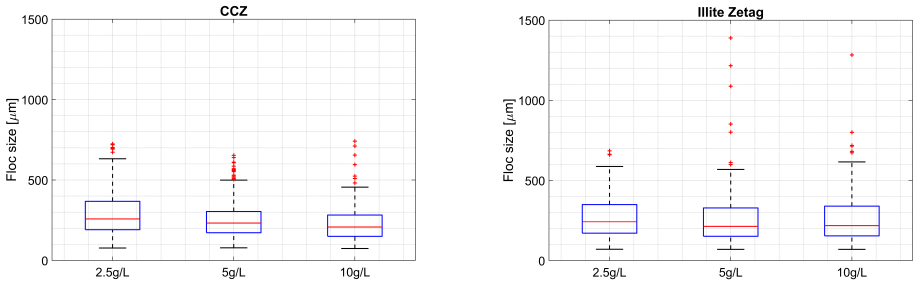

(a) CCZ (b) Illite–Zetag

Figure 6.16: Floc size obtained from FlocCAM

Here, the median floc sizes for CCZ and illite-zetag are presented. For CCZ, the median floc-sizes are very similar across the tested concentrations, with only minor variations observed. In the case of illite-zetag, the median floc size also remains relatively consistent, with the largest median size occurring at 2.5g/L, followed by 10g/L and then 5g/L. This shows that for the illite-zetag system, the aggregation efficiency does not increase linearly with concentration under the current circumstances.

6.5. DISCUSSION

6.5.1. PERFORMANCE OF OBS AND ADV FOR SUSPENDED SOLIDS MEASUREMENTS

The concentration measurements obtained using the OBS and the ADV demonstrate clear strengths and limitations associated with both techniques, particularly with respect to the sediment type, concentration range, and aggregation processes. Although both the sensor techniques (optical and acoustic) are widely applied in field and as well as in laboratory settings, the current experiments were performed in a controlled environment, which revealed that their behavior is strongly influenced by the characteristics of the sediments and cannot be interpreted solely as a function of concentration.

For OBS, the calibration curves showed a linear relationship between turbidity and concentration for illite and CCZ, whereas quartz exhibited a non-linear relationship above 3g/L. It was seen that at lower concentrations, the output concentrations for illite and illite-zetag were comparable, indicating that the addition of zetag did not substantially alter the bulk suspended concentration measured by the OBS. However, it may still have an impact on the floc size and settling behavior of the formed flocs later. CCZ sediments showed higher fluctuations in the signal output, with a peak at 1.9g/L. This could be attributed to their heterogeneity in PSD with irregularly shaped particles and higher opacity. Quartz on the other hand, produced lower OBS-derived concentrations, likely due to its light color and reduced light scattering efficiency compared to illite and CCZ sediments (Sutherland et al., 2000, Downing, 2006).

In case of 5g/L, the output signal for illite-zetag remained below 2g/L. As previously shown in Wahab et al., 2024, higher sediment concentrations lead to enhanced flocculation and larger flocs, and this is what happened in this case as well. Larger flocs were being formed, which settled down during the propagation of the current. Thus the OBSs observed the remaining materials in suspension, resulting in lower measured concentrations. For CCZ, all sensors reached saturation limits at this concentration, while at 10 g/L, saturation occurred for all cases except quartz. It did not saturate even at 10g/L input concentration. This delayed saturation for quartz confirms that OBS saturation is primarily governed by the optical properties of the particles rather than the sediment concentration. Thus, saturation thresholds are highly dependent on the sediment properties.

The ADV-derived concentrations exhibit a different response in comparison to the OBS. Since it does not measure concentration directly, the signal-to-noise ratio (SNR) values were converted to concentration using a calibration curve based on the Sonar equation. For illite and CCZ sediments, the SNR-concentration relationship followed the fit well, whereas deviations were observed for quartz. These deviations are likely linked

to differences in acoustic scattering efficiency associated with particle size, with quartz particles (23 μm) producing stronger acoustic backscatter than the finer CCZ sediments (5 μm). Additionally, it was seen that the calibration curves for illite and CCZ reached saturation at around 4g/L, whereas quartz reached saturation at 10g/L. This can be due to the fact that illite and CCZ contain smaller particles, which caused stronger acoustic attenuation. The sound energy is rapidly absorbed and scattered, causing the returned echo to weaken quickly. Thus, the SNR reaches its maximum range earlier compared to the case with larger particles, where the signal remains measurable over a wider concentration range.

By comparing both sensor types, it is evident that they are highly material-specific. The OBS tends to saturate early for optically opaque and fine sediments, whereas ADV favors coarse and acoustically reflective particles. Furthermore, both sensors are sensitive to flocculation, but in different ways. The OBS response is affected indirectly through sediment removal from suspension due to settling of larger flocs, whereas the ADV response is modified by changes in effective particle size. As a result, neither of the sensors can be considered universally applicable without sediment specific calibration. In environments such as deep-sea mining or dredging, where sediment behavior change rapidly (aggregation), careful determination of calibration curves and saturation thresholds under controlled conditions is necessary.

6.5.2. MULTI-SENSOR IDENTIFICATION OF PRIMARY AND AGGREGATED PARTICLES

The combined use of OBS, ADV, LISST, FlocCAM, and Malvern Mastersizer provided a robust framework to differentiate between primary and aggregated particles during a turbidity current propagation. On their own, it would be difficult to identify the aggregation process. The present experiments present a combination of information on concentrations, particle size distributions, and (ex situ) floc characteristics that collectively enable identification of flocculation dynamics in a controlled environment.

The OBS measurements are based on optical backscatter intensity and are sensitive to particle concentration and optical properties. It cannot directly identify aggregation. However, it can indirectly point towards the occurrence of flocculation, with rapid decay of signal even at higher concentrations, meaning that the larger particles (flocs) have settled down.

In the case of ADV, low signal outputs were observed for the illite-zetag case (except for 5g/L, where illite was the lowest, due to some anomaly in the signal), due to the formation of aggregates, which settled down. Since ADV is more sensitive to larger particles, this indicates that withthe larger particles settled down, the ADV only observed fines, which resulted in stronger acoustic attenuation and hence lower SNR.

Direct evidence of aggregation was provided by LISST measurements, as it provides temporal evolution in PSD. For CCZ sediments, the PSDs were in the size class of 100 μm across all concentrations. Illite-zetag cases showed polymodal distributions at 2.5g/L and 5g/L, indicating the coexistence of primary particles and aggregates during propagation. In case of 10g/L the PSD was found to be monomodal. The PSD did not change much for illite and quartz as they did not form flocs. The temporal evolution observed by LISST shows the transition from primary particles to aggregated flocs.

FlocCAM is an ex-situ measurement device that enables detailed floc analysis that helps to distinguish between primary particles and formed flocs. In this study, a broader range of settling velocities was observed for CCZ flocs compared to illite-zetag flocs. These flocs were naturally formed during the propagation of turbidity currents and are composed of a wide range of densities, compared to the flocculant-induced illite-zetag flocs, which had flocs with more uniform settling velocities.

In the CCZ case, the median settling velocities gradually increased with sediment concentration. For the illite-zetag case, the median settling velocity at 2.5g/L was higher than at larger concentrations. This is likely due to the formation of flocs with mineral particles bound by a lesser amount of flocculant (Wahab et al., 2024). It could also be that some flocs fell into the wake of larger flocs, which can further enhance their effective settling velocity (Ali et al., 2024a). In terms of floc sizes, the median values were comparable across all concentrations.

The experiments in this study thus demonstrate that a multi-sensor array can reliably distinguish between primary and aggregated flocs when sensor outputs are compared to analyse a similar pattern. This integrated approach is particularly relevant for deep-sea mining and dredging applications, where sediment particles evolve rapidly, and single sensor interpretations may lead to uncertainty in plume analysis.

6.5.3. COMPARISON BETWEEN IN SITU AND EX SITU MEASUREMENTS

The particle size distribution (PSD) obtained from the Malvern Mastersizer (ex situ device) and LISST (in situ device) is compared in Section 6.4.12. For CCZ sediments, the Malvern Mastersizer measurements show a consistent bimodal distribution across all three initial concentrations, indicating the presence of two distinct particle populations representing fine primary particles and coarser flocculated aggregates.

At higher concentrations (10g/L), the CCZ PSD exhibits a slight leftward shift with time, indicating a reduction in particle size, which may be attributed to floc breakage or folding under continuous shear during the measurement period in the Malvern Mastersizer. In contrast, at 5g/L and 2.5g/L, the PSD peaks shift towards larger sizes, indicating progressive aggregation and floc growth over time. It should be noted that measurements with the Malvern Mastersizer involve longer residence and analysis times compared to the LISST or FlocCAM, allowing additional opportunities for particle-particle collisions, aggregation, restructuring, along with breakage processes. In these measurement methods, the obtained values are also influenced by the prolonged hydrodynamic exposure (shear, in case of Malvern Mastersizer) along with the properties of the sediment. Furthermore, the bimodal distribution indicates the coexistence of two different size classes in a single sample.

For illite-zetag suspensions, the PSD is monomodal and peaks exhibit only minor temporal shifts, with the overall distribution being relatively stable. This points towards the observation that flocculant induced aggregates are mechanically stronger compared to naturally occurring CCZ flocs and are less sensitive to shear induced breakage under moderate conditions over time. A narrow distribution in case of illite-Zetag further points towards a more homogeneous size distribution compared to the bimodal CCZ distribution.

Measurements obtained from LISST showed a similar trend across both the sediment

types for 10g/L and 2.5g/L. In both of these concentrations, the PSD peak shifts towards larger sizes with time, indicating aggregation processes. However, at 5g/L, a slight leftward shift is observed, suggesting limited floc fragmentation or restructuring. Owing to considerably shorter analysis time of LISST relative to the Malvern Mastersizer, the particles experienced reduced interaction time, which may not be sufficient to ensure growth in particle size. Also, in the study of Wahab et al., 2024, it was seen that the floc size is strongly influenced by the sediment concentration. So in case of lower concentrations such as 5g/L and 2.5g/L, the LISST distribution is found to be considerably smaller, proving the presence of mostly primary particles, due to shorter residence time and lesser materials being available.

6.6. CONCLUSION

This chapter investigated the performance of optical and acoustic sensors for monitoring suspended sediment concentration and flocculation processes during turbidity current propagation. The calibration analysis showed that both OBS and ADV require sediment-specific calibrations, with saturation thresholds varying significantly between the sediments. The results obtained showed that the sensors exhibit distinct sensitivities to particle characteristics. The OBS response is governed mainly by optical properties such as color and opacity of the material. Whereas for ADV, the response mainly depended on the particle size and acoustic scattering efficiency of the material. The experiments also showed that a multi-sensor array combining OBS, ADV, and LISST is capable of distinguishing between primary particles and aggregated flocs, which cannot be achieved reliably with any single sensor. Measurement techniques such as FlocCAM and Malvern mastersizer proved that ex-situ laboratory analysis is essential for the interpretation of in-situ sensor measurements and to further validate flocculation behavior. This study highlights the significance of reliable plume monitoring using an array of acoustic and optical sensors.

Suspended sediments concentration measurements are strongly influenced by the properties of the sediments and the aggregation process. The experiments conducted in this study reveal that a combination of acoustic and optical devices supported by ex situ measurements is reliable to distinguish between primary and aggregated particles. It also underlines the significance of sediment-specific calibration and a multi-sensor approach for accurate plume monitoring in offshore engineering applications.

7

CONCLUSIONS AND RECOMMENDATIONS

This chapter presents the main findings of the thesis and addresses the research questions in Chapter 1. It also presents the recommendations for future work.

7.1. CONCLUSION

This section aims to answer the main research questions tackled in this thesis.

7.1.1. RESEARCH QUESTION 1

How does the presence of organic matter in the water column influence flocculation and the propagation of turbidity currents?

Lock exchange experiments were conducted to study the influence of organic matter on the propagating turbidity current. The experimental results have shown that

1. The presence of organic matter (flocculant/polymer, in this case) in the water column led to the occurrence of flocculation within 30-60 seconds i.e., within the propagation duration of the turbidity current. This implies that flocculation can occur rapidly in a propagating turbidity current.

2. The presence of flocculant increased the front velocity of the turbidity current across all concentrations in the absence of a bed. The hypothesis behind it was that due to the addition of flocculant in the outflow compartment, there was a lubrication effect that formed a thin, slippery, polymer-rich layer at the flume bottom, thus reducing bottom friction.

3. The characteristics of the formed flocs depend strongly on the type and dosage of flocculant used. Anionic polymers produced larger and more open-structured flocs compared to those formed with cationic polymer, which produced smaller and more compact flocs. However, their impact on the front velocity was similar, causing the turbidity currents with polymers to propagate faster than their no-polymer counterparts.

4. The floc size varied depending on the location within the turbidity current from which they were sampled. Flocs sampled via siphons from the body of the turbidity current were larger than the ones collected through the bottom outlets. This could be attributed to the convective motion within the turbidity current that promotes the formation of open-structured flocs due to interactions between clay particles and flocculant in the water column. On the contrary, flocs sampled from the bottom outlet likely traveled further downstream, leading to reconformation of the polymeric tails and thus smaller flocs.

5. The comparison between Malvern Mastersizer and FlocCAM showed that FlocCAM consistently measured larger flocs. This is attributed to the continuous pumping and therefore shearing of flocs within the mastersizer.

7.1.2. RESEARCH QUESTION 2

How does the presence of a bed and its age influence flocculation dynamics and propagation behavior of the turbidity current?

This research question was addressed by conducting lock exchange turbidity current experiments, which led to the following key findings:

1. Lock exchange experiments showed that the presence of a bed significantly affected turbidity current propagation, with current velocity being lower than that propagating over the smooth flume bottom (compared to the no-bed case).

2. The age of the bed played a critical role in influencing the propagation velocity of turbidity currents. Freshly formed bed (here, 1-day bed) had a stronger impact on reducing the front velocity compared to an older bed (here, 3-day bed). This is due to the fact that as bed ages, the flocs undergo reconformation, with the surface becoming smoother, leading to a reduction in frictional resistance to flow.

3. The presence of a bed had an influence on flocculation. Turbidity currents propagating over a bed produced larger and denser flocs compared to the no-bed case. This is attributed to materials being picked up during propagation.

4. Higher initial sediment concentration inside the turbidity current resulted in a wider range of floc settling velocity due to the availability of more materials.

5. The increased floc size and density in the presence of a bed suggested that sediment resuspension and erosion played a crucial role in flocculation.

The results from this experimental study suggest that freshly disturbed beds near deep-sea mining operations sites may reduce turbidity current propagation through reduced front velocities and enhanced flocculation potential.

7.1.3. RESEARCH QUESTION 3

What is the role of bed composition on flocculation dynamics and the propagation behavior of turbidity currents?

This question has been answered by conducting lock exchange experiments with different bed types, and the following observations have been recorded:

1. It has been found that the presence of a (any type of) bed reduced the front velocity of the turbidity current, compared to a smooth (plexiglass) bed.

2. Beds with flocculated illite on top had the greatest impact on front propagation velocity. The velocities were reduced by 5-17 %. The flocs on top of the beds protruded beyond the viscous layer, making the bed hydraulically rough with increased bed friction.

3. Beds with illite on top resulted in enhanced flocculation. The particles were incorporated within the propagating turbidity current, leading to a reduction in its front velocity compared to the cases that had no loose materials on top.

4. Flocs formed in the bed case with no loose materials on top were larger and fluffier, with visible voids.

5. The flocs formed on top of the bed with illite were denser compared to the flocs formed with no illite on top of the bed.

7.1.4. RESEARCH QUESTION 4

How effectively can different sensing methods provide quantitative parameters regarding plume properties (concentration and particle size)? This question has been answered using multiple sensors in a lock exchange flume and the following key findings are stated here:

1. Sensor response depends strongly on the sediment type, as both OBS and ADV outputs vary significantly with particle size and optical/acoustic properties, and not just the concentrations.
2. The saturation threshold for OBS depends on the optical opacity of the sediments rather than the concentration alone.
3. ADV calibration follows the Sonar equation fit for finer particles and deviates for larger ones.
4. ADV saturation occurs at lower concentrations for finer sediments.
5. In situ LISST measurements showed the occurrence of aggregation of particles inside the turbidity current.
6. Lower OBS signal and its decay point towards the formation of flocs.
7. Lower ADV signals in flocculation-favorable environments indicate settling of larger flocs, with only finer particles in suspension. These fine sediments cause strong acoustic attenuation, which reduces the returned backscatter and thus results in lower SNR values.
8. Ex situ device, such as FlocCAM can be used along with the in situ devices to study the flocs in detail.
9. Single sensors cannot reliably distinguish primary particles from aggregates. Therefore, a multi-sensor array is essential to identify aggregated flocs in a highly dynamic environment, such as in dredging and deep-sea mining.

7.2. RECOMMENDATIONS

This section outlines the recommendations for future research based on the key findings and limitations identified in this study.

1. The CCZ clay used in the experiments was not stored under optimal conditions. ideally, it should have been preserved in a refrigerated environment under controlled conditions, rather than being kept in a jar in room temperature. This may have affected the physicochemical properties of the clay, potentially affecting its aggregation behavior and experimental repeatability.
2. The CCZ clay used in these experiments was obtained from box cores collected from the top 30 cm of the bed. However, the top few centimeters, which typically contain the highest amount of organic matter, was not present in the batch provided. Hence, the influence of organic matter on flocculation and, in turn, turbidity current propagation may be underrepresented in the experimental study.

3. The amount of organic matter in the sample that was provided was not quantified. Moreover, the material was used over a period of approximately three years, during which the organic matter content may have changed due to degradation, microbial activity. Such temporal variability should be avoided in the future studies by conducting experiments within a shorter time frame.

4. In order to study turbidity current propagation under varying bed conditions, it would be interesting to examine the distance the turbidity current dies out. For this purpose, experiments conducted in a longer flume, such as a 10 m flume tank, are recommended. This would let the turbidity current to evolve during the course of its propagation including deceleration, sediment settling and interactions with the bed.

5. In the present study, only a limited range of bed durations was considered. Investigating a broader spectrum of bed durations would provide a deeper insight into how bed age play a role in turbidity current propagation. Such experiments would help understand the impact of temporal evolution of beds on the turbidity current dynamics and improve understanding oh how bed age influences flocculation.

6. In the future experiments it would be interesting to install a camera beneath the flume, facing the transparent plexiglass bottom, inorder to visually capture the internal dynamics of the turbidity current. This can help understand sediment- flow interactions including flocculation, erosion and deposition.

7. Temperature differences between the mixing section and the outflow compartment should be avoided. Maintaining uniform temperatures between both the sections is necessary to avoid aby unwanted behavior of the turbidity current during its propagation and to ensure experimental reproducibility.

8. Using a material of contrasting color would facilitate identification of bed erosion and help in identifying whether eroded materials is incorporated into flocs. This approach would provide better visual and qualitative evidence of sediment entrainment from bed.

9. The experimental setup could be adapted to enable in situ measurements of floc settling velocities. This would minimize disturbances associated due to sampling and better represent the natural settling of flocs inside a turbidity current.

Understanding how organic matter accelerates turbidity currents is essential for predicting plume spread in dredging and deep-sea mining.

The findings of this thesis have implications beyond laboratory-scale investigations. For deep-sea mining and dredging operations, the results highlight the importance of flocculation, seabed characteristics, and sediment-specific behavior when assessing plume dispersion and environmental impacts. The influence of flocculation on settling and plume dynamics suggests that future numerical models should incorporate aggregation processes and bed interactions to improve the prediction of sediment transport and its

deposition. Furthermore, the demonstrated variability in sensor response between sediment types emphasizes the need for sediment-specific calibration and integrated monitoring approaches. These insights can support practical engineering applications, including the design of plume monitoring programs, optimization of operational strategies to reduce sediment dispersion, and the development of more reliable environmental impact assessments for offshore activities.

Appendices

A

FLOC CHARACTERISTICS

A

A.0.1. FLOCCAM SNAPSHOTS

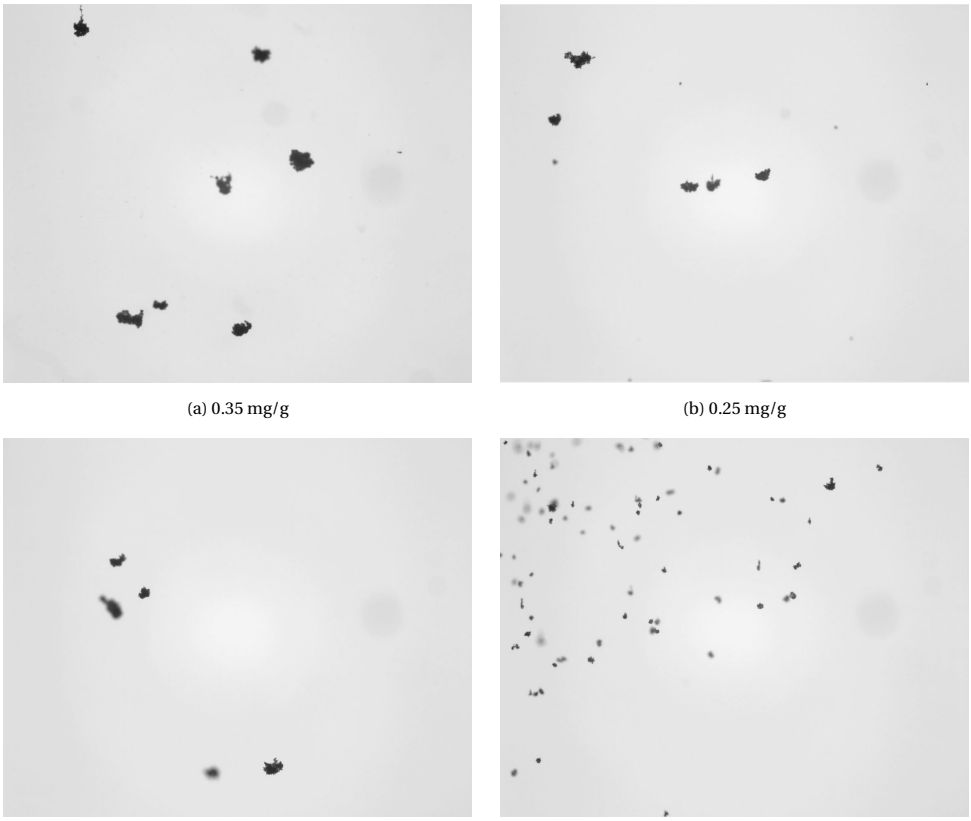

(a) 0.35 mg/g

(b) 0.25 mg/g

(c) 0.20 mg/g

(d) 0.10 mg/g

Figure A.1: Floc snapshots obtained from FlocCAM videos with different dosages of Zetag 4120.

A.0.2. Comparison of floc size obtained from Malvern and FlocCAM

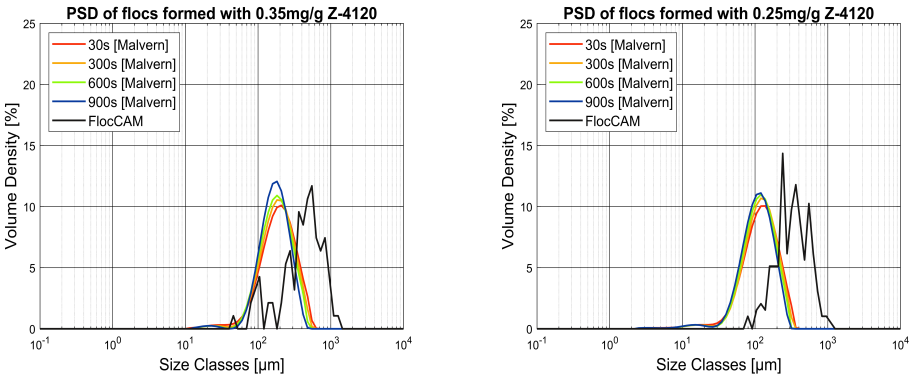

(a) 0.35 mg/g

(b) 0.25 mg/g

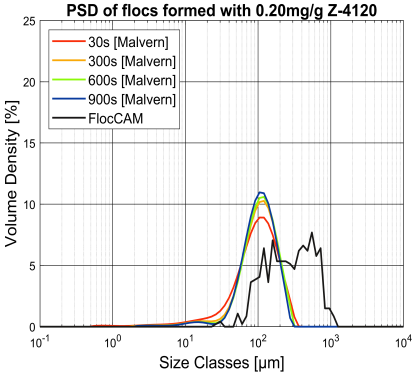

(c) 0.20 mg/g

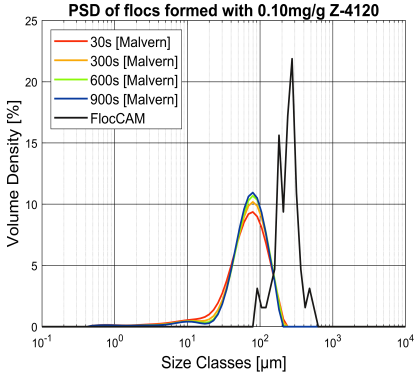

(d) 0.10 mg/g

Figure A.2: Comparison between floc size obtained from Malvern and FlocCAM for different dosages of Zetag 4120.

A

A.0.3. FLOC SIZE OF SAMPLES FROM TURBIDITY CURRENT WITH ZETAG 4120

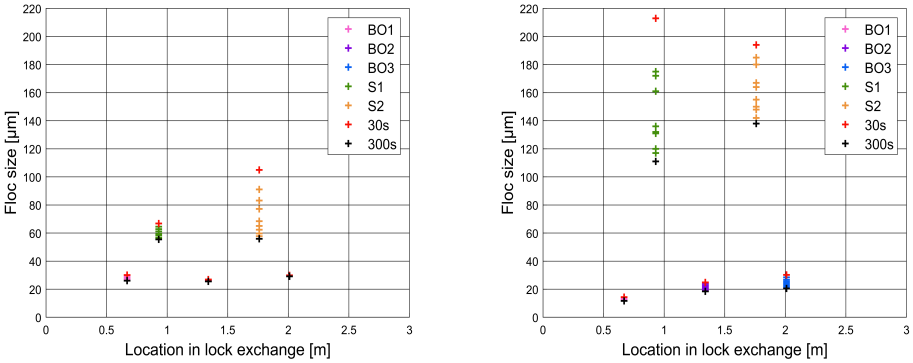

(a) 10 g/L

(b) 5 g/L

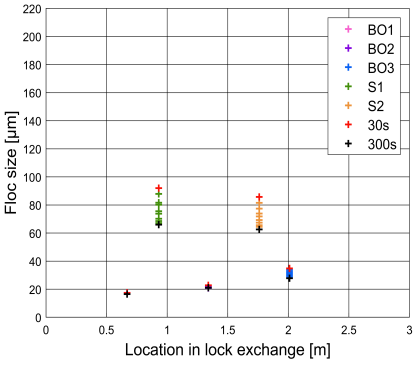

(c) 2.5 g/L

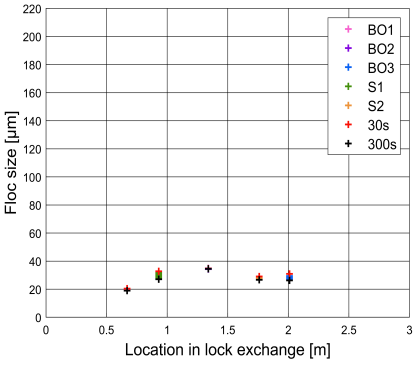

(d) 0.5 g/L

Figure A.3: Evolution of the d_{50} of flocs collected along the flume. BO and S stand for Bottom Outlet and Siphon. The floc size evolution is measured using the Malvern particle sizer. Red and black crosses represent flocs formed at 30 s and 300 s, respectively.

A.0.4. FLOC SIZE OF SAMPLES FROM TURBIDITY CURRENT WITH ZETAG 7587

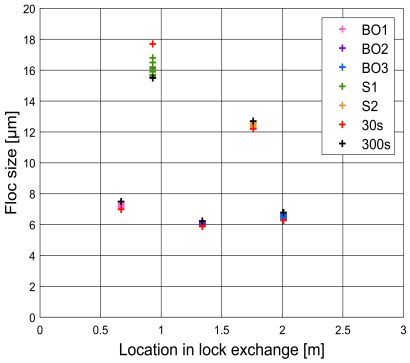

(a) 5 g/L

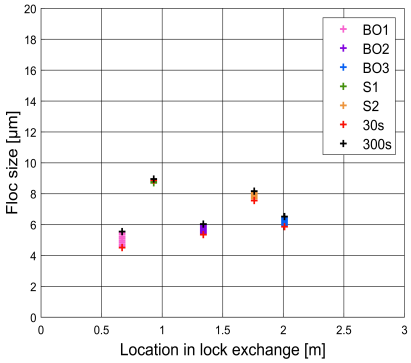

(b) 2.5 g/L

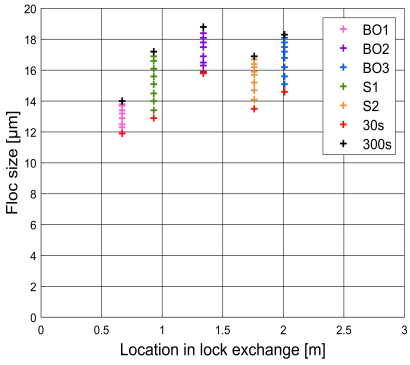

(c) 0.5 g/L

Figure A.4: Evolution of the d_{50} of flocs collected along the flume. BO and S stand for Bottom Outlet and Siphon. The floc size evolution is measured using the Malvern particle sizer. Red and black crosses represent flocs formed at 30 s and 300 s, respectively.

A

A.0.5. d_{50} OF FLOCS FROM SIPHON SAMPLES

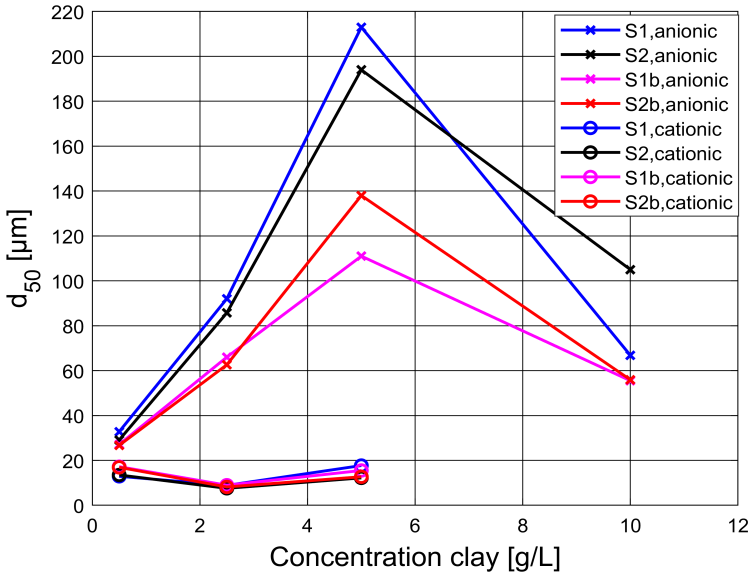

Figure A.5: d_{50} of flocs from siphon samples as a function of clay concentration.

A.0.6. Comparison of floc size obtained from Malvern and FlocCAM (samples from turbidity current) with Zetag 4120

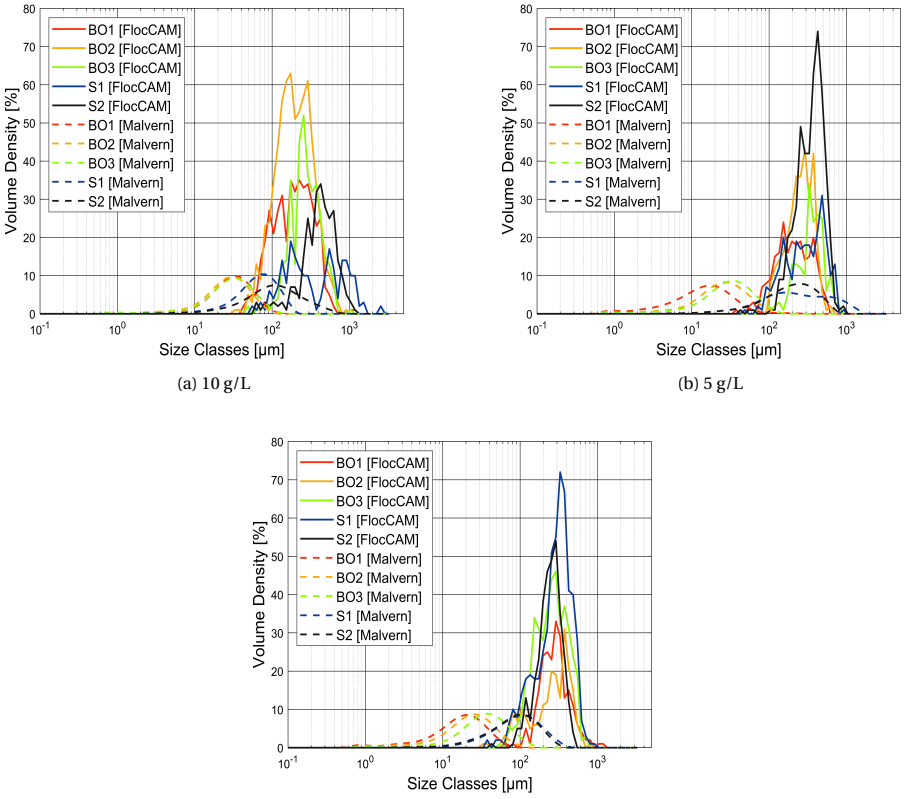

(a) 10 g/L

(b) 5 g/L

(c) 2.5 g/L

Figure A.6: PSD of flocs obtained from Malvern and FlocCAM with Zetag 4120.

A

A.0.7. COMPARISON OF FLOC SIZE OBTAINED FROM MALVERN AND FLOCCAM (SAMPLES FROM TURBIDITY CURRENT) WITH ZETAG 7587

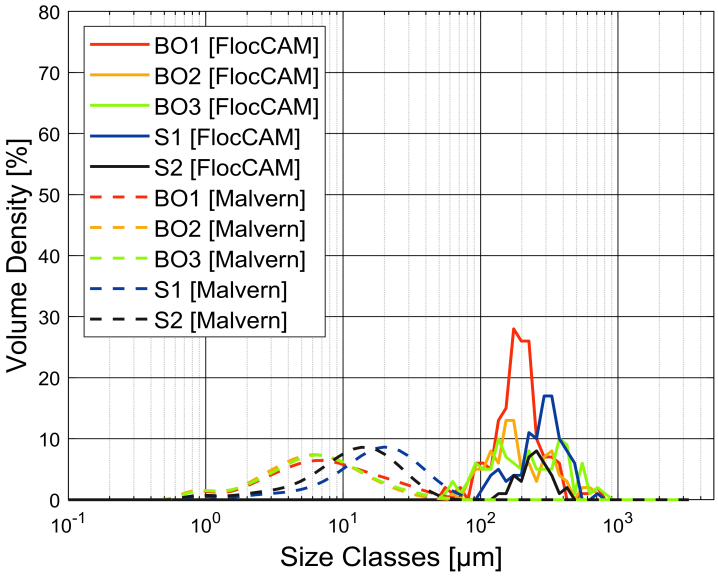

Figure A.7: PSD of flocs obtained from Malvern and FlocCAM with Zetag 7587 for 5 g/L clay concentration.

A.0.8. FLOCCAM SNAPSHOTS OF FLOCS OBTAINED FROM TURBIDITY CURRENT (5 G/L WITH ZETAG 4120)

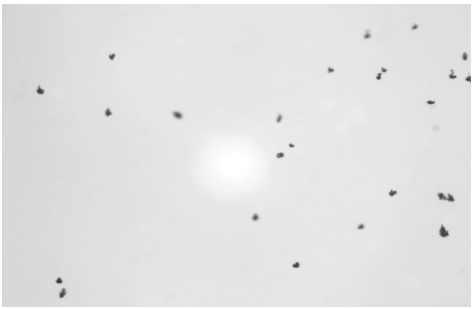

(a) BO1

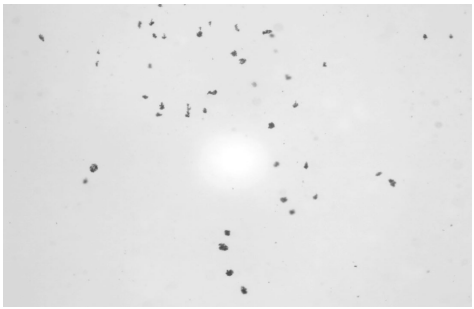

(b) BO2

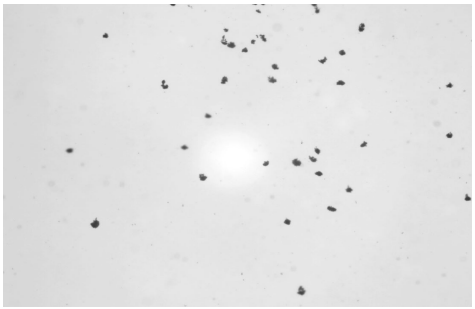

(c) BO3

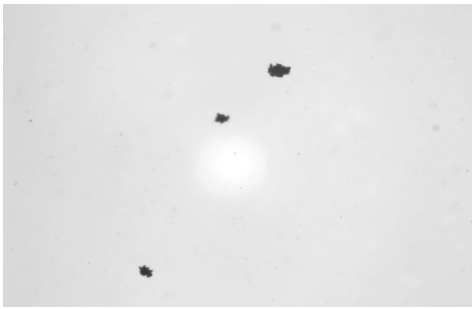

(d) S1

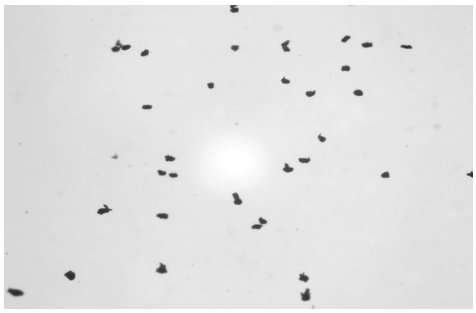

(e) S2

Figure A.8: FlocCAM snapshots for 5 g/L clay concentration with Zetag 4120.

A

A.0.9. FLOCCAM SNAPSHOTS OF FLOCS OBTAINED FROM TURBIDITY CURRENT (5 G/L WITH ZETAG 7587)

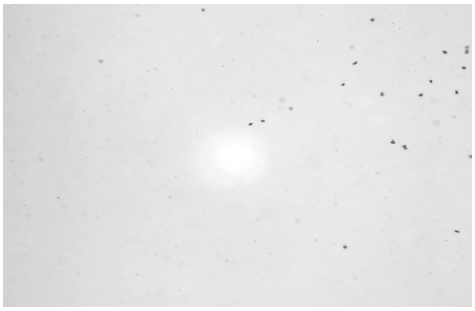

(a) BO1

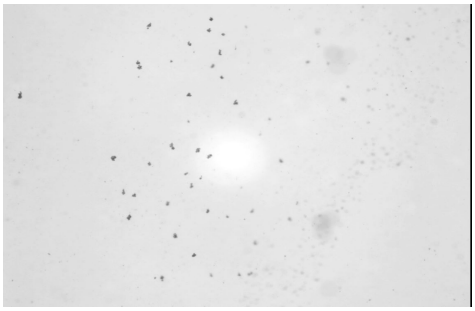

(b) BO2

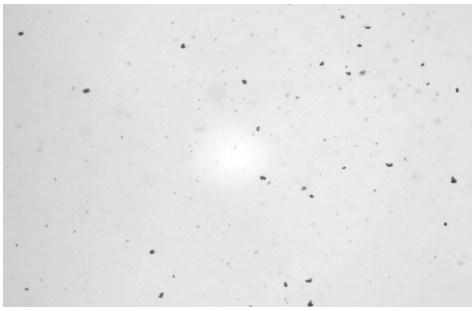

(c) BO3

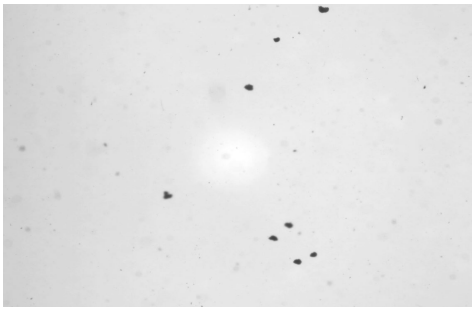

(d) S1

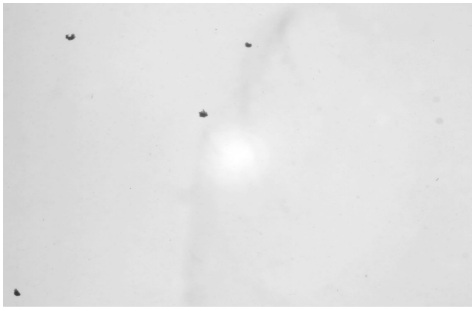

(e) S2

Figure A.9: FlocCAM snapshots for 5 g/L clay concentration with Zetag 7587.

A.0.10. FLOCCAM SNAPSHOTS OF FLOCS OBTAINED FROM TURBIDITY CURRENT (2.5 G/L WITH ZETAG 4120)

(a) BO1

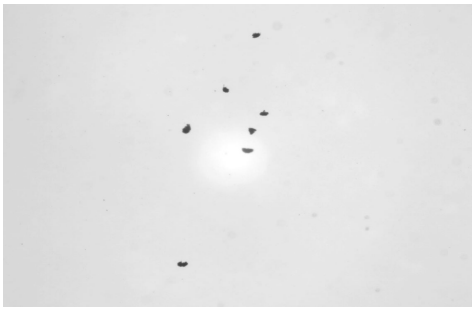

(b) BO2

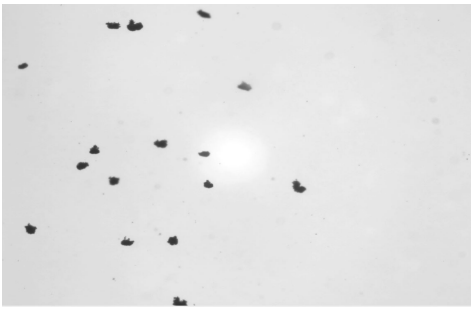

(c) BO3

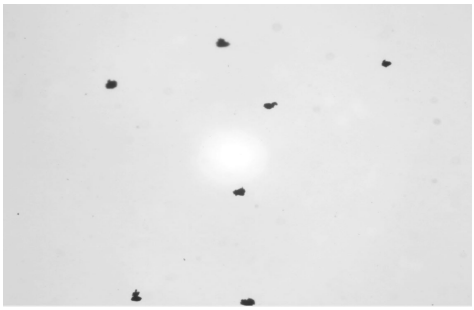

(d) S1

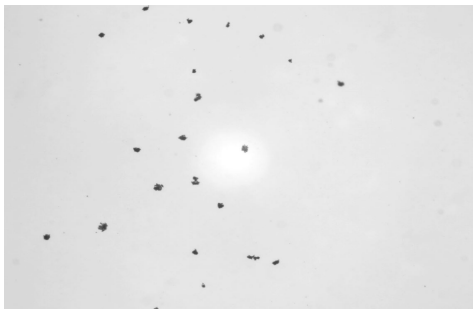

(e) S2

Figure A.10: FlocCAM snapshots for 2.5 g/L clay concentration with Zetag 4120.

A

A.0.11. FLOCCAM SNAPSHOTS OF FLOCS OBTAINED FROM TURBIDITY CURRENT (2.5 G/L WITH ZETAG 7587)

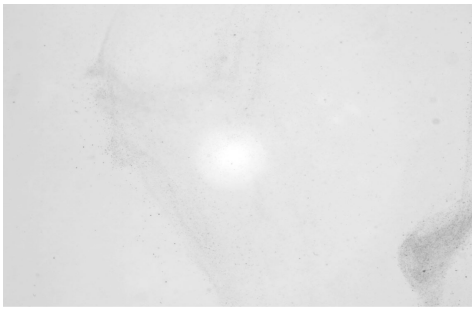

(a) BO1

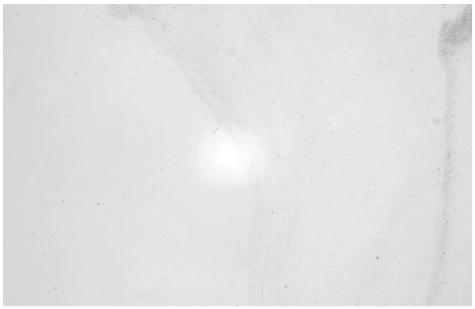

(b) BO2

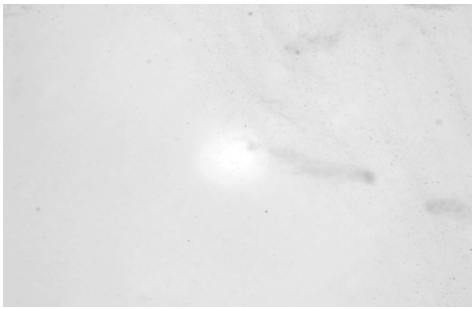

(c) BO3

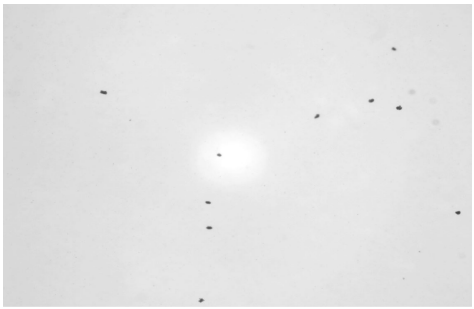

(d) S1

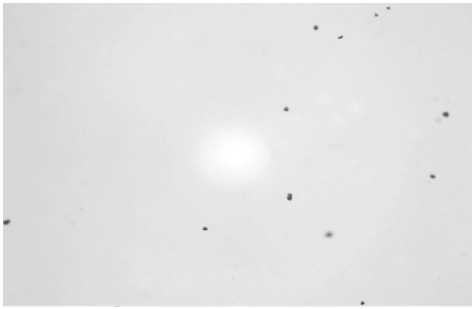

(e) S2

Figure A.11: FlocCAM snapshots for 2.5 g/L clay concentration with Zetag 7587.

B

FLOC IMAGES FOR BED EXPERIMENTS

B

B.1. FLOCS 10G/L

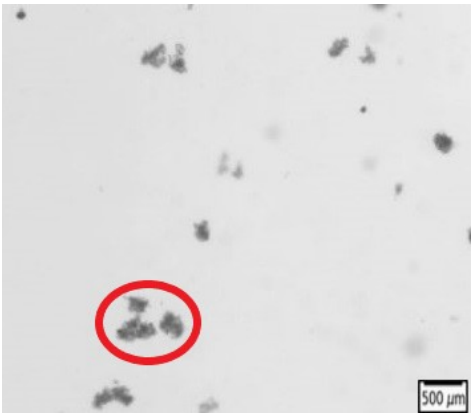

(a) No bed: Largest floc

(b) No bed: Smallest floc

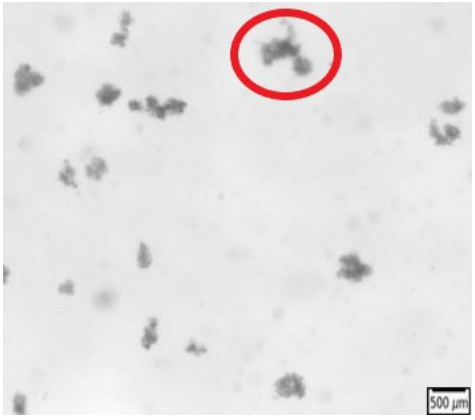

(c) 1-day bed: Largest floc

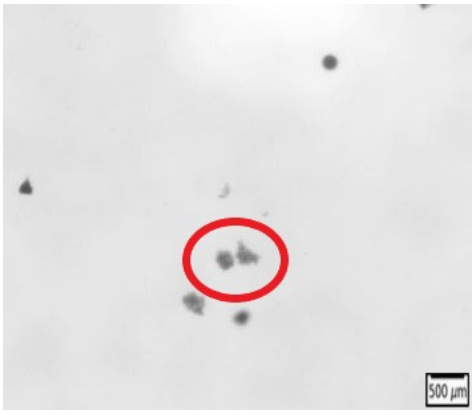

(d) 1-day bed: Smallest floc

Figure B.1: Snapshots of flocs from FlocCAM video recordings for 10g/L for No bed and 1-day bed cases

B.2. FLOCS 5G/L

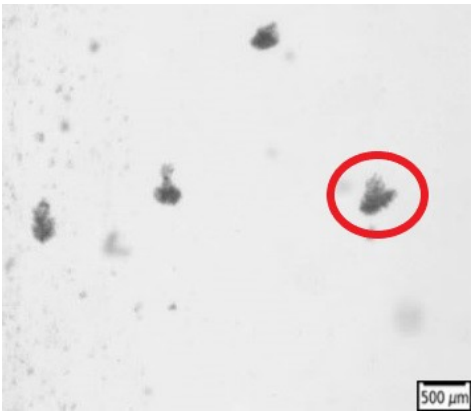

(a) No bed: Largest floc

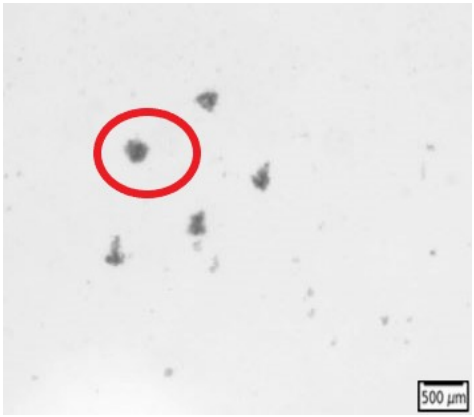

(b) No bed: Smallest floc

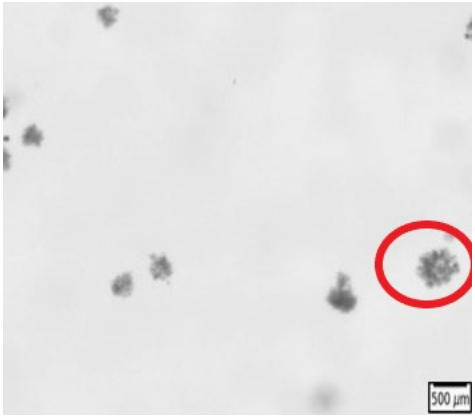

(c) 1-day bed: Largest floc

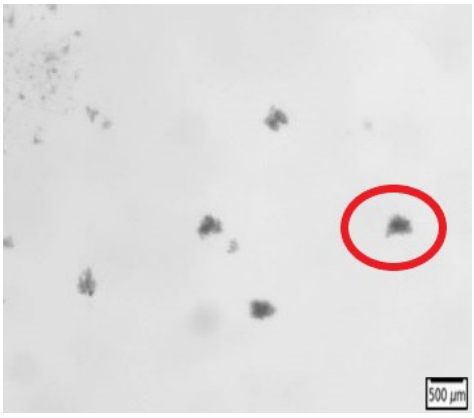

(d) 1-day bed: Smallest floc

Figure B.2: Snapshots of flocs from FlocCAM video recordings for 5g/L for No bed and 1-day bed cases

B.3. FLOCS 2.5G/L

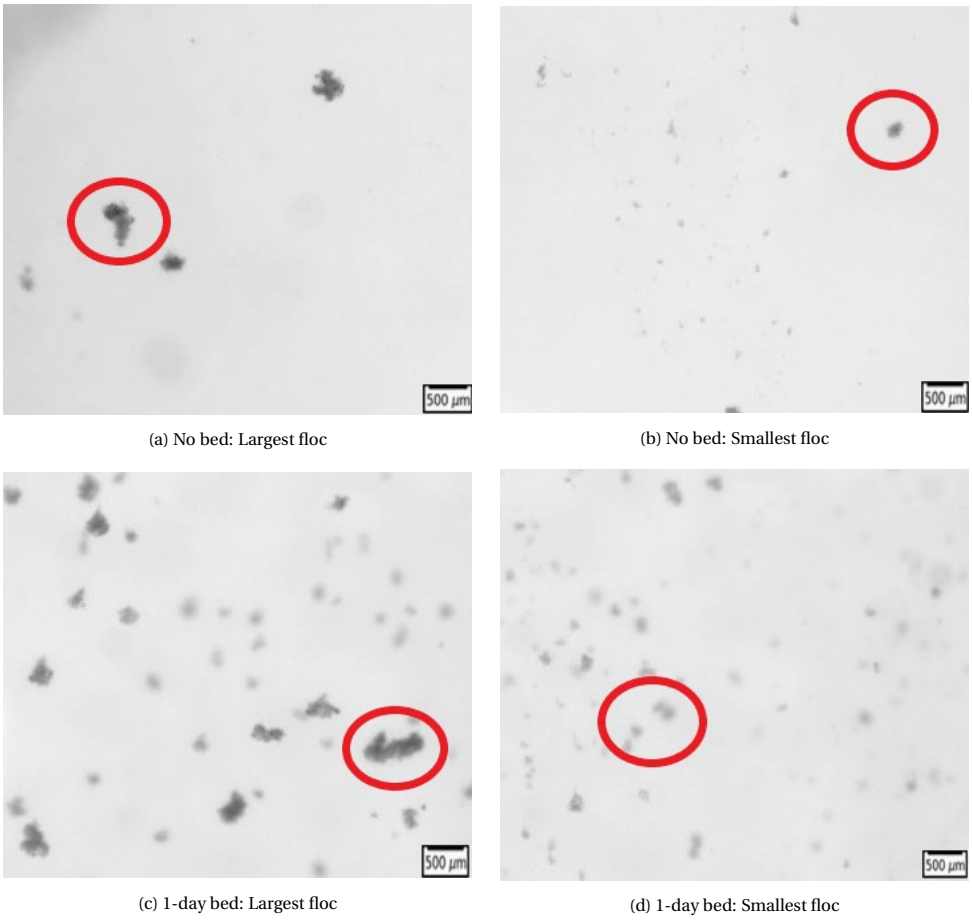

(a) No bed: Largest floc

(b) No bed: Smallest floc

(c) 1-day bed: Largest floc

(d) 1-day bed: Smallest floc

Figure B.3: Snapshots of flocs from FlocCAM video recordings for 2.5g/L for No bed and 1-day bed cases

B.3.1. TEST FOR EROSION

Two samples of CCZ clay were prepared in beakers and were left undisturbed for 1 day and 3 days, respectively. The thickness of the beds in the beakers was kept at 1.5 mm, similar to the bed thickness that would be on the flume bottom in case of 10g/L sediment concentration. The samples were then placed in a Velp Scientifica FP4 Portable Jar test apparatus. They were mixed at 40 rpm just above the bed to see how the beds would erode. The snapshots are shown here.

B.3.2. SNAPSHOTS OF LOCK EXCHANGE EXPERIMENTS

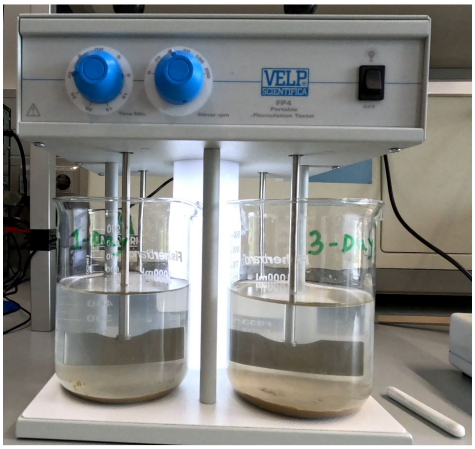

(a) t=0s

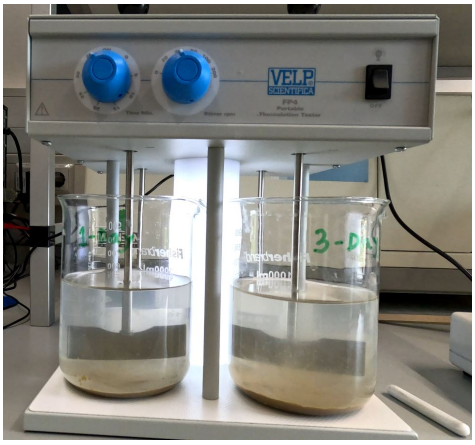

(b) t=4s

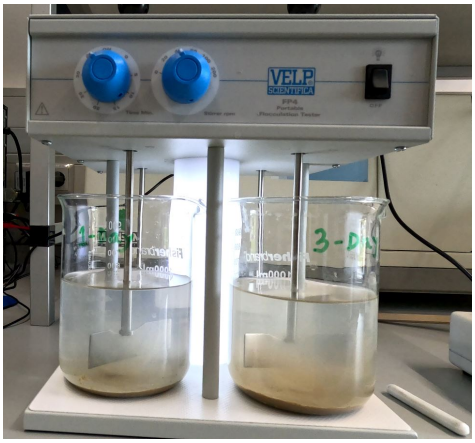

(c) t=6s

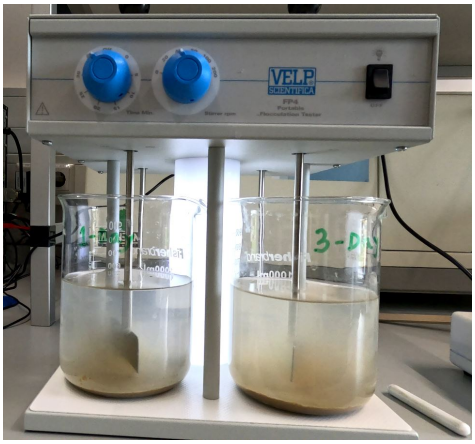

(d) t=8s

Figure B.4: Snapshots of erosion of bed at different time stamps

B

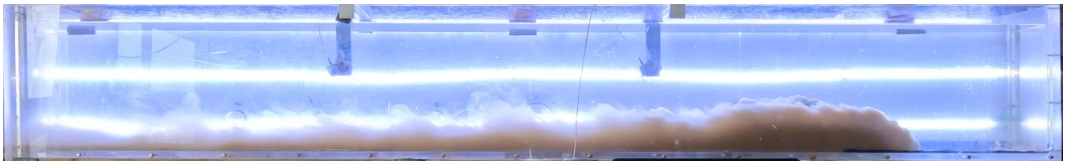

(a) No bed

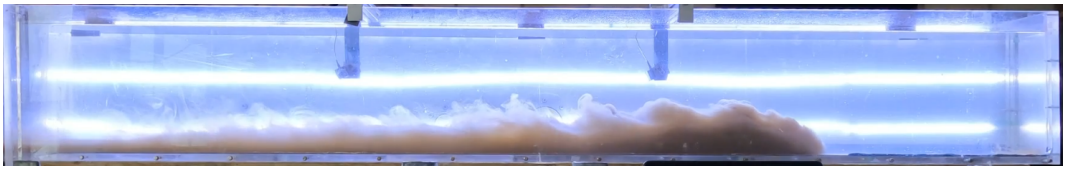

(b) 1-day bed

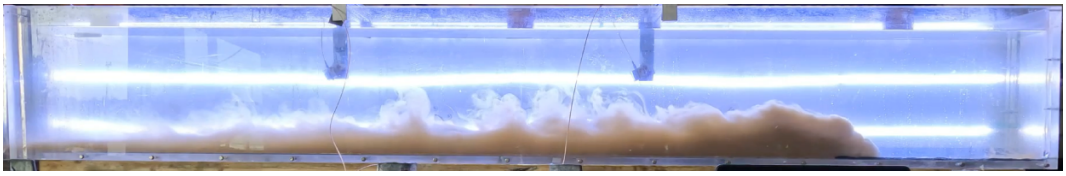

(c) 3-day bed

Figure B.5: Turbidity current propagating on 3 types of beds at t=75 s for 5g/L

C

FLOC IMAGES FOR BED EXPERIMENTS

C

C.1. FLOCS 10G/L

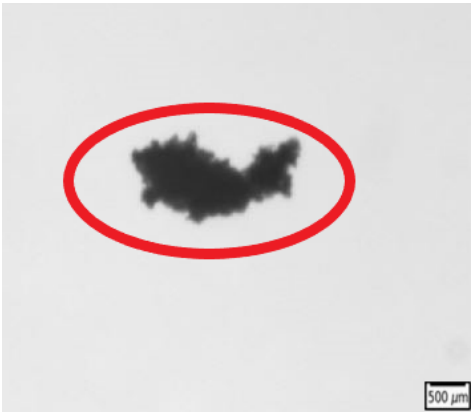

(a) Quartz bed with Zetag: Largest floc

(b) Quartz bed with Zetag: Smallest floc

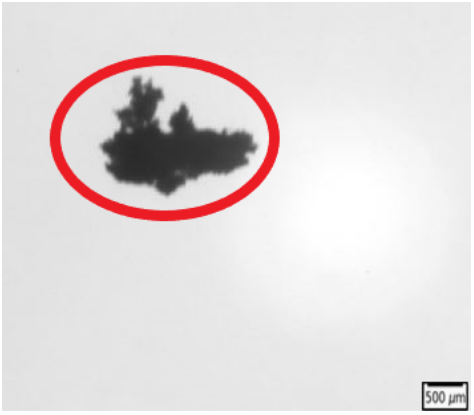

(c) Quartz bed with Zetag and Illite: Largest floc

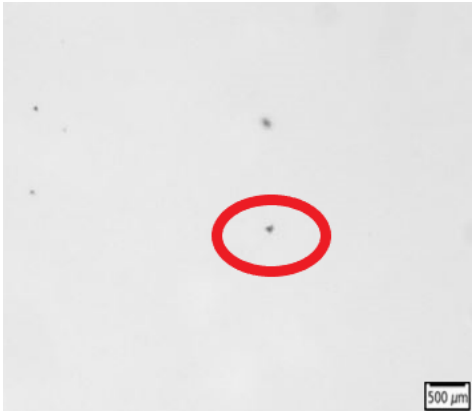

(d) Quartz bed with Zetag and Illite: Smallest floc

Figure C.1: Snapshots of flocs extracted from FlocCAM video recordings at an initial sediment concentration of 10 g/L for (i) quartz bed with Zetag and (ii) quartz bed with Zetag and Illite conditions.

C.2. FLOCS 5G/L

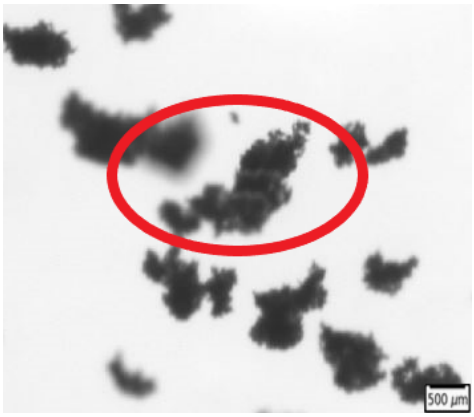

(a) Quartz bed with Zetag: Largest floc

(b) Quartz bed with Zetag: Smallest floc

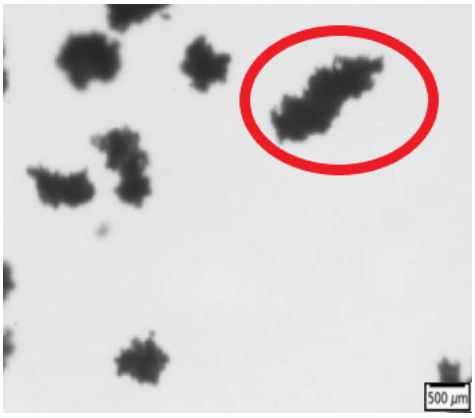

(c) Quartz bed with Zetag and Illite: Largest floc

(d) Quartz bed with Zetag and Illite: Smallest floc

Figure C.2: Snapshots of flocs extracted from FlocCAM video recordings at an initial sediment concentration of 5 g/L for (i) quartz bed with Zetag and (ii) quartz bed with Zetag and Illite conditions.

C.3. FLOCS 2.5G/L

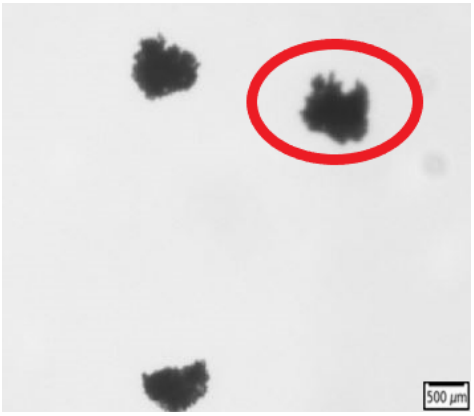

(a) Quartz bed with Zetag: Largest floc

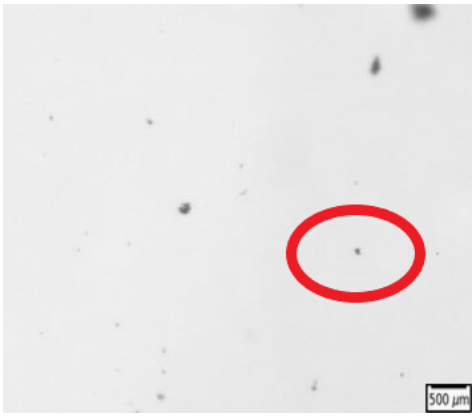

(b) Quartz bed with Zetag: Smallest floc

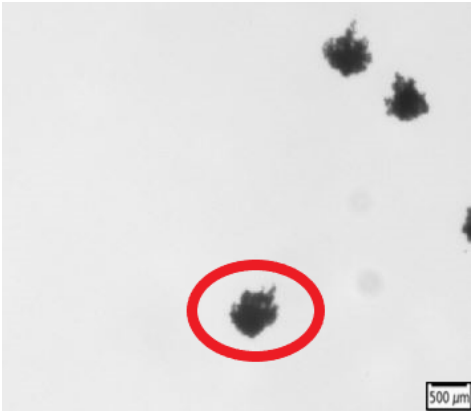

(c) Quartz bed with Zetag and Illite: Largest floc

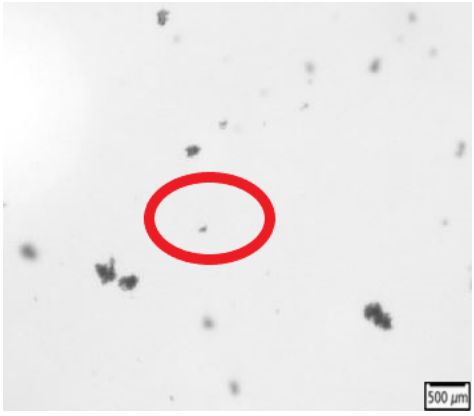

(d) Quartz bed with Zetag and Illite: Smallest floc

Figure C.3: Snapshots of flocs extracted from FlocCAM video recordings at an initial sediment concentration of 2.5 g/L for (i) quartz bed with Zetag and (ii) quartz bed with Zetag and Illite conditions.

BIBLIOGRAPHY

Adduce, C., Lombardi, V., Sciortino, G., & Morganti, M. (2009). Roughness effects on gravity currents dynamics. *Proceedings of 33rd IAHR congress, Vancouver, Canada*.

Ali, W., et al. (2022a). Effect of flocculation on turbidity currents. *Frontiers in Earth Science*, *10*, 1014170.

Ali, W., & Chassagne, C. (2022). Comparison between two analytical models to study the flocculation of mineral clay by polyelectrolytes. *Continental Shelf Research*, *250*, 104864.

Ali, W., Enthoven, D., Kirichek, A., Helmons, R., & Chassagne, C. (2022b). Can flocculation reduce the dispersion of deep sea sediment plumes. *Proceedings of the World dredging conference, Copenhagen, Denmark*.

Ali, W., Kirichek, A., & Chassagne, C. (2024a). Collective effects on the settling of clay flocs. *Applied Clay Science*, *254*, 107399.

Ali, W., Kirichek, A., & Chassagne, C. (2024b). Flocculation of deep-sea clay from the clarion clipperton fracture zone. *Applied Ocean Research*, *150*, 104099.

Ali, W., Kirichek, A., & Chassagne, C. (2023). Collective effects on the settling of clay flocs [manuscript submitted for publication]. *Faculty of Civil Engineering and Geosciences, Delft University of Technology*.

Alldredge, A. L., & Silver, M. W. (1988). Characteristics, dynamics and significance of marine snow. *Progress in oceanography*, *20*(1), 41–82.

Baghalian, S., & Ghodsian, M. (2022). Experimental study of obstacle and bed roughness effects on behavior of turbidity current. *Journal of Hydro-Environment Research*, *40*, 77–90.

Baker, M. L., Baas, J. H., Malarkey, J., Jacinto, R. S., Craig, M. J., Kane, I. A., & Barker, S. (2017a). The effect of clay type on the properties of cohesive sediment gravity flows and their deposits. *Journal of Sedimentary Research*, *87*(11), 1176–1195.

Baker, M. L., Baas, J. H., Malarkey, J., Jacinto, R. S., Craig, M. J., Kane, I. A., & Barker, S. (2017b). The effect of clay type on the properties of cohesive sediment gravity flows and their deposits. *Journal of Sedimentary Research*, *87*(11), 1176–1195. https://doi.org/10.2110/jsr.2017.63

Barany, S., Kozakova, I., Marcinova, L., & Skvarla, J. (2010). Electrokinetic potential of bentonite and kaolin particles in the presence of polymer mixtures. *Colloid Journal*, *72*(5), 595–601. https://doi.org/10.1134/s1061933x10050030

Barany, S., Meszaros, R., Kozakova, I., & Skvarla, I. (2009). Kinetics and mechanism of flocculation of bentonite and kaolin suspensions with polyelectrolytes and the strength of floccs. *Colloid Journal*, *71*(3), 285–292. https://doi.org/10.1134/s1061933x09030016

Bárány, S., Meszaros, R., Marcinova, L., & Skvarla, J. (2011). Effect of polyelectrolyte mixtures on the electrokinetic potential and kinetics of flocculation of clay min-

eral particles. *Colloids and Surfaces A: Physicochemical and Engineering Aspects*, *383*(1–3), 48–55. https://doi.org/10.1016/j.colsurfa.2011.01.051

BGR. (2019). *Environmental impact assessment for the testing of a pre-protoype manganese nodule collector vehicle in the eastern german license area (clarion- clipperton zone) in the framework of the european jpi-o miningimpact 2 research project*. (tech. rep.).

Blue Nodules Summary- Deep Sea Mining. (2020). Blue nodules.

Boetius, A., & Lochte, K. (1994). Regulation of microbial enzymatic degradation of organic matter in deep-sea sediments. *Marine Ecology Progress Series*, 299–307.

Boschen, R. E., Rowden, A. A., Clark, M. R., & Gardner, J. P. (2013). Mining of deep-sea seafloor massive sulfides: A review of the deposits, their benthic communities, impacts from mining, regulatory frameworks and management strategies. *Ocean & coastal management*, *84*, 54–67.

Bray, R. N. (2008). *Environmental aspects of dredging*. CRC Press.

Brown, D., Christian, W., & Hanson, R. (2008, June). Tracker video analysis and modeling tool. https://physlets.org/tracker/

Bruun, P., Gayes, P., Schwab, W., & Eiser, W. (2005). Dredging. In *Port and coastal engineering: Developments in science and technology*. Coastal Education; Research Foundation.

Cacchione, D., Sternberg, R., & Ogston, A. (2006). Bottom instrumented tripods: History, applications, and impacts. *Continental Shelf Research*, *26*(17-18), 2319–2334.

CEDA. (2011). Ceda position paper: Underwater sound in relation to dredging. *Terra Et Aqua*.

Chassagne, C. (2021). *Introduction to colloid science: Applications to sediment characterization*. TU Delft OPEN Publishing.

Chmiel, O., Baselt, I., & Malcherek, A. (2018). Applicability of acoustic concentration measurements in suspensions of artificial and natural sediments using an acoustic doppler velocimeter. *Acoustics*, *1*(1), 59–77.

Clare, M., Lintern, D. G., Rosenberger, K., Clarke, J. E. H., Paull, C., Gwiazda, R., Cartigny, M. J., Talling, P. J., Perara, D., Xu, J., et al. (2020). Lessons learned from the monitoring of turbidity currents and guidance for future platform designs.

Clare, M. A., Vardy, M. E., Cartigny, M. J., Talling, P. J., Himsworth, M. D., Dix, J. K., Harris, J. M., Whitehouse, R. J., & Belal, M. (2017). Direct monitoring of active geohazards: Emerging geophysical tools for deep-water assessments. *Near Surface Geophysics*, *15*(4), 427–444.

Craig, M. J., Baas, J. H., Amos, K. J., Strachan, L. J., Manning, A. J., Paterson, D. M., Hope, J. A., Nodder, S. D., & Baker, M. L. (2019). Biomediation of submarine sediment gravity flow dynamics. *Geology*, *48*(1), 72–76. https://doi.org/10.1130/g46837.1

Craig, M. J., Baas, J. H., Amos, K. J., Strachan, L. J., Manning, A. J., Paterson, D. M., Hope, J. A., Nodder, S. D., & Baker, M. L. (2020). Biomediation of submarine sediment gravity flow dynamics. *Geology*, *48*(1), 72–76.

Dantec Dynamics A/S & Met-Flow SA. (2025). Uvp-duo ultrasonic velocity profiler [Accessed: October 30, 2025]. *Dantec Dynamics A/S & Met-Flow SA*.

de Wit, L. (2015). *3d cfd modelling of overflow dredging plumes* [Doctoral Thesis]. Delft University of Technology. https://doi.org/10.4233/uuid:ef743dff-6196-4c7b-8213-fd28684d3a58

de Wit, L., Mosca, C., Buschman, F., Jaksic, L., van der Deijl, E., & van der Biezen, T. (2025). Accurate determination of far-field source terms of barge overflow dredge plumes based on near-field monitoring and modeling. *Journal of Waterway, Port, Coastal, and Ocean Engineering, 151*(2), 04024026.

Deng, Z. (2022). The role of algae in fine cohesive sediment flocculation.

Deng, Z., He, Q., Safar, Z., & Chassagne, C. (2019). The role of algae in fine sediment flocculation: In-situ and laboratory measurements. *Marine Geology, 413*, 71–84.

Diaz, M., De Stigter, H. C., Palanques, A., Arjona-Camas, M., Puig, P., Helmons, R., Thomsen, L., & Jonge, L. d. (2023). Monitoring flocculation in a sediment plume produced by a deep-sea mining test in shallow water: Preliminary results.

Downing, J. (2006). Twenty-five years with obs sensors: The good, the bad, and the ugly. *Continental Shelf Research, 26*(17-18), 2299–2318.

Drexhage, J., La Porta, D., Hund, K., McCormick, M., & Ningthoujam, J. (2017). The growing role of minerals and metals for a low carbon future. *World Bank, Washington, DC*.

Droppo, I., & Ongley, E. (1994). Flocculation of suspended sediment in rivers of southeastern canada. *Water Research, 28*(8), 1799–1809. https://doi.org/10.1016/0043-1354(94)90253-4

Eisma, D. (1986). Flocculation and de-flocculation of suspended matter in estuaries. *Netherlands Journal of sea research, 20*(2-3), 183–199.

Elerian, M., Alhaddad, S., Helmons, R., & van Rhee, C. (2021). Near-field analysis of turbidity flows generated by polymetallic nodule mining tools. *Mining, 1*(3), 251–278.

Elerian, M., Huang, Z., van Rhee, C., & Helmons, R. (2023a). Flocculation effect on turbidity flows generated by deep-sea mining: A numerical study. *Ocean Engineering, 277*, 114250. https://doi.org/10.1016/j.oceaneng.2023.114250

Elerian, M., Huang, Z., van Rhee, C., & Helmons, R. (2023b). Flocculation effect on turbidity flows generated by deep-sea mining: A numerical study. *Ocean Engineering, 277*, 114250.

Erftemeijer, P. L. A., Riegl, B., Hoeksema, B. W., & Todd, P. A. (2012). Environmental impacts of dredging and other sediment disturbances on corals: A review. *Marine Pollution Bulletin, 64*(9), 1737–1765. https://doi.org/10.1016/j.marpolbul.2012.05.008

Erftemeijer, P. L., & Lewis III, R. R. R. (2006). Environmental impacts of dredging on seagrasses: A review. *Marine pollution bulletin, 52*(12), 1553–1572.

Erftemeijer, P. L., Riegl, B., Hoeksema, B. W., & Todd, P. A. (2012). Environmental impacts of dredging and other sediment disturbances on corals: A review. *Marine pollution bulletin, 64*(9), 1737–1765.

Flemming, H.-C., & Wingender, J. (2001). Relevance of microbial extracellular polymeric substances (epss)-part i: Structural and ecological aspects. *Water science and technology, 43*(6), 1–8.

Gausepohl, F., Hennke, A., Schoening, T., Köser, K., & Greinert, J. (2020). Scars in the abyss: Reconstructing sequence, location and temporal change of the 78 plough tracks of the 1989 discol deep-sea disturbance experiment in the peru basin. *Biogeosciences*, *17*(6), 1463–1493. https://doi.org/10.5194/bg-17-1463-2020

Gazis, I.-Z., de Stigter, H., Mohrmann, J., Heger, K., Diaz, M., Gillard, B., Baeye, M., Veloso-Alarcón, M. E., Purkiani, K., Haeckel, M., et al. (2025). Monitoring benthic plumes, sediment redeposition and seafloor imprints caused by deep-sea polymetallic nodule mining. *Nature Communications*, *16*(1), 1229.

Gilkinson, K., Fader, G., Gordon Jr, D., Charron, R., McKeown, D., Roddick, D., Kenchington, E., MacIsaac, K., Bourbonnais, C., Vass, P., et al. (2003). Immediate and longer-term impacts of hydraulic clam dredging on an offshore sandy seabed: Effects on physical habitat and processes of recovery. *Continental Shelf Research*, *23*(14-15), 1315–1336.

Gillard, B., & Thomson, L. (2022). *Appendix 6: Characterization of sediment plumes behind mining vehicles in the nori area* (tech. rep.).

Gillard, B., Purkiani, K., Chatzievangelou, D., Vink, A., Iversen, M. H., & Thomsen, L. (2019). Physical and hydrodynamic properties of deep sea mining-generated, abyssal sediment plumes in the clarion clipperton fracture zone (eastern-central pacific). *Elem Sci Anth*, *7*, 5.

Glé, P., Gourdon, E., Arnaud, L., Horoshenkov, K.-V., & Khan, A. (2013). The effect of particle shape and size distribution on the acoustical properties of mixtures of hemp particles. *The Journal of the Acoustical Society of America*, *134*(6), 4698–4709.

Global Sea Mineral Resources NV. (2018). *Environmental impact statement* (tech. rep.). Global Sea Mineral Resources.

Gollner, S., Kaiser, S., Menzel, L., Jones, D. O., Brown, A., Mestre, N. C., Van Oevelen, D., Menot, L., Colaço, A., Canals, M., et al. (2017). Resilience of benthic deep-sea fauna to mining activities. *Marine Environmental Research*, *129*, 76–101.

Goodwin, J. (2009). *Colloids and interfaces with surfactants and polymers*. John Wiley & Sons.

Haalboom, S., de Stigter, H. C., Mohn, C., Vandorpe, T., Smit, M., de Jonge, L., & Reichart, G.-J. (2023). Monitoring of a sediment plume produced by a deep-sea mining test in shallow water, málaga bight, alboran sea (southwestern mediterranean sea). *Marine Geology*, *456*, 106971.

Hein, J. R., Mizell, K., Koschinsky, A., & Conrad, T. A. (2013). Deep-ocean mineral deposits as a source of critical metals for high-and green-technology applications: Comparison with land-based resources. *Ore Geology Reviews*, *51*, 1–14.

Hein, J. R., & Petersen, S. (2013). The geology of cobalt-rich ferromanganese crusts. Secretariat of the Pacific Community (SPC).

Helmons, R., de Wit, L., de Stigter, H., & Spearman, J. (2022). Dispersion of benthic plumes in deep-sea mining: What lessons can be learned from dredging? *Frontiers in earth science*, *10*, 868701.

Ho, Q. N., Fettweis, M., Spencer, K. L., & Lee, B. J. (2022). Flocculation with heterogeneous composition in water environments: A review. *Water Research*, *213*, 118147.

Hu, P., & Cao, Z. (2009). Fully coupled mathematical modeling of turbidity currents over erodible bed. *Advances in Water Resources*, *32*(1), 1–15.

Hughes Clarke, J. E. (2016). First wide-angle view of channelized turbidity currents links migrating cyclic steps to flow characteristics. *Nature communications*, *7*(1), 11896.

International Seabed Authority (ISA). (2010). *A geological model of polymetallic nodule deposits in the clarion-clipperton fracture zone*. International Seabed Authority.

JFE Advantech Co., Ltd. (2025). Company profile [Accessed: October 30, 2025]. *JFE Advantech Co., Ltd.*

Karl, D. M., Knauer, G. A., & Martin, J. H. (1988). Downward flux of particulate organic matter in the ocean: A particle decomposition paradox. *Nature*, *332*(6163), 438–441.

Khripounoff, A., Crassous, P., Bue, N. L., Dennielou, B., & Jacinto, R. S. (2012). Different types of sediment gravity flows detected in the var submarine canyon (northwestern mediterranean sea). *Progress in Oceanography*, *106*, 138–153.

Kiørboe, T. (2001). Formation and fate of marine snow: Small-scale processes with large-scale implications. *Scientia marina*, *65*(S2), 57–71.

Kirsten Hund, D. L. P., Thao P. Fabregas, T. L., & Drexhage, J. (2020). *Minerals for climate action: The mineral intensity of the clean energy transition* (tech. rep.). World Bank Group. Washington, DC.

Köllner, T., Meredith, A., Nokes, R., & Meiburg, E. (2020). Gravity currents over fixed beds of monodisperse spheres. *Journal of Fluid Mechanics*, *901*, A32.

Laboyrie, P., Van Koningsveld, M., Aarninkhof, S., Van Parys, M., Lee, M., Jensen, A., Csiti, A., & Kolman, R. (2018). *Dredging for sustainable infrastructure*. CEDA/IADC The Hague, The Netherlands.

Lang, M., Dasselaar, S., Aasly, K., & Larsen, E. (2019). *Blue nodules deliverable report d3.4 report describing the process flow overview pu. pp. 1–23*. (tech. rep.).

Lee, B. J., Schlautman, M. A., Toorman, E., & Fettweis, M. (2012). Competition between kaolinite flocculation and stabilization in divalent cation solutions dosed with anionic polyacrylamides. *Water Research*, *46*(17), 5696–5706. https://doi.org/10.1016/j.watres.2012.07.056

Lee, J. (2024, July). 'dark oxygen' discovery highlights the need to stop deep sea mining [Accessed: 2025-10-22]. https://www.greenpeace.org/aotearoa/press-release/dark-oxygen-discovery-highlights-need-stop-deep-sea-mining/

Li, M., Dong, H., Shi, B., Chi, W., & Bai, T. (2026). Flocculation and settling of in-situ deep-sea sediments under mining disturbance. *Ocean Engineering*, *347*, 124054.

Lintern, D. G., & Hill, P. R. (2010). An underwater laboratory at the fraser river delta. *Eos, Transactions American Geophysical Union*, *91*(38), 333–334.

Lunt, J., & Smee, D. L. (2020). Turbidity alters estuarine biodiversity and species composition. *ICES Journal of Marine Science*, *77*(1), 379–387.

Maggi, M. R., Adduce, C., & Negretti, M. E. (2022). Lock-release gravity currents propagating over roughness elements. *Environmental Fluid Mechanics*, *22*(2), 383–402.

Malvern Panalytical. (2024). *Mastersizer user guide*. Malvern Panalytical. Malvern, UK. Retrieved January 6, 2025, from https://www.malvernpanalytical.com/en/learn/knowledge-center/user-manuals/man0474en

Manning, A., Friend, P., Prowse, N., & Amos, C. (2007). Estuarine mud flocculation properties determined using an annular mini-flume and the labsfloc system. *Continental Shelf Research*, *27*(8), 1080–1095.

Manning, A. (2001). Study of the effect of turbulence on the properties of flocculated mud.

Mestres, M., Sierra, J. P., Mösso, C., Sánchez-Arcilla, A., Hernáez, M., & Morales, J. (2014). Numerical assessment of the dispersion of overspilled sediment from a dredge barge and its sensitivity to various parameters. *Marine pollution bulletin*, *79*(1-2), 225–235.

Met-Flow SA. (2024). UVP-DUO Profilers – Ultrasonic Velocity Profiling Technology [Accessed: 2025-02-10]. https://www.met-flow.com/technology/products/uvp-duo-profilers

Middleton, G. V. (1993). Sediment deposition from turbidity currents. *Annual Review Of Earth And Planetary Sciences, Volume 21, pp. 89-114.*, *21*, 89–114.

Mietta, F. (2010). Evolution of the floc size distribution of cohesive sediments.

Miller, K. A., Thompson, K. F., Johnston, P., & Santillo, D. (2018). An overview of seabed mining including the current state of development, environmental impacts, and knowledge gaps. *Frontiers in Marine Science*, *4*, 312755.

Mousadik, S. E., Ouillon, R., Muñoz-Royo, C., Slade, W., Pottsmith, C., Leeuw, T., Alford, M. H., Mikkelsen, O. A., & Peacock, T. (2024). In situ optical measurement of particles in sediment plumes generated by a pre-prototype polymetallic nodule collector. *Scientific Reports*, *14*(1), 23894.

M.Ryan MacIver. (2019). Safas: Sedimentation and floc analysis software.

Muñoz-Royo, C., Ouillon, R., El Mousadik, S., Alford, M. H., & Peacock, T. (2022). An in situ study of abyssal turbidity-current sediment plumes generated by a deep seabed polymetallic nodule mining preprototype collector vehicle. *Science advances*, *8*(38), eabn1219.

Nichols, C. M., Guezennec, J., & Bowman, J. (2005). Bacterial exopolysaccharides from extreme marine environments with special consideration of the southern ocean, sea ice, and deep-sea hydrothermal vents: A review. *Marine biotechnology*, *7*(4), 253–271.

Nichols, M., Diaz, R. J., & Schaffner, L. C. (1990). Effects of hopper dredging and sediment dispersion, chesapeake bay. *Environmental Geology and Water Sciences*, *15*(1), 31–43.

Nogueira, H. I., Adduce, C., Alves, E., & Franca, M. J. (2013a). Analysis of lock-exchange gravity currents over smooth and rough beds. *Journal of Hydraulic Research*, *51*(4), 417–431. https://doi.org/10.1080/00221686.2013.798363

Nogueira, H. I., Adduce, C., Alves, E., & Franca, M. J. (2013b). Analysis of lock-exchange gravity currents over smooth and rough beds. *Journal of hydraulic Research*, *51*(4), 417–431.

Nortek AS. (2018). *Comprehensive manual – velocimeters* [Accessed: October 30, 2025]. https://www.nortekgroup.com/assets/software/N3015-030-Comprehensive-Manual-Velocimeters_1118.pdf

Ojiambo, M. N., & Adachi, T. (2023). Selected critical metals for a low-carbon future. *Mineral Economics*, *36*(3), 519–534.

Özgökmen, T. M., & Fischer, P. F. (2008). On the role of bottom roughness in overflows. *Ocean Modelling*, *20*(4), 336–361.

Parker, G., Garcia, M., Fukushima, Y., & Yu, W. (1987). Experiments on turbidity currents over an erodible bed. *Journal of Hydraulic Research*, *25*(1), 123–147.

Parsons, J. D., Friedrichs, C. T., Traykovski, P. A., Mohrig, D., Imran, J., Syvitski, J. P., Parker, G., Puig, P., Buttles, J. L., & García, M. H. (2007). The mechanics of marine sediment gravity flows. *Continental margin sedimentation: from sediment transport to sequence stratigraphy*, 275–337.

Peters, W. D., & Venart, J. (2000). Visualization of rough-surface gravity current flows using laser-induced fluorescence. *Proceedings of 9th international symposium of flow visualization, Edinburgh, Scotland*.

Riza, M., Ehsan, M. N., Pervez, M. N., Khyum, M. M. O., Cai, Y., & Naddeo, V. (2023). Control of eutrophication in aquatic ecosystems by sustainable dredging: Effectiveness, environmental impacts, and implications. *Case Studies in Chemical and Environmental Engineering*, *7*, 100297.

Safar, Z., Deng, Z., & Chassagne, C. (2023). Applying a logistic growth equation to model flocculation of sediment in the presence of living and dead organic matter. *Frontiers in Marine Science*, *10*, 1227849.

Safar, Z., Rijnsburger, S., Sanz, M. I., Chassagne, C., Manning, A., Pietrzak, J., Souza, A., van Kessel, T., Horner-Devine, A., Flores, R., et al. (2019). Characterization and dynamics of suspended particulate matter in the near field of the rhine river plume during a neap tide. *Geophysical research abstracts*, *21*.

Sanz, M. I. (2018). *Flocculation and consolidation of cohesive sediments under the influence of coagulant and flocculant* [Doctoral dissertation, Delft University of Technology].

Sequeiros, O. E., Mosquera, R., & Pedocchi, F. (2018). Internal structure of a self-accelerating turbidity current. *Journal of Geophysical Research: Oceans*, *123*(9), 6260–6276.

Sequoia Scientific, Inc. (2016). *Lisst-200x user's manual version 2.35* [Accessed: October 30, 2025]. https://www.sequoiasci.com/wp-content/uploads/2016/02/LISST-200X_Users_Manual_v2_35.pdf

Sequoia Scientific, Inc. (2018, January). *LISST-200X User's Manual: Version 1.3B* [Version 1.3B]. Sequoia Scientific, Inc. Bellevue, WA, USA. https://www.sequoiasci.com/wp-content/uploads/2016/02/LISST-200X_Users_Manual_v1_3B.pdf

Serra, T., Soler, M., Mancini, M., Solari, L., & Colomer, J. (2025). Sedimentary rates driven by laboratory lock-exchange turbidity currents flowing over gravel and vegetated beds. *Sedimentary Geology*, 106978.

Shakeel, A., MacIver, M. R., van Kan, P. J., Kirichek, A., & Chassagne, C. (2021). A rheological and microstructural study of two-step yielding in mud samples from a port area. *Colloids and Surfaces A: Physicochemical and Engineering Aspects*, *624*, 126827.

Shakeel, A., Safar, Z., Ibanez, M., van Paassen, L., & Chassagne, C. (2020). Flocculation of clay suspensions by anionic and cationic polyelectrolytes: A systematic analysis. *Minerals*, *10*(11), 999. https://doi.org/10.3390/min10110999

Sharma, R. (2015). Environmental issues of deep-sea mining. *Procedia Earth and Planetary Science*, *11*, 204–211.

Shih, H. (2012). Real-time current and wave measurements in ports and harbors using adcp. *2012 Oceans-Yeosu*, 1–8.

Smith, S. J., & Friedrichs, C. T. (2011). Size and settling velocities of cohesive flocs and suspended sediment aggregates in a trailing suction hopper dredge plume. *Continental Shelf Research*, *31*(10), S50–S63.

Spearman, J., Taylor, J., Crossouard, N., Cooper, A., Turnbull, M., Manning, A., & Lee, M. (2019). The measurement and modelling of plumes resulting from deep sea mining of fe-mn crusts. *22nd World Dredging Congress, WODCON 2019*, 203–214.

Spearman, J., Taylor, J., Crossouard, N., Cooper, A., Turnbull, M., Manning, A., Lee, M., & Murton, B. (2020). Measurement and modelling of deep sea sediment plumes and implications for deep sea mining. *Scientific reports*, *10*(1), 1–14.

Sutherland, T., Lane, P., Amos, C., & Downing, J. (2000). The calibration of optical backscatter sensors for suspended sediment of varying darkness levels. *Marine Geology*, *162*(2-4), 587–597.

Thorne, P. D., & Hanes, D. M. (2002). A review of acoustic measurement of small-scale sediment processes. *Continental shelf research*, *22*(4), 603–632.

Todd, V. L., Todd, I. B., Gardiner, J. C., Morrin, E. C., MacPherson, N. A., DiMarzio, N. A., & Thomsen, F. (2014). A review of impacts of marine dredging activities on marine mammals. *ICES Journal of Marine Science*, *72*(2), 328–340. https://doi.org/10.1093/icesjms/fsu187

van Grunsven, F., Keetels, G., & van Rhee, C. (2018). The initial spreading of turbidity plumes–dedicated laboratory experiments for model validation. *48th Underwater Mining vation Conference (UMC)*.

Varriale, A. C., Crema, R., Galletti, M. C., Zunarelli, R. V., et al. (1985). Environmental impact of extensive dredging in a coastal marine area. *Marine Pollution Bulletin*, *16*(12), 483–488.

Vergne, A., Le Coz, J., & Berni, C. (2023). Some backscatter modeling issues complicating the sonar-based monitoring of suspended sediments in rivers. *Water Resources Research*, *59*(6), e2022WR032341.

Victor, O., Ikenna, O. C., & Ndubuisi, I. G. (2018). Environmental effect of dredging and geochemical fractionation of heavy metals in sediments removed from river. *Modern Chemistry*, *6*.

Wahab, S. A., Ali, W., Chassagne, C., & Helmons, R. (2024). Role of organic matter present in the water column on turbidity flows. *Journal of Marine Science and Engineering*, *12*(10), 1884.

Wahab, S. A., Chassagne, C., & Helmons, R. (2025). Effects of bed composition on turbidity flow dynamics in relation to flocculation. *Frontiers in Marine Science*, *12*, 1656243.

Wahab, S. A., Chassagne, C., & Helmons, R. (2026). Influence of bed age and flocculation dynamics on turbidity current propagation. *Frontiers in Earth Science*, *13*, 1720768.

Weaver, P., Aguzzi, J., Boschen-Rose, R., Colaço, A., De Stigter, H., Gollner, S., Haeckel, M., Hauton, C., Helmons, R., Jones, D. O., et al. (2022). Assessing plume impacts caused by polymetallic nodule mining vehicles. *Marine Policy*, *139*, 105011.

Wells, M. G., & Dorrell, R. M. (2021). Turbulence processes within turbidity currents. *Annual Review of Fluid Mechanics*, *53*(1), 59–83.

Xu, J. (2011). Measuring currents in submarine canyons: Technological and scientific progress in the past 30 years. *Geosphere*, *7*(4), 868–876.

Ye, L., Manning, A. J., & Hsu, T.-J. (2020). Oil-mineral flocculation and settling velocity in saline water. *Water Research*, *173*, 115569.

Zawadzki, D., Maciag, L., Abramowski, T., & McCartney, K. (2020). Fractionation trends and variability of rare earth elements and selected critical metals in pelagic sediment from abyssal basin of ne pacific (clarion-clipperton fracture zone). *Minerals*, *10*(4), 320.

ACKNOWLEDGEMENTS

This PhD journey has been one of the most transformative experiences of my life. It still feels surreal to think about how it all began. On the 15th of September 2021, around noon (IST), I received a phone call that I unfortunately missed. Curious, I checked the number and found it was from TU Delft; immediately, I felt a rush of excitement and nervous anticipation.

Two hours later, the phone rang again. It was Dr. Rudy Helmons. I will never forget that conversation. It remains one of the most special moments of my life, the moment when he informed me that I had been selected for the PhD position. Little did I know then that this call would mark the beginning of an extraordinary journey that would shape me both as a researcher and as a person.

What began with a single phone call soon evolved into four years of mentorship, support, and encouragement from two exceptional supervisors, without whom this journey would not have been the same. Throughout this journey, my supervisors, Dr. Rudy Helmons and Dr. Claire Chassagne, were my constant source of guidance and support. Their dedication, patience, and unwavering belief in me have played a fundamental role in helping me reach this milestone.

Dr. Rudy, thank you for always taking the time to listen, no matter how big or small the challenge was. Your patience, understanding, and thoughtful advice helped me navigate many difficult moments throughout my PhD. Dr. Claire, thank you for your encouragement, positivity, and the confidence you instilled in me whenever I doubted myself. Your kind words often gave me the motivation to keep going.

A PhD is a journey filled with challenges, uncertainties, and moments of self-doubt. However, I firmly believe that supervisors have the unique ability to shape this experience, not only by guiding the research but also by helping candidates find joy and purpose in their work. I feel incredibly fortunate to have worked with both of you. You made these four years not only intellectually rewarding but also truly enjoyable and memorable. You helped me develop a genuine love for what I do, and for that I will always be grateful.

Words cannot fully express the depth of my gratitude for everything you have done for me. Thank you for your guidance, your support, your patience, and your belief in me. I will carry the lessons I learned from both of you throughout my career and beyond.

While my supervisors guided me throughout this journey, many other wonderful people also contributed to making this achievement possible.

I would like to thank the technical staff of the Dredging Laboratory: Andre, Ed, Huib, and Marcel, and Mateusz at Deltares, for their invaluable support during my experiments. A special thank you goes to Paul van Kan for his expertise, patience, and guidance

in working with the sensors used throughout this research.

I am also grateful to my colleagues in the Offshore and Dredging Engineering section for creating a supportive and inspiring work environment. Special thanks to Xiuhan, Edwin, and Mossaab for their friendship, guidance, and willingness to help throughout my PhD. I would also like to thank Geert for the many enjoyable and insightful conversations, and Antonio, Rick, Said, Arno, Mark, Mohamed Elerian, Jian, Stefano, Justus, Thijs, Elbert, Pauline, Patty, Tessa, and Gracia for making the department such a welcoming place to work. Among the many friendships I formed during these years, I am especially thankful for the bond I shared with my dear colleague-turned-brother, Lalit.

I would like to pay tribute to the late Professor Cees van Rhee, whose vision and dedication shaped the Offshore and Dredging Engineering section. His legacy continues to inspire us and will always be remembered.

As the section continued to grow, I was particularly happy to see greater diversity within it. To be the first woman to join the Offshore and Dredging Engineering section in over a hundred years, I was delighted to see more women joining our circle. Sterre and later Chatarina brought friendship, laughter, and companionship to everyday life at TU Delft. From shared lunches and celebrations to unforgettable trips, including our adventure to Orlando Walt Disney World and Universal Studios, these moments made the PhD journey far more enjoyable and created friendships I will always treasure.

I am grateful to my colleagues at Deltares: Fatemeh, Waqas, Sidra, Ismail, Adarsh, Saghar, and Saskia, for their friendship, support, and countless moments of laughter throughout my PhD. Their kindness, encouragement, and companionship made my time at Deltares both enjoyable and memorable.

One of the highlights of my PhD was the research expedition aboard the RV Pelagia in 2023. I am grateful to all the scientists and crew members who made it such a memorable experience. A special thank you to Henko de Stigter for his kindness, humility, and invaluable guidance throughout my PhD journey. It has been a privilege to learn from and work alongside him. I would also like to thank Melanie for her support and kindness throughout the expedition.

I would also like to thank the MSc students whom I supervised: Koen, Arjan, Arjun, and Jan. I had such an amazing time in the lab, conducting experiments, making mistakes, and, most importantly, learning from each other.

The collaborative nature of this research extended beyond the university as well. To the members of the PLUMEFLOC team- Laurens from Royal IHC, Mark from Boskalis, Frans and Britt from Allseas, Lynyrd from Deltares, Henko and Melanie from NIOZ- thank you for the many insightful discussions and annual meetings.

I would also like to thank the wonderful MUDNET community for the many enjoyable team dinners, presentations, and memorable trips, including our visit to Efteling. My sincere thanks to Alex, Julia, Deyan, Geert, Dr. Rudy, and Dr. Claire for creating so many opportunities to share our work, learn from one another, and enjoy great moments together.

Beyond academia, I was fortunate to find friendships that made the Netherlands feel like home. To my friends at Don Pepe Tower: Abhishek, Skirmantas, Kostas K., Kostas Z., Apostolos, and our dear Kris- thank you for the friendship, laughter, and countless memories we shared.

To my Assamese family in the Netherlands: Mayuri, Iftikhar, Prantik, Ashraf, and Sajib-thank you for the friendship, laughter, and sense of home you gave me. Special thanks to Shrinjay for his constant support and to Dwijashish dada and Barsha for making life away from home a little easier and a lot brighter.

To my best friend and paranymph, Xue, your friendship has been a source of strength, joy, and comfort throughout this journey. I could not have asked for a better companion along the way.

The Netherlands also gifted me friendships that became family. To Maitry, my sister in the Netherlands-thank you for being family when I was far from home. Your love, care, and unwavering support carried me through some of the most challenging moments of this journey. I am grateful to have you in my life.

To a very special friend I met along this journey, Corine, thank you for your friendship, unwavering support, and kindness throughout the years. Your presence has meant more to me than words can express. I will always cherish our friendship and the wonderful memories we have shared together.

My gratitude also extends to my family, whose encouragement never wavered despite the distance.

To my nani (grandmother), whose constant prayers always protected me, and to my mama and mami, thank you for all your love and support.

A special mention goes to my uncle, Haroon Rashid. Your unwavering support, constant encouragement, and sincere interest in my work have meant more to me than you know. Thank you for always believing in me and celebrating every milestone along the way. I am so grateful to have you in my life.

To my incredibly patient husband, Tarit-I think you deserve a percentage of this PhD. From reading blogs and watching videos on how to support a partner through PhD stress, to living through it all with me, you did an exceptional job. You have seen me at my lowest and celebrated me at my highest. Through every setback, doubt, and success, you have been my greatest supporter, my biggest cheerleader, and my safe place. There were many moments I could not share with anyone else, but you were always there to listen, encourage, and believe in me. This journey would have been so much harder without you, and I am endlessly grateful to have had you by my side every step of the way.

To my dearest Papa, Mehbubul Wahab, and Ammi, Abida Wahab, thank you for always believing in me and giving me the confidence to dream big and spread my wings from a very young age. Papa, your love, encouragement, and faith in me have been the foundation of every achievement in my life. Ammi, your strength, resilience, and sacrifices have always inspired me; I have never known a stronger woman. Everything I am today is because of the values, love, and support you both have given me. I am incredibly proud to be your daughter, and I love you both more than words can ever express.

Above all, my deepest gratitude belongs to Almighty Allah, whose grace carried me through every challenge and every triumph. I am equally thankful to the saints whose blessings have been a constant source of strength, hope, and guidance.

Looking back, this journey feels even more remarkable when I think about where it began.

Growing up in a small tea-garden town in Assam, India, I could never have imagined that one day I would be completing a doctorate at one of the world's leading universities.

This journey has taught me that dreams can take us far beyond what we dare to imagine.

Finally, I would like to thank myself for being brave enough to leave home, resilient enough to overcome every challenge, and persistent enough to turn a dream into a PhD.

Shaheen Akhtar Wahab
Delft, The Netherlands
June 2026

CURRICULUM VITÆ

Shaheen Akhtar Wahab

15-07-1992 Born in Golaghat, India.

EDUCATION

1997–2011 Sacred Heart School (1997-2002)
St. Mary's School, (2003)
St. Stephen's High School (2004-2009)
Salt Brook Academy, India (2009–2011)

2011–2015 Bachelor of Technology in Civil Engineering
Assam Don Bosco University, India

2016–2019 Master of Science in Water Resources Engineering and Management
University of Stuttgart, Germany

2022–2026 Doctor of Philosophy (PhD)
Delft University of Technology, The Netherlands
Thesis: From particles to plumes: Role of Flocculation in Turbidity flows
Promotor: Dr. Rudy Helmons and Dr. Claire Chassagne

WORK EXPERIENCE

2017–2018 Student Research Assistant, University of Stuttgart, Germany

2018–2019 Intern and Master Thesis Student
International Marine and Dredging Consultants, Belgium

2020–2021 Lecturer
Kaziranga University, India

2022–2026 PhD Candidate
Delft University of Technology, The Netherlands

AWARDS

2015 Assam Don Bosco University Gold Medal for securing the highest CGPA

LIST OF PUBLICATIONS

Journal papers

4. **S. A. Wahab**, C. Chassagne, and R. Helmons, *Sensor suitability for turbidity and flocculation monitoring*, Manuscript under preparation (2026).

3. **S. A. Wahab**, C. Chassagne, and R. Helmons, *Influence of bed age and flocculation dynamics on turbidity current propagation*, Frontiers in Earth Science **13**, 1720768 (2025).

2. **S. A. Wahab**, C. Chassagne, and R. Helmons, *Effects of bed composition on turbidity flow dynamics in relation to flocculation*, Frontiers in Marine Science **12**, 1656243 (2025).

1. **S. A. Wahab**, W. Ali, C. Chassagne, and R. Helmons, *Role of organic matter present in the water column on turbidity flows*, Journal of Marine Science and Engineering **12**(10), 1884 (2024).

Oral and Poster presentations

3. **S. A. Wahab**, C. Chassagne, and R. Helmons, *Influence of Flocculation on dynamics of turbidity currents*, 53rd Underwater Minerals Conference, St. Pete Beach, Florida, USA, November 9-14, 2025 (Oral presentation).

2. **S. A. Wahab**, C. Chassagne, and R. Helmons, *Laboratory experiments to explore the effect of flocculation on sediment dispersion*, CEDA Dredging Days 2024, Rotterdam, Netherlands, 27-29 May, 2024 (Oral presentation).

1. K. v. Pelt, **S. A. Wahab**, and R. Helmons, *Sediment dispersion from a moving source*, 51st Underwater Minerals Conference, Rotterdam, the Netherlands, October 1-5, 2023 (Poster presentation).